
# Tesis Doctoral

# Digital Signal and Image Processing For Autonomic Nervous System Function Evaluation

**Autor:**

***Mohammed El Yaagoubi***

**Directores:**

***Dra. Rebeca Goya Esteban***

***Dr. Younes Jabrane***

**Tutor:**

***Dr. José Luis Rojo-Álvarez***

**Programa de Doctorado en Tecnologías de la Información y las Comunicaciones**

**Escuela Internacional de Doctorado**

**2020**

# Resumen


## Antecedentes

El sistema nervioso autónomo regula ciertas funciones automáticas del cuerpo, como los músculos lisos, la digestión, la respiración, los músculos del corazón o ciertas glándulas. De este modo, permite el mantenimiento de la homeostasis interna del cuerpo. El sistema nervioso autónomo se divide en **el sistema nervioso simpático** y **el sistema nervioso parasimpático**, los cuales controlan simpáticamente las acciones antagónicas más frecuentes a través de diferentes neurotransmisores, entre los cuales encontramos la norepinefrina y la adrenalina (catecolaminas) a nivel simpático, mientras que a nivel parasimpático encontramos la acetilcolina. Por otro lado, **el sistema nervioso entérico** regula el sistema digestivo, así como las actividades motoras y secretoras. Estos tres sistemas gestionan la actividad de muchos órganos, tales como actividad cardíaca y vasos sanguíneos, pulmones, tracto digestivo, vejiga, dilatación o contracción de la pupila del ojo, entre muchos otros.

El reciente auge de la ingeniería biomédica reside en buena parte en el uso de las técnicas de procesamiento digital de señales e imágenes médicas con el objetivo de buscar nuevas herramientas y soluciones en numerosos ámbitos. En esta Tesis se han seleccionado dos problemas específicos de ingeniería biomédica relacionados con el sistema nervioso autónomo: (1) en cardiología, abordamos el ámbito de la variabilidad de la frecuencia cardíaca (HRV, del inglés Heart Rate Variabillity) y la prevención de muerte cardíaca súbita (MCS); (2) en neurología, estudiamos la pigmentación del iris y su relación con las cefaleas en racimo (CH, del inglés Cluster Headache).

Respecto al primer ámbito, la identificación de pacientes con mayor riesgo de MCS se ha estudiado ampliamente durante las últimas décadas y se han propuesto varios índices a partir del análisis del electrocardiograma (ECG) almacenado en registros Holter de 1 día. Los índices basados en la dinámica no lineal de la variabilidad de la HRV han demostrado transmitir información predictiva en términos de factores relacionados con la regulación cardíaca por el sistema nervioso autónomo, y entre ellos, los métodos multiescala tienen como objetivo proporcionar descripciones más completas que las medidas basadas en en escalas individuales. Sin embargo, existe un conocimiento limitado sobre la idoneidad de las mediciones no lineales para caracterizar la dinámica cardíaca en los escenarios actuales de monitoreo a lo largo de un plazo de varios días.

En cuanto al segundo ámbito, la dificultad de diagnóstico de las CH entre las diferentes clases de cefaleas patológicas conlleva a la necesidad de investigar métodos que ayuden al diagnóstico y con ello mejorar la administración de tratamiento específico para las mismas. El ser humano recién nacido tiene un color de iris indeterminado y la coloración del iris se realiza en los primeros meses de vida. El color final es heredado y determina la pigmentación progresiva, que se culmina en los primeros meses de vida por la actividad de las células pigmentadoras (melanóforos). El sistema nervioso simpático ejerce una acción trófica sobre la actividad de los melanóforos. Cuando existe un defecto simpático congénito o adquirido en el periodo neonatal, se produce un déficit de la pigmentación en el iris del lado de la hipofunción simpática. El resultado es la heterocromia, esto es, el individuo tiene un ojo de cada color, típicamente un ojo azul y el otro marrón, siendo el ojo claro el

defectuosamente pigmentado. La heterocromia con clara diferencia de color se reconoce fácilmente a simple vista. Sin embargo, si la diferencia es sutil, se precisa de un método sensible para reconocerla.

**Objetivos**

El objetivo de esta Tesis es contribuir con técnicas de procesamiento digital emergentes al conocimiento y la evaluación de la función de autorregulación del sistema nervioso autonomo. Según las consideraciones anteriores, la presente Tesis aborda dos objetivos específicos:

- $O1$. Estudiar la información diagnóstica adicional proporcionada por la HRV en escalas de largo plazo disponibles en Holter de monitorización prlongada.

- $O2$. Estudiar la pigmentación del iris con el objetivo de distinguir el color entre los dos ojos de un indivíduo con cefaleas y con ello ayudar a decidir si padece o no cefaleas en racimo.

**Metodología**

En el objetivo de la primera línea de investigación, se examinan las propiedades a largo plazo de tres métodos no lineales para la caracterización de HRV, a saber, la Entropía Multiescala (MSE, del inglés Multiscal Entropy), la Irreversibilidad Temporal Multiescala (MTI, del inglés Multiscal Time Irreversibility) y el Espectro Multifractal (MFS, del inglés Multifractal Spectrum). Estos índices fueron seleccionados porque todos ellos han sido diseñados teóricamente para tener en cuenta las múltiples escalas de tiempo inherentes tanto en la fisiológica saludable como en la dinámica cardiaca patológica. Estas mediciones multiescala han sido analizadas hasta el momento en el monitoreo de hasta 24 horas de señales de ECG, correspondientes a aproximadamente 20 escalas de tiempo. Los analizamos en registros Holter de 7 días de dos conjuntos de datos, a saber, pacientes con fibrilación auricular (FA) e insuficiencia cardíaca crónica (ICC), hasta 100 escalas de tiempo, gracias a la monitorización a largo plazo disponile en sistemas actuales de Holter.

En cuanto a la segunda línea, se ha desarrollado un método de cuantificación del color del iris (Iridocolorímetro) que permite detectar diferencias sutiles de pigmentación. Para ello, se han empleado técnicas de aprendizaje estadístico, en concreto basadas en Máquinas de Vectores Soporte, que mediante su probabilidad de error al comparar imágenes en los dos ojos permiten dar una medida cuantitativa sobre las diferencias de coloración en el iris. Se han realizado pruebas sistemáticas sobre una base de datos con imágenes de 25 pacientes, y se han comparado las prestaciones de los diferentes espacios de color.

## Resultados

En el primer objetivo se destaca que las escalas más largas de los intervalos inter-latido, que están disponibles en el monitoreo a largo plazo, contienen información adicional sobre el estado del paciente. El MSE (MTI) exhibió el sesgo y la varianza más bajos (más elevados) a grandes escalas, mientras que todos los métodos mostraron una descripción consistente de los procesos a gran escala en términos de robustez del índice multiescala, con una sensibilidad a las diferentes dinámicas en las diferentes longitudes. Uno de los resultados más ilustrativos es que estos algoritmos multiescala, aunque probablemente informativos, deberían confiar no sólo en el aumento de la longitud de las señales para su consistencia, sino también en la mejora de su robustez.

Una vez desarrollado el método para detectar diferencias en el color del iris, se testeó en los primeros pacientes diagnosticados de cefalea en racimos proporcionados por el Hospital Universitario Fundación de Alcorcón. En todos los pacientes se demostró que el iris del lado sintomático estaba menos pigmentado que el del lado asintomático. Este hallazgo indica que la hipofunción simpática del lado sintomático es congénita o adquirida en el periodo neonatal que condiciona la lateralización del dolor. Con esto se mejora la detección así como la prescripción de tratamientos específicos para esta patología. En un futuro próximo se pretende aplicar el método a otras cefaleas que cursan con defecto simpático. La iridocolorimetría puede además, aportar claves patogénicas en diversos trastornos que cursan con afectación del sistema nervioso vegetativo.

## Conclusiones

Estos resultados allanan el camino de estas técnicas hacia su uso en escenarios de monitoreo con Holter cardíaco a largo plazo. Los índices basados en la dinámica no lineal de la HRV han mostrado información predictiva en términos de factores relacionados con la regulación cardiaca por el sistema nervioso autónomo, y entre ellos, los métodos multiescala que proporcionan descripciones más completas que las medidas basadas en una única escala.

Se ha desarrollado un método de cuantificación del color de los iris (iridocolorímetro) que permite detectar diferencias sutiles de pigmentación. Los ensayos preliminares de aplicación clínica demuestran en los pacientes analizados y afectos de cefalea en racimos una hipopigmentación del iris del lado sintomático. Este hallazgo es de importancia patogénica crucial puesto que indica que, en la cefalea en racimos, existe una hipofunción simpática congénita o desarrollada en el periodo neonatal, que sugiere una predisposición genética a sufrir el trastorno y que condiciona la lateralización del dolor. La iridocolorimetría se perfila como una técnica de interés en el estudio de trastornos que cursan con afectación del sistema simpático.

Las técnicas de procesamiento digital de señal e imagen médica pueden contribuir cada vez más en la evaluación de la función del ANS, detectando deficiencias que se traducen en patologías, mejorar del diagnóstico, y con su ayuda mejorar la prescripción de tratamientos específicos.

# Abstract


## Background

The autonomic nervous system regulates certain automatic body functions, such as smooth muscles, digestion, breathing, heart muscles, or certain glands. In this way, it allows the maintenance of the body's internal homeostasis. The autonomic nervous system is divided into **the sympathetic nervous system** and **the parasympathetic nervous system**, which sympathetically control the most frequent antagonistic actions through different neurotransmitters, among which we find norepinephrine and adrenaline (catecholamines) at the sympathetic level, while at the parasympathetic level we find acetylcholine. On the other hand, **the enteric nervous system** regulates the digestive system, as well as motor and secretory activities. These three systems manage the activity of many organs, such as cardiac activity and blood vessels, lungs, digestive tract, bladder, dilation or contraction of the pupil of the eye, among many others.

The recent boom in biomedical engineering lies largely in the use of digital signal and medical image processing techniques with the aim of finding new tools and solutions in many areas. In this Thesis, two specific problems of biomedical engineering related to the autonomic nervous system have been selected: (1) in cardiology, we address the field of heart rate variability (HRV) and the prevention of sudden cardiac death (SCD); (2) in neurology, we study iris pigmentation and its relationship with cluster headaches (CH).

With respect to the first area, the identification of patients at greater risk of SCD has been extensively studied over the last few decades and several indices have been proposed based on the analysis of the electrocardiogram (ECG) stored in 1-day Holter records. Indices based on the non-linear dynamics of HRV variability have been shown to convey predictive information in terms of factors related to cardiac regulation by the autonomic nervous system, and among these, multiscale methods aim to provide more complete descriptions than measures based on individual scales. However, there is limited knowledge about the suitability of non-linear measurements to characterize cardiac dynamics in current monitoring scenarios over a period of several days.

As for the second area, the difficulty in diagnosing CH among the different types of pathological headaches leads to the need to investigate methods that help diagnosis and thus improve the administration of specific treatment for them. The newborn human being has an indeterminate iris colour and the iris is coloured during the first months of life. The final color is inherited and determines the progressive pigmentation, which is culminated in the first months of life by the activity of the pigmenting cells (melanophores). The sympathetic nervous system exerts a trophic action on the activity of the melanophores. When there is a congenital or acquired sympathetic defect in the neonatal period, there is a deficit of pigmentation in the iris on the side of the sympathetic hypofunction. The result is heterochromia, that is, the individual has one eye of each color, typically one blue eye and the other brown, with the light eye being the one that is defective in pigmentation. Heterochromia with clear color difference is easily recognized with the naked eye. However, if the difference is subtle, a sensitive method is required to recognize it.

## Objectives

The objective of this Thesis is to contribute with emerging digital processing techniques to the knowledge and evaluation of the self-regulatory function of the autonomic nervous system. According to the previous considerations, this Thesis addresses two specific objectives:

- $O1$. Study the additional diagnostic information provided by the HRV on long-term scales available in extended monitoring Holter.
- $O2$. To study the pigmentation of the iris with the aim of distinguishing the colour between the two eyes of an individual with headaches and thus help to decide whether or not to suffer from cluster headaches.

## Methodology

In the first line of research, the long-term properties of three non-linear methods for the characterization of HRV are examined, namely Multiscale Entropy (MSE), Multiscale Time Irreversibility (MTI) and Multifractal Spectrum (MFS). These indices were selected because they have all been theoretically designed to take into account the multiple time scales inherent in both healthy physiology and pathological cardiac dynamics. These multiscale measurements have been analyzed so far in monitoring up to 24 hours of ECG signals, corresponding to approximately 20 time scales. We analyzed them in 7-days Holter records of two data sets, namely patients with atrial fibrillation (AF) and chronic heart failure (CHF), up to 100 time scales, thanks to the long-term monitoring available in current Holter systems.

As for the second line, a method for quantifying iris colour (Iridocolourmeter) has been developed to detect subtle differences in pigmentation. For this purpose, statistical learning techniques have been used, specifically based on Support Vector Machines, which by means of their error probability when comparing images in the two eyes allow a quantitative measure of the differences in colour in the iris. Systematic tests have been carried out on a database with images of 25 patients, and the performance of the different colour spaces has been compared.

## Results

In the first objective, it is emphasized that the longer scales of the inter-beat intervals, which are available in long-term monitoring, contain additional information about the patient's condition. The MSE (MTI) exhibited the lowest (highest) bias and variance at large scales, while all methods showed a consistent description of large-scale processes in terms of robustness of the multiscale index, with sensitivity to different dynamics at different lengths. One of the most illustrative results is that these multiscale algorithms, although probably informative, should rely not only on increasing the length of the signals for consistency, but also on improving their robustness.

Once the method for detecting differences in iris colour was developed, it was tested on the first patients diagnosed with CH provided by the Hospital Universitario Fundación

de Alcorcón. In all patients it was shown that the iris on the symptomatic side was less pigmented than the one on the asymptomatic side. This finding indicates that sympathetic hypofunction on the symptomatic side is congenital or acquired in the neonatal period which conditions the lateralization of pain. This improves the detection as well as the prescription of specific treatments for this pathology. In the near future, it is intended to apply the method to other headaches with sympathetic defect. Iridocolourimetry can also provide pathogenic clues in various disorders affecting the vegetative nervous system.

**Conclusions**

These results pave the way for these techniques to be used in long-term cardiac holter monitoring scenarios. Indices based on the non-linear dynamics of HRV have shown predictive information in terms of factors related to cardiac regulation by the autonomic nervous system, and among them, multiscale methods that provide more complete descriptions than measures based on a single scale.

A method of quantifying iris colour (iridocolourimeter) has been developed to detect subtle differences in pigmentation. Preliminary trials of clinical application show a hypopigmentation of the iris on the symptomatic side in patients analysed and affected by cluster headache. This finding is of crucial pathogenic importance since it indicates that, in cluster headache, there is a congenital or developed sympathetic hypofunction in the neonatal period, suggesting a genetic predisposition to the disorder and conditioning the lateralization of pain. Iridocolourimetry is a technique of interest in the study of disorders that affect the sympathetic system.

Digital signal processing and medical imaging techniques can increasingly contribute to the evaluation of the function of the ANS, detecting deficiencies that translate into pathologies, improving diagnosis, and with their help improve the prescription of specific treatments.

*"That whose existence is necessary must necessarily be one essence."*

*Avicenna*

*A mis padres*
*A mi mujer Nadia, mis hijos Ismail y Ghali*
*A mis hermanos Aissam, Amal y Soumia*
*A toda mi familia*

# Acknowledgment

*Siempre parece imposible hasta que se hace (Nelson Mandela).* Es innegable que sin ellos, cualquier proyecto no sería posible, y en particular la investigación, es poco probable que dé frutos. Sin embargo, de todos los que han tenido la oportunidad de vivir esta experiencia, nadie negará el hecho de que, a pesar de de nuestras fortalezas y cualidades, aunque sean numerosas, no pueden lograrse sin el apoyo de nuestro séquito profesional, personal y familiar, tal es el tortuoso y tortuoso curso de este recorrido tortuoso y arduo. Además, aprecio mucho la invaluable contribución de esta enriquecedora experiencia tanto a nivel intelectual como humano, y me alegro del inmenso orgullo que siento por tener contribuyó, aunque poco, al avance de la investigación académica. Por lo tanto, es natural que, al terminar esta tesis, me gustaría expresar mi gratitud a todos aquellos que han contribuido de una forma u otra a su éxito.

Quiero expresar mi sincero agradecimiento al Prof. Dr. José Luis Rojo-Álvarez, que me ha propuesto esta oportunidad y que, como tutor de tesis, me proporcionó consejos sólidos, herramientas metodológicas indispensables para llevar a cabo esta investigación, y siempre estuvo disponible y dedicado. Su ayuda fue inestimable desde la primera reflexión hasta la organización y la defensa de esta tesis.

Nunca podré agradecer suficientemente a la Prof Dra. Rebeca Goya Esteban la confianza que ha depositado en mí al aceptar supervisar la primera línea de investigación por todo el interés que ha mostrado en mi trabajo. Su guía y estímulo fueron fructíferos. Además, me permitió descubrir el mundo de las HRV y me introdujo en la investigación, momentos inestimables que quedarán grabados en mi memoria para siempre.

Estoy, pues, muy agradecido al Prof. Dr. Younes Jabrane por la ayuda y el tiempo considerables que ha dedicado: desde la ENSA de la universidad UCA de Marrakech; a todas las horas que ha dedicado a hacer avanzar esta investigación, a corregir publicaciones, el informe y la presentación; a su disponibilidad siempre que le he pedido ayuda.

No hace falta decir que la Prof. Dra. Inamculada Mora Jimńez desempeñó un papel notable durante los años de mi tesis. Su vigilancia y observaciones de calidad hicieron mi tarea mucho más fácil. Siempre deseoso de compartir su abundante conocimiento y experiencia conmigo. Por lo tanto, debo saludar muy calurosamente su extensa contribución al éxito de este trabajo.

También quisiera expresar mi sincero agradecimiento por un lado al equipo del Hospital Universitario Fundación Alcorcón dirigido por el Prof. Dr. Juan Antonio Pareja Grande y por otro lado al equipo del Hospital Universitario Virgen de la Arrixaca de Murcia dirigido Prof. Dr. Arcadi García-Alberola por la acogida y las condiciones de trabajo privilegiadas que reservaron.

Sin duda, me gustaría agradecerle al Dr. Sergio Muñoz su disponibilidad y compromiso en las aportaciones en optimizar los algoritmos, gracias Sergio.

A mis amigos y compañeros muchas gracias por el apoyo que recibí durante todo el transcurso de esta tesis.

# Acronyms

**AF:** Atrial Fibrillation.
**AI:** Artificial Intelligence.
**ANS:** Autonomic Nervous System.
**BPV:** Blood Preasure Variability.
**CAD:** Coronary Artery Disease.
**CH:** Cluster Headaches.
**CHF:** Congestive Heart Failure.
**CI:** Confidence Intervals.
**ECG:** Electrocardiogram.
**EF:** Ejection Fraction.
**ENS:** Enteric Nervous System.
**HRV:** Heart Rate Variability.
**HSI:** Hue-Saturation-Intensity.
**HSV:** Hue-Saturation-Value.
**HUFA:** Hospital Universitario Fundación de Alcorcón.
**ICD:** Implantation of an Cardioverter Defibrillators.
**IHS:** International Headache Society.
**KNN:** K-Nearest Neighbour.
**LAB:** Lightness Red/Green Value and Blue/Yellow Value.
**LTM:** Long-Term Monitoring.
**LVEF:** Left Ventricular Ejection Fraction.
**MFS:** Multifractal Spectrum.
**MI:** Mutual Information.
**ML:** Machine Learning.
**MSE:** Multiscale Entropy.
**MTI:** Multiscale Time Irreversibility.
**RBF:** Radial-Basis Function.
**RGB:** Red Green Blue.
**SCD:** Sudden Cardiac Death.
**SVC:** Support Vector Clussifier.
**SVM:** Support Vector Machines.
**VF:** Ventricular Fibrillation.
**VT:** Ventricular Tachycardia.
**WHO:** World Health Organization.

# List of Figures

# List of Tables

# Contents

# Chapter 1

# Introduction

The present chapter provides an overview of the addressed topics. Initially, the physiological and technical background that feeds the motivation of this doctoral dissertation are described. Subsequently, the main objectives of the Thesis are stated and the methodology adopted for this work is also described. Finally, the outline of the Thesis and its contributions to the scientific literature are indicated.

## 1.1 Background

Biomedical Engineering arising from the Information and Communications technologies and applied to the medicine field provides an extended diagnosis of several pathologies, through signal and image processing. This allows specifying accurately the appropriated medical treatment, and it also promotes advanced methods for preventing sudden death.

Biomedical research [1, 2] over the past 25 to 30 years has led to a remarkable increase in knowledge and its practical applications. These advances have been made in many disciplines, ranging from biochemistry to various specialized clinical areas, but the most important and far-reaching contributions are undoubtedly those of molecular biology. The clinical sciences have also made great strides, both in terms of diagnostic procedures and therapeutic methods. This progress has been and will continue to be largely dependent on the results of basic research, particularly in molecular biology and immunology. It should be pointed out that in some cases they have been made possible by techniques borrowed from disciplines other than those normally forming part of the Biomedical Sciences, such as Physics and Mathematics. Examples of diagnostic methods include magnetic resonance imaging and positron emission tomography. In general, progress has been more rapid in the field of diagnosis than in therapeutics, but progress in this area should not be underestimated. Suffice it to mention that, in developed countries, many common cancers have a cure rate of 50 %, that artificial joints have transformed the lives of many people with various forms of arthritis, and that organ transplants, especially kidney transplants, are a true miracle for patients once condemned to an early death. In some cases, therapeutic procedures have been developed using techniques developed outside the Biomedical Sciences [3]. One example is the increasingly widespread use of lasers. Lasers have long been used in ophthalmic, gynaecological and otolaryngological surgery, but they are now increasingly used in other forms of surgery. Perhaps the most promising area of use is in cardiovascular surgery. Although still an experimental technique, it appears

that the laser will be increasingly used in the surgical treatment of obstructed blood vessels, particularly coronary arteries. If the experiment proves successful, the indications for coronary artery bypass surgery will become much more rare. Even technologies and physical sciences, some of which can undoubtedly facilitate directly or indirectly the improvement of health care increasing products and processes that are of real or potential interest in improving the health care system. As an example, ancillary technologies are expected to play an equally important role in facilitating healthcare planning and problem solving [4].

Currently, hundreds of millions of people worldwide are affected by nervous system abnormalities which induce the development of disorders such as cardiovascular diseases (CVD) and neurological pathologies [5]. Many diseases of the central nervous system can be accompanied by cardiovascular changes such as stroke, epilepsy, or degenerative diseases. These may include changes in the electrocardiogram (ECG), atrial or ventricular cardiac arrhythmias, specific cardiac lesions (myocytolysis), changes in blood pressure or subclinical manifestations, detected by non-invasive tests such as sinus variability. The pathogenesis of these cardiovascular manifestations is not fully elucidated. It could result from an imbalance of the vagosympathetic balance leading to sympathetic hyperactivity. The asymmetry of cardiac innervation suggests that right brain lesions are more likely to result in changes in heart rate or supraventricular arrhythmias and that left brain lesions are more likely to be associated with atrioventricular conduction disorders or ventricular arrhythmias. A better understanding of these cardiac consequences could lead to the identification of subgroups at risk that could benefit from specific monitoring or therapeutic measures.

The autonomic nervous system (ANS) is divided into three parts:

- The sympathetic nervous system in which we find norepinephrine and adrenaline (catecholamines).
- The parasympathetic nervous system, which controls antagonistic actions through different neurotransmitters, such as acetylcholine.
- The enteric nervous system, which regulates the digestive system, as well as the motor and secretory activities.

These three systems manage the activity of many organs (heart and blood vessels, lungs, digestive tract, bladder, dilatation or contraction of the pupil of the eye, among many others). In this dissertation, two major conditions related to the state of the ANS are investigated by means of signal and image digital processing techniques.

### Risk on Sudden Cardiac Death

Sudden Cardiac Death (SCD) is defined as natural death with abrupt loss of consciousness within one hour of the onset of symptoms, in a person with or without known heart disease. The timing and mode of occurrence are unexpected. SCD is a public health issue, which justifies major efforts to improve the management of the accident itself when it occurs unexpectedly. The specificity of this definition varies depending on whether the event was observed or not. However, most studies include cases associated with an observed collapse, death within one hour of an acute change in clinical status, or unexpected death

within the previous 24 hours [5, 6, 7, 8]. There are other causes of sudden death, but cardiac is the most usual origin, specifically including: (a) Arrhythmic causes, such as ventricular tachycardia (VT), ventricular fibrillation (VF), or asystole; (b) Several other structural heart disease origins, for instance, those ones corresponding to congenital heart disease; And (c) abnormal function of the ANS, which is not itself a death cause, but it can promote others such as arrhythmic or hypertensive death [8]. The SCD mechanism in the last case is often VT or VF. Given the incidence of SCD as major cause of mortality in the world, methods have been proposed aiming to provide with risk stratification tools for cardiac patients [9]. SCD episodes can happen not only in patients with coronary or cardiomyopathic disease, but also they can occur in people with no previous heart alteration, which makes the risk stratification extremely complex.

The prognostic significance of noninvasive studies and the efficacy of the therapeutic actions have been pointed to be etiology dependent [10]. The most widely used SCD-risk marker in the clinical practice is the Left Ventricular Ejection Fraction (LVEF), but given its low specificity, many other techniques have been proposed. A relevant subset of them is given by the computational indices that are obtained from the signal analysis of the ECG, including a variety of proposed biomarkers such as late potentials, heart rate variability (HRV), T-wave alternans, or deceleration capacity. The interested reader can refer to [11] for a detailed review on issues related with signal processing, technology transfer, and scientific evidence for all of them. Many of these SCD markers are obtained in a Holter recording, which is a diagnostic tool consisting of 24 to 48 hour signal registers in two or three chest leads to be subsequently processed by using a computer program, so that a variety of cardiac events can be identified by the clinician. Probably one of the most scrutinized markers of SCD risk from Holter recordings is HRV, which measures the time changes between consecutive cardiac beats [12]. Its interest partially comes from its non-invasive nature and its easy for analysis, only needing to know the time instants of the beat occurrences. The heart does not behave like a periodic oscillator, but instead its rhythm is modulated by the ANS, and the simultaneous actuation of its two branches (sympathetic and parasympathetic) causes dynamic oscillations of the cardiac frequency, producing the presence of HRV [13]. Among the many methods that have been proposed in the literature to quantify the HRV indices, the nonlinear methods extract relevant information from HRV signals in terms of their complexity. Nonlinear indices are based on the underlying idea that fluctuations in the between-beat intervals (also known as $RR$ intervals) can exhibit characteristics that are well known from Complex Dynamic Systems Theory, and broadly speaking, healthy states are expected to correspond to more complex patterns than pathological states. However, some pathologies are associated with highly erratic fluctuations with statistical properties resembling uncorrelated noise [11], and traditional algorithms could yield higher irregularity indices for such pathological signals when compared to healthy dynamics, even though the latter represent more physiologically complex states [14]. This possible inconsistency may be due to the fact that traditional algorithms are based on single scale analysis, and they can not take into account the complex temporal fluctuations inherent to healthy physiologic control systems. It is usual that studies based on 1-day Holter monitoring [15] envision that relevant information could be obtained from longer duration recordings, however, few studies [16, 17] have scrutinized nonlinear indices in several-day Holter monitoring, despite its current and increasing availability in the clinical practice. Note in the following that, whereas some

authors refer to long-term Holter as those with duration about 24 h, we will use *long-term* to refer to the Holter recordings when measured for several days.

Several of the nonlinear HRV measurements (based either on Chaos Theory, Information Theory, or Fractal Theory) have been paid special attention according to the electrophysiological hypothesis that the long-term regulation is a homeostatic yet dynamical equilibrium, which can be expected to be complex and multi-cause enough to require a set of indices that should be calculated at different scales. This has motivated the extension of several of those indices to what can be called their *multiscale* versions. Remarkable examples of this effort are the Multiscale Entropy (MSE) method [18, 19, 20, 21], the Multiscale Time Irreversibility (MTI) method [19], and the Multifractal Spectrum (MFS) method [22, 23].

#### Cluster Headache

On the other hand, Headache is a local pain felt in the skull or sometimes in the neck. This pain can be lateral, often unilateral, or diffuse and generalized. It manifests itself in a wide variety of ways through sensations of tightness or compression, pounding, hammering, sinking, burning, tingling, or crushing, as well as a hyper-sensitivity to noise and light.

Trigeminal Autonomic Cephalalgias (TAC) belong to the Group III of the International Headache Society (IHS), and they share the clinical features of pain felt in the area supplied by the first division (V-1) of the trigeminal nerve, accompanied by a variable combination of cranial autonomic features [24, 25]. Cluster Headache (CH) is the most frequent TAC [26]. It is a male-predominant disorder with a usual age at onset in the late twenties. CH typically presents with very severe strictly unilateral, orbital/periorbital pain, accompanied by a variable combination of autonomic features, such as conjunctival injection, lacrimation, rhinorrhea, nasal stuffiness, ptosis, miosis, eyelid edema and facial/forehead sweating. The attacks last 15-180 minutes and recur with a frequency from one every other day to 8 per day, during symptomatic periods (cluster periods).

During attacks of CH, a sympathetic hypofunction is manifested clinically as ptosis and miosis on the painful side. The sympathetic hypofunction remains latent (subclinical) in between attacks, throughout the symptomatic period but can be unveiled by provocative tests with appropriate eye drops substances. If there is a persistent but subtle and constitutional (since birth) sympathetic hypofunction in the symptomatic side, the iris of the symptomatic side would have been less pigmented. In these cases the sympathetic defect would be congenital or would have occurred in the neonatal period [27, 28]. One of the CH signs could be the different iris color in the patient's eyes, which is not always noticeable by simple visual inspection. Accordingly, the screening and early detection of CH could be addressed by creating a biomarker from subtle color changes in the iris.

## 1.2 Motivation and Objectives

Digital signal processing and medical imaging techniques are increasingly contributing to the evaluation of the function of the ANS, detecting deficiencies that translate into pathologies, improving diagnosis, and helping doctors to objectify the prescription with an appropriate treatment.

The most significant motivation of this dissertation is to evaluate the auto-regulation function of the ANS and contribute to the solution of related diagnostic problems through the use of appropriate digital signal and data processing techniques. The ANS is a part of the nervous system that regulates certain automatic functions of the body and allows the maintenance of the internal homeostasis, such as cardiovascular and neurological systems.

Cardiovascular diseases are statistically the major cause of morbidity, unfortunately, classical invasive-based treatment methods present high risk and expensive cost [5]. On the other hand, the cluster headache is a specific pain which is difficult to detect among different pathologies having the same clinical signs. Up to now, the specialists prescribe classical headache medicines to alleviate the pain [6].

The main objective of this Thesis is to improve the analysis using statistical tools and multimedia processing methods to design two automatic non-invasive systems, the first one able to provide improved SCD risk markers, and the second one able to detect the cluster headache and objectify its treatment. Therefore, two specific aims are clearly distinguished:

- The first specific objective is to scrutinize the HRV analysis methods proposed for the SCD risk-stratification and to improve the robustness of non-linear methods through a set of indices in long-term holter monitoring, namely Multiscale Entropy (MSE), Multiscale Time Irreversibility (MTI), and Multifractal Spectrum (MFS).

- The second specific is to propose a multimedia concept for quantifying the color of the iris, which allows the documentation and quantification of subtle pigmentation differences. This concept is to be made operative though different machine learning methods namely Support Vector Classifier (SVC), and K-Nearest Neighbour (K-NN).

## 1.3 Methodology

To achieve the first objective, we studied the suitability of nonlinear multiscale HRV measurements to characterize different cardiac health states in LTM recordings. Specifically, we made a comparative analysis of the three mentioned multiscale methods on a database consisting of patients with 7-day Holter in two cardiac conditions, namely, Congestive Heart Failure (CHF) and Atrial Fibrillation (AF) [29]. This study aims to give basic knowledge on the usefulness and current limitations of these methods towards their future and principle use for SCD risk stratification. For this purpose, a nonparametric statistical test is proposed in order to compare and give cut-off comparison levels between two different situations in terms of the confidence intervals (CI) for the median difference across multiscale representations of poblational representations. This method can be used either for establishing comparisons among patients or subjects with different conditions, or to scrutinize the impact of preprocessing or data length on the statistical properties of the multiscale representations. The procedure can be seen as an extension of previously used statistical comparisons [30, 31] in terms of nonparametric bootstrap tests for confidence bands [32, 16].

For the second objective, we developed an automatic CH diagnosis method using machine learning classification (in particular, the SVC and K-NN principles) to analyze differences in the iris color of a cephalea patient. We hypothesized that subtle differences

in eyes color could be quantified in terms of the error probability of a pixel classification system which is suitably designed and trained to identify color space differences in color-pixel spaces. We built this system by using a specifically created database with images of both eyes in 25 subjects, with images taken under the same conditions. It is worth noting that the used database is completely new, and though the number of patients is limited, it represents a trade-off for technically scrutinizing our method before large-scale data assembling. First, we studied the applicability of statistical classifiers to detect differences in the iris color under a pixel-by-pixel approach. Then, we analyzed the robustness of the classifier to regional changes due to substructures possibly present in the iris images, as well as the impact of simultaneously using different color spaces and the contribution of the pixel neighborhood to the classifier performance.

## 1.4 Thesis Structure and Contributions

This Dissertation is outlined as follows:

- In the next chapter, an overview of the research field is exposed: ANS background, cardiovascular system regulation, and the CH.
- Chapter 3 spreads our first contribution in SCD risk-stratification applying nonlinear dynamics and multiscale indices in large scales of cardiac signals.
- Chapter 4 presents the second proposal in ANS function evaluation for CH diagnosis support by classifying the iris color-pixel vectors of both eyes.
- Chapter 5 contains the discussion, the conclusions, and future perspectives.

Results of the described works of this Thesis have been previously published on journals indexed in the Journal Citation Reports service and presented in international conferences. The contributions of the first line of research have been published in two international conferences and one journal article as follows:

- El-Yaagoubi, M.; Goya-Esteban, R.; Jabrane, Y.; Muñoz-Romero, S.; García-Alberola, A.; Rojo-Álvarez, J.L. "On the Robustness of Multiscale Indices for Long-Term Monitoring in Cardiac Signals", Entropy 2019, 21, 594.
- M. El Yaagoubi, R. Goya, Y. Jabrane, S. Muñoz-Romero, J.L. Rojo Álvarez and A. García-Alberola "Multifractal Spectrum Analysis of Long-term Monitoring in Cardiac Signals", International Conference on Biomedical Engineering, 4-5 October 2018, Marrakech, Morocco.
- M. El Yaagoubi, R. Goya, Y. Jabrane, S. Muñoz-Romero, J.L. Rojo Álvarez and A. García-Alberola "Multiscale Entropy and Multiscale Time Irreversibility for Atrial Fibrillation and Heart Failure from 7-Day Holter", Congreso Anual de la Sociedad Española de Ingeniería Biomédica, 29 November - 1 December 2017, Bilbao, Spain.

As for the second line of research, the results have been published in two international conferences with a journal article to be submitted:

- M. El Yaagoubi, I. Mora Jiménez, Y. Jabrane, S. Muñoz-Romero, J.L. Rojo Álvarez and J.A. Pareja Grande "Quantitative Cluster Headache Analysis for Neurological Diagnosis Support using Statistical Classification", submitted to MDPI-Information.
- M. El Yaagoubi, I. Mora Jiménez, J.L. Rojo Álvarez, Y. Jabrane and J.A. Pareja Grande "Extended Iris Color Features Analysis and Cluster Headache Diagnosis Based On Support Vector Classifier", International Conference on Intelligent Systems and Computer Vision, 17-19 April 2017, Fes, Morocco.
- M. El Yaagoubi, I. Mora Jiménez, J.L. Rojo Álvarez, and J.A. Pareja Grande "Cluster Headache Diagnosis Using Iris Color Features and Statistical Pixel Classification", 2016 - XIV Mediterranean Conference on Medical and Biological Engineering and Computing.

# Chapter 2

# Overview of the Research Field

This chapter presents a brief background of the ANS, its relation with the cardiovascular system regulation, and the brief overview of the CH.

## 2.1 Autonomous Nervous System

The ANS or visceral nervous system, also called the vegetative nervous system, is the part of the nervous system responsible for functions not under voluntary control [33].

The ANS regulates certain physiological processes, such as blood pressure and breathing rate. This system works automatically (autonomously), without conscious effort on the part of a person. ANS disorders can affect any part of the body or any physiological process. Autonomous disorders can be reversible or progressive. This system connects the brain stem and spinal cord to the internal organs and it regulates internal physiological processes that do not require any voluntary effort and of which people are normally unaware, for example, the heart rate and power of heart contractions, blood pressure, breathing rate and the rate of food transit through the digestive tract [34]. The ANS is divided into three parts [35], as it can be seen in Figure 2.1:

- The sympathetic system: Its main function is to prepare the body to react in case of stress or emergency, to fight or escape. Its action is regulated by the norepinephrine and adrenaline (catecholamines).

- The parasympathetic system: Its main function is to maintain the body's normal functions during ordinary situations. Its action is regulated through different neurotransmitters such as acetylcholine.

- A third part of the ANS is known as the Enteric Nervous System (ENS), as it can be seen in Figure 2.2. The ENS regulates the digestive system, as well as the motor functions, local blood flow, mucosal transport and secretions, and it also modulates immune and endocrine functions.

Sympathetic and parasympathetic systems interact with each other, in general, one system activates the actions of the internal organs while the other inhibits them. For example, sympathetic activity increases pulse rate, blood pressure and respiratory rate, while parasympathetic activity reduces them.

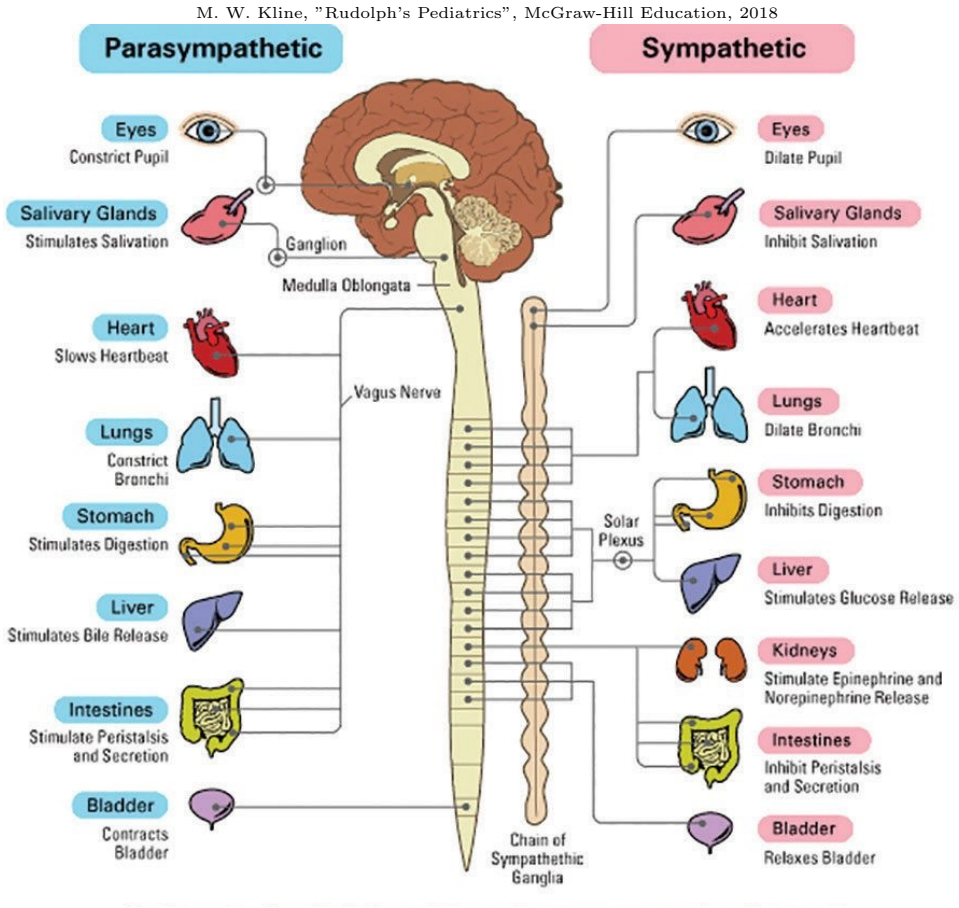


Figure 2.1: ANS organs and function regulation.

Many organs are mainly controlled by the sympathetic or parasympathetic systems. Sometimes the two systems have opposite effects on the same organ. For example, the sympathetic system increases blood pressure, while the parasympathetic system reduces it. Overall, these two systems work together to ensure that the body responds appropriately to different situations.

The sympathetic system prepares the body to react in case of stress or emergency, to fight or escape. It increases the heart rate and strength of cardiac contractions, and it dilates the airways to facilitate breathing. It causes the release of energy stored in the body. Muscle strength is also increased. This system is also responsible for sweating the palms, dilating the pupils, and making the hair stand up. It slows down physiological processes that are less important in emergencies, such as digestion and urination.

The parasympathetic system controls physiological processes during ordinary situations. In general, the parasympathetic system preserves and restores. It slows the heart rate and reduces blood pressure. It stimulates the digestive tract to digest food and eliminate waste. The energy of digested food is used to restore and build tissues.

Both the sympathetic and parasympathetic systems are involved in sexual activity, as well as those parts of the nervous system that control voluntary actions and transmit skin sensations.

These three systems manage the activity of many organs (heart and blood vessels,

https://www.pinterest.com/pin/473300242076693204/ (accessed 02 March 2020)

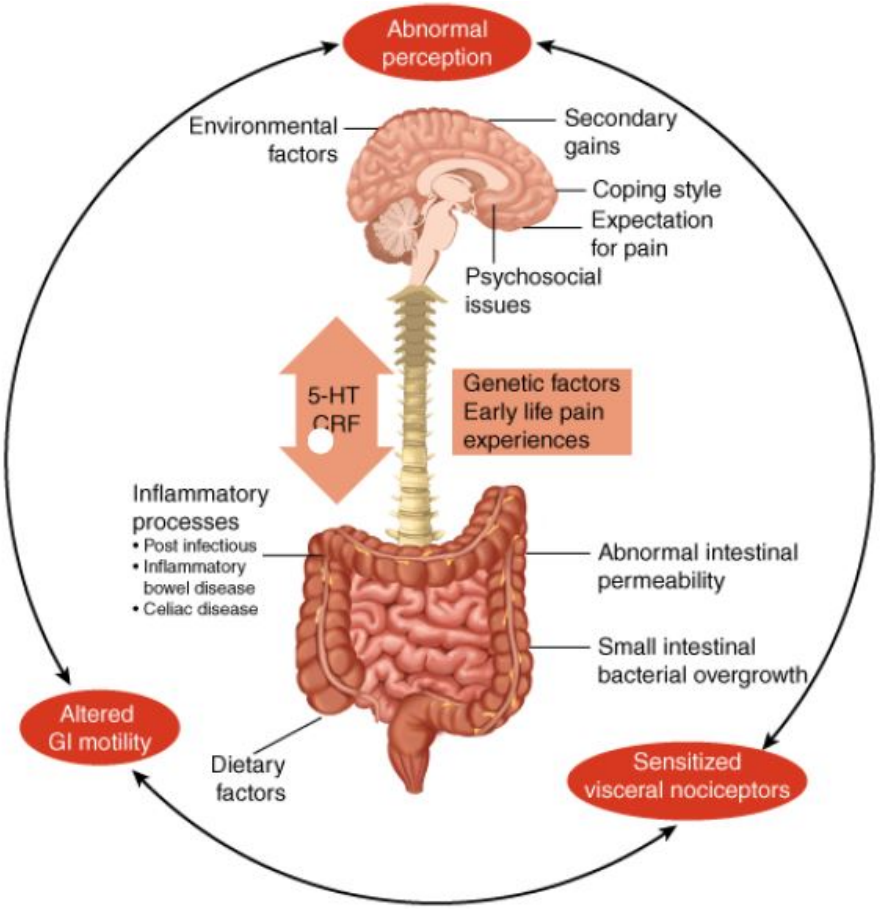


Figure 2.2: Enteric Nervous System functions.

lungs, digestive tract, bladder, dilatation or contraction of the pupil of the eyes).

After the ANS has received information about the body and the external environment, it responds by stimulating physiological processes, usually through the sympathetic system, or by inhibiting them, usually through the parasympathetic system.

An autonomous nerve pathway connects two nerve cells located in two major structures, one in the brain stem, and the other in the spinal cord. It is connected by nerve fibres to the other cell, which is located in a network of nerve cells (called the autonomous ganglion). The nerve fibres in these lymph nodes are connected to the internal organs. Most of the lymph nodes of the sympathetic system are located just outside the spinal cord, on either side of it. The nodes of the parasympathetic system are located near or in the organs to which they are attached.

## 2.2 ANS Regulation of the Cardiovascular System

It is well known that central neural system acts on the circulation as well as the emotional stress which causes an increase in heart rate or a blushing of the skin [36]. Moreover, it has been observed that stimulation of peripheral sympathetic nerves causes vasoconstriction and that interruption of the spinal cord in the lower cervical region drastically reduces

E. L. Boulpaep, "Regulation of arterial pressure and cardiac output", Medical Physiology A Cellular and Molecular Approach

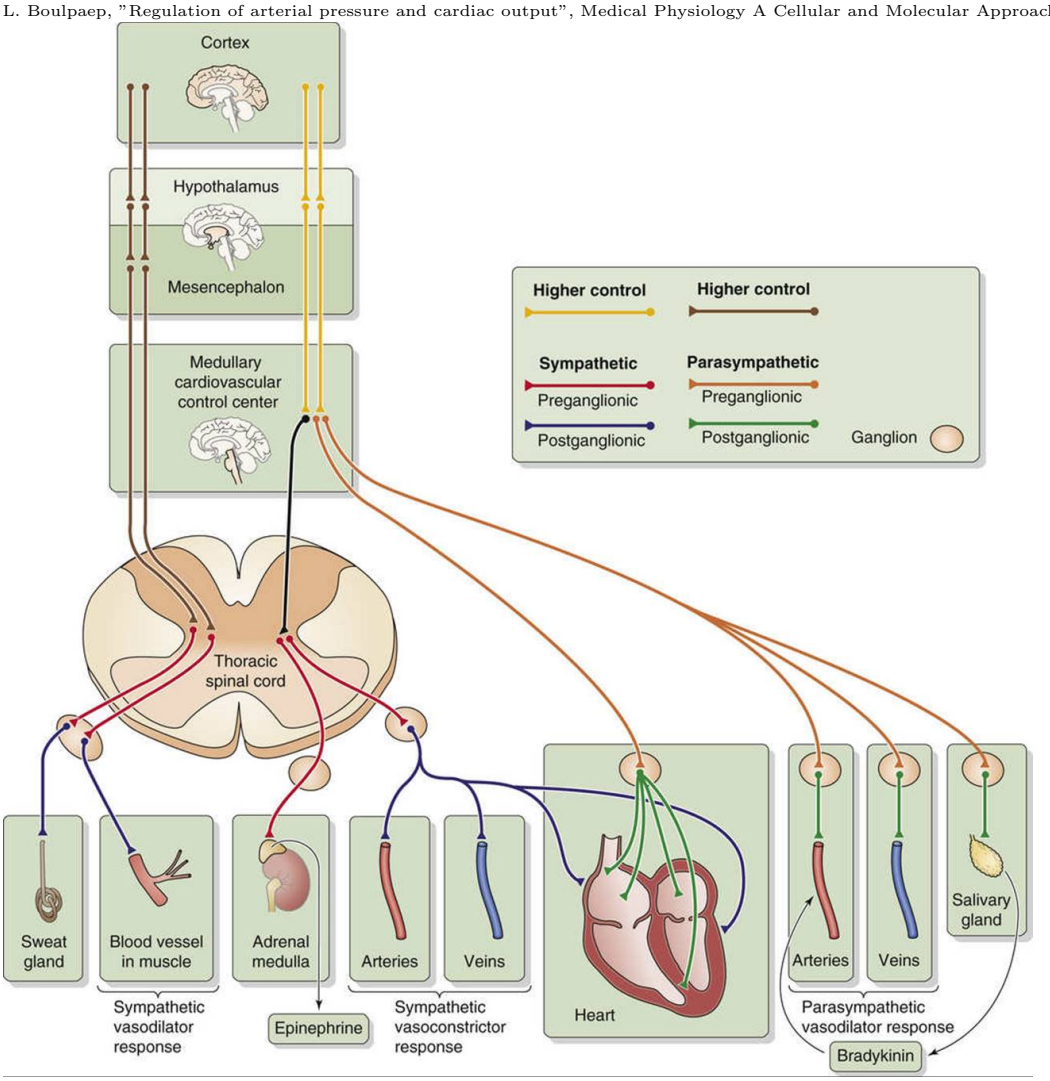


Figure 2.3: ANS and Cardiovascular System Regulation. Hypothetical section through the medulla.

blood pressure. All the experiments made suggest that the depressor and sinus nerves carry sensory information to the brain and that the brain in some fashion uses this information to control cardiovascular function. In Figure 2.3 a synoptic is shown of the relation between the ANS and the cardiovascular system, and the behaviour of this relation is described in [37] and summarized next.

The main variable controlled by the ANS is the systemic arterial blood pressure. The mean arterial pressure must be both constant and high enough for glomerular filtration to occur in the kidneys or to overcome high tissue pressures in organs such as the eye. Corneille Heymans was the first to demonstrate that pressure receptors (called baroreceptors) are located in arteries and they are part of a neural feedback mechanism that regulates mean arterial pressure. Heymans hypothesized that increased blood pressure stimulates arterial sensors, which send a neural signal to the brain, and that the brain in turn transmits a neural signal to the heart, resulting in bradycardia (decreased heart rate). The negative-feedback loop, when increased mean arterial pressure, causes vasodilation

A. Henika, "The circulatory system", http://www.humananatomychart.us (accessed 08 March 2020)

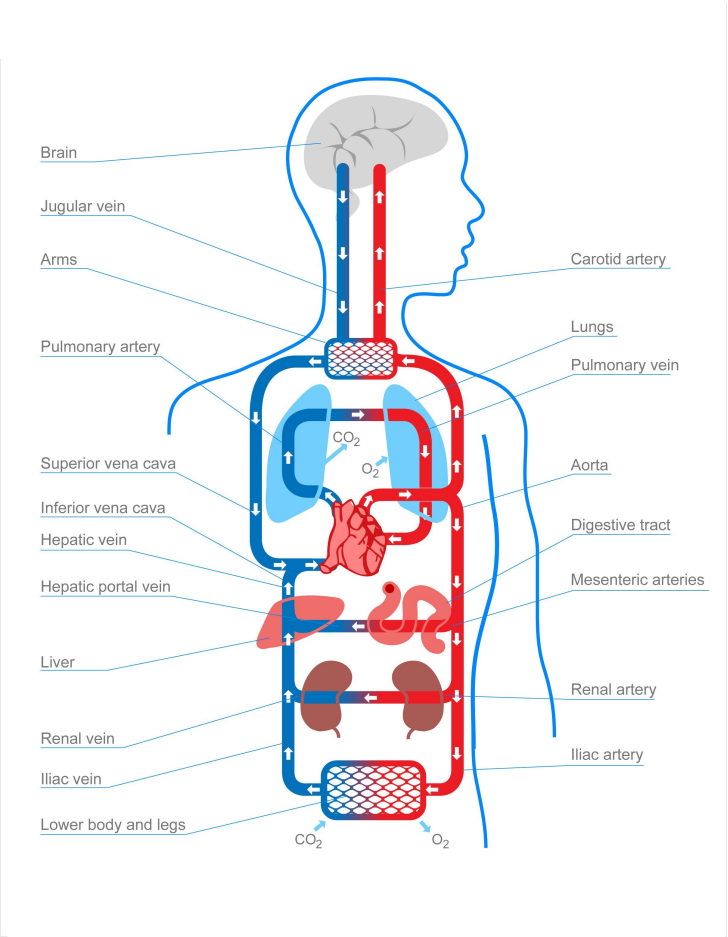


Figure 2.4: The blood circulation, oxygen distribution way, and the path of the blood charged with carbon dioxide.

and bradycardia, whereas decreased mean arterial pressure causes vasoconstriction and tachycardia (increased heart rate). Sympathetic and parasympathetic divisions of the autonomic nervous system are both included in the efferent pathways of the baroreceptor response:

- **Sympathetic Efferents**. Increased sympathetic activity produces vasoconstriction. Indeed, the baroreceptor reflex produces vasodilation.

- **Parasympathetic Efferents**. Increased baroreceptor activity instructs the nervous system to stimulate neurons in the nucleus ambiguus and the dorsal motor nucleus of the vagus (cardioinhibitory area).

## 2.3 Cardiovascular System Overview

Consisting of the heart and vessels (arteries and veins), the cardiovascular system distributes oxygen and nutrients essential to life to the organs through blood, while eliminating waste.

The blood circulates within a network of pipes, with calibres perfectly adapted to their functions:

- The arteries, from the large aorta (2.5 centimetres in diameter) to the small arterioles (no more than 2 millimetres), carry oxygen-laden blood from the heart to the organs.
- The capillars, thin as hair, ensure the circulation of blood inside each organ.
- The veins bring back blood loaded with carbon dioxide to the heart.

### 2.3.1 Blood Circulation

The oxygen-laden blood is propelled into the aorta, which is the main artery of our body. It then passes through the many secondary arteries that lead to the different parts of the body. Then, blood is carried to the various organs from the arteries, which are narrower and narrower (arterioles). In each organ, the blood, circulating in the capillaries, distributes to the cells their ration of oxygen and nutrients, in exchange for carbon dioxide and waste. The blood, charged with carbon dioxide, is brought back to the heart by the venous circuit.

Venous blood is ejected from the heart to the lungs through the pulmonary artery. It joins the pulmonary alveoli, a kind of small bags located on the bronchi, where the air breathed ends. The blue blood then regenerates by drawing oxygen through the permeable membrane of the alveoli, which is supported by the red blood cells, while evacuating carbon dioxide. The pulmonary veins are responsible for bringing the regenerated blood - rich in oxygen and low in carbon dioxide - back to the left heart, and ready for a new journey through the arterial network.

### 2.3.2 Brain Circulation

Like all organs, the brain receives the oxygen and energy it needs to function through the blood vessels. Four arteries provide blood to the brain:

- Two internal carotids (right and left) are born at the front of the neck of the common carotid arteries. They penetrate the skull through the bone of the rock.
- Two vertebral arteries, at the back of the neck, penetrate through the occipital hole and join into a single artery, the basilar trunk.

These four arteries are at the origin of the cerebral arteries.

### 2.3.3 The Heart

The heart is composed of two compartments (right / left heart), as it can be seen in Figure 2.5.

Inside each of these cavities there are two cavities, namely, atrium and ventricle. The blood circulation is divided into two parts that correspond to the right and left cavities of the heart. Oxygen-poor blood reaches the right heart through the vein cave, enters through the right atrium and moves to the right ventricle owing to the pressure differences, and to

R. Bailey, "Anatomy of the Heart: Valves", http://www.thoughtco.com/anatomy-of-the-heart-valves-373203 (accessed 12 March 2020)

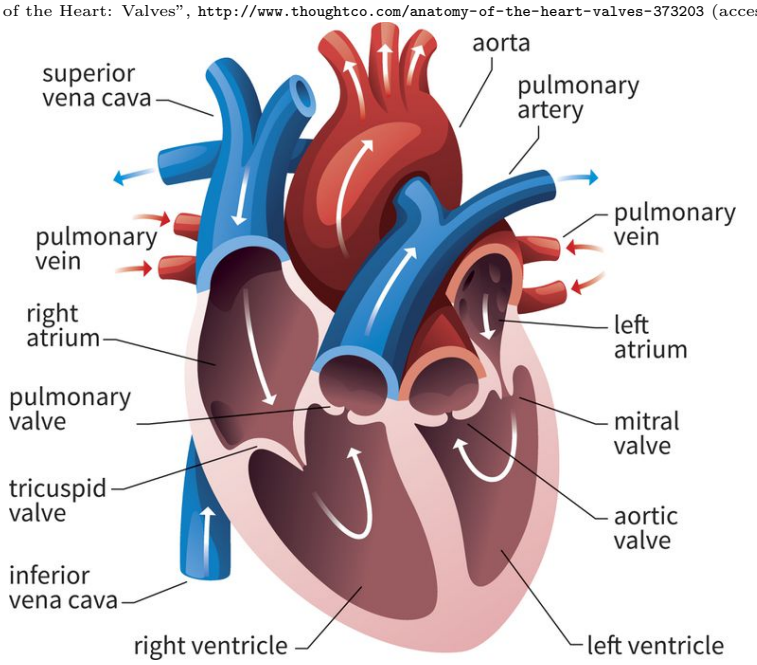


Figure 2.5: The Heart.

a lesser extent, to the atrial systole. The ventricular systole (ventricular contraction) in turn ejects the blood from the right ventricle to the lungs where it is oxygen-enriched. This blood returns through the pulmonary veins and accumulates in the left atrium and passes to the left ventricle owing to pressure differences to the atrial systole. The ventricular systole also ejects blood to the peripheral organs through the aorta artery. Figure 2.6 shows the phases of the cardiac cycle.

### 2.3.4 ECG, Tachogram, and Long-Term Monitoring

The electrical function of the heart is based on the propagation of an electrical impulse along the tissue of the myocardium (His bundle). This impulse is initially generated in the sinus node and spreads due to the depolarization of the atrial muscle cells. The impulse arrives at the atrio-ventricular node and spreads through the purkinje Fibres that propagates it to several points of the ventricles, and then to the ventricular muscle cells. The cycle can be seen as divided into two phases:

- The depolarization of cells, which causes systole in the phase of contraction (ejection of blood), originating the following cardic waves:
  - P wave, corresponding to atrial depolarization which causes the atrial systole (contraction);
  - PQ segment, corresponding to the atrio-ventricular conduction time delay of the blood.
  - QRS complex, corresponding to the ventricular depolarization causing the ventricular systole (contraction of ventricles).

"Phases of the Cardiac Cycle", http://www.englishstudytoday.com/downloads/phases-of-the-cardiac-cycle/(accessed 20 March 2020)

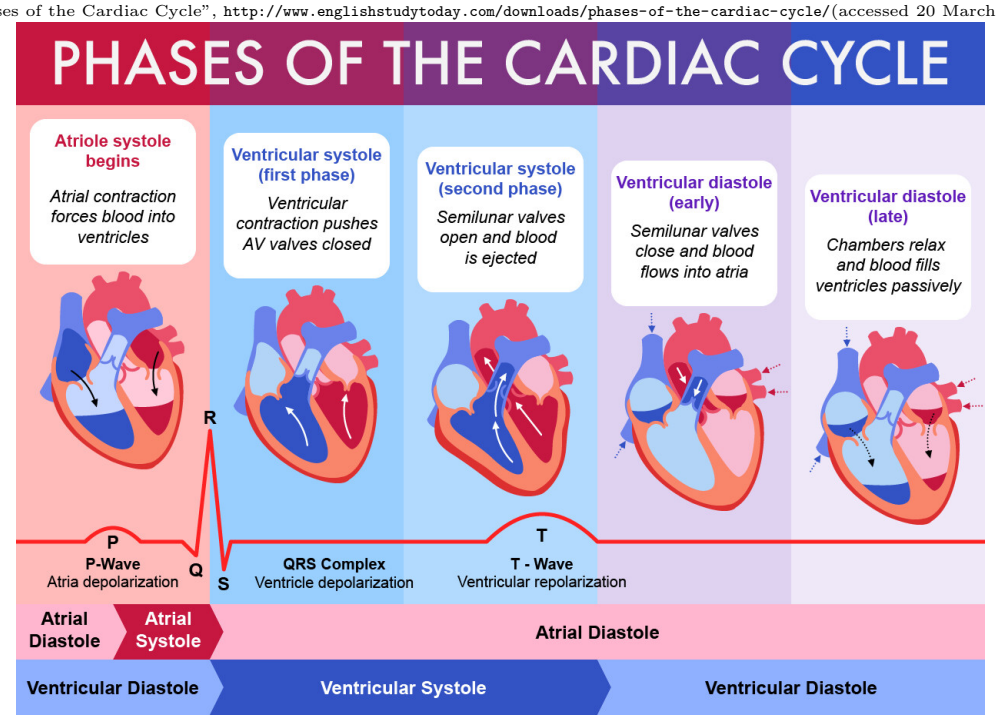


Figure 2.6: Cardiac cycle.

- The repolarization of cells, leading to the diastole or the relaxation phase (filling of atrial and ventricles):
  - ST segment, corresponding to the repolarization time of the ventricles;
  - T wave, corresponding to the repolarization of the ventricles and the ventricular diastole (relaxation)

### 2.3.5 Physio-pathology and Cardiac Disorders

CHF and AF are two disorders that increase in prevalence as the population ages. This combination is a problem with which the cardiologist is increasingly confronted. CHF promotes AF which in turn worsens CHF [38]. The therapeutic management of these patients is complex. It can be considered in several ways: Frequency control, i.e. compliance with AF and prescription of decelerating drugs, or rhythm control, i.e. cardioversion when the patient is in persistent AF, and sinus rhythm maintenance by anti-arrhythmic drugs. However, class I antiarrhythmics are contraindicated in these patients, with the best results being provided by amiodarone, which can have deleterious extracardial effects. Non-pharmacological therapeutic methods can also have their place, whether it is ablation or resynchronization. There is currently growing interest in drugs in the renin-angiotensin system for CHF and AF. Beyond their therapeutic effect on CHF, they can also have a preventive effect on AF when used in hypertensive patients [39].

https://www.researchgate.net/publication/262384778_Hiding_Patients_Confidential_Datainthe_ECG_Signal_viaa_Transform-Domain_Quantization_Scheme/figures?lo=1 (accessed 25 March 2020)

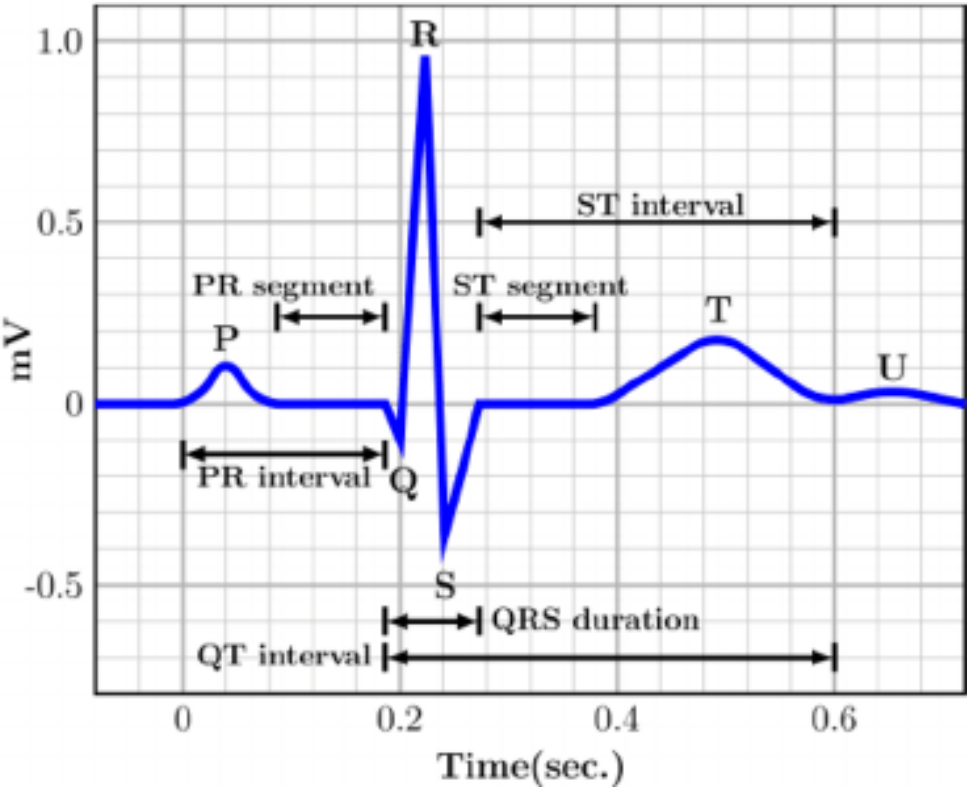


Figure 2.7: ECG waveform.

### 2.3.6 ANS Heartbeat regulation and SCD Risk Stratification

#### ANS and Heart Rate Regulation

The heart contraction is controlled by special neurological mechanisms which induce the propagation of the action potentials through the myocardium resulting on a rhythmic beats. The sympathetic and parasympathetic vagus nerves controls the blood pumping. The heart rate can be affected by sympathetic stimulation going from 70 to 200 beats per minute. The increased force of heart contraction, in turn, increases the volume of blood pumped as well as the ejection pressure. The inhibition of the sympathetic nerve that reaches the heart can decrease the heart rate and the volume of blood pumped. The heartbeat can be stopped for a few seconds with a strong stimulation of parasympathetic nerve fibers in the vagus nerve to the heart. Although, the heart changes response and beats at a frequency of 20 to 40 beats per minute during the parasympathetic stimulation.

#### Risk stratification in SCD

A heart attack occurs when the blood supply to a part of the heart is interrupted by the obstruction of a coronary artery. Without oxygen, the cells in this part of the heart muscle gradually die until the supply is restored. The extent of damage varies according to the duration of the interruption: cardiac damage can be benign, severe or irreversible. In some cases, a heart attack can be fatal. Even if the two are often confused, cardiac arrest is different from a heart attack. A heart attack is a circulatory problem (blocking a vessel

that supplies blood to the heart) that can cause irreversible heart damage. Cardiac arrest is caused by an electro-physiological problem (electrical dysfunction of the heartbeat). Among the populations subject to the problem, there is a subgroup of patients with shortened life expectancy. The main areas of analysis are: The study of ventricular arrhythmias (ventricular extrasystoles and unsupported ventricular tachycardias) and their frequency of occurrence; The study of the autonomic nervous system (HRV and HRT); And the study of ventricular activity (duration of the QRS complex, length of the QT segment and amplitude variability of the T-wave). These studies, which most often focus on the predictive power of sudden death of a single descriptor (univariate studies) or sometimes a linear combination of descriptors (multivariate studies), are generally consistent. The main risk criteria identified are: a reduced HRV, a prolonged QRS complex, a QT segment $> 440$ ms and the presence of T-Wave Alternans.
However, not all these studies conducted to better characterize the at-risk population have necessarily made it possible to optimize the selection criteria for patients likely to benefit from the prophylactic implantation of an cardioverter defibrillators (ICD), particularly because the results obtained are not robust. A multivariate non-linear analysis of the Holter recording descriptors has not yet been conducted, but it could improve, through the combined contribution of each of the relevant descriptors, the specification of the patient at risk of SCD and, ultimately, the recommendations for implementing an ICD in primary prevention. Moreover, given the complex nature of the interactions present in physiological systems, the interpretation and explanation of these indices are questionable, while the study of the long-term evolution of these indices may well provide a new approach.

### 2.3.7 HRV Measurements and Analysis Methods

HRV [40, 41] can be measured using temporal, statistical, geometric, spectral, and non-linear methods that can help us to describe the quantitative and qualitative aspects of the oscillations of the NN interval around its mean value. The NN-intervals are defined as the distance between R-waves of consecutive beats, excluding the ectopic beats.

#### Temporal, Statistical, and Geometrical Measurements

Statistical analysis of a dataset, which in our case is the temporal sequence of NN intervals. The calculation methods used in this analysis family remain very simple and all these operations can be done in a spreadsheet. Table 2.1 summarizes some of the statistical methods for HRV.

Geometric methods are derived and constructed from the conversion of NN interval sequences. There are different geometric forms for the evaluation of HRV: the histogram, the triangular index HRV and its modification, the triangular interpolation histogram of interval NN, and the method based on the Lorentz or Poincaré plots. The histogram evaluates the relationship between the total number of detected NN intervals and the variation of NN intervals. The triangular HRV index estimates the main peak of the histogram as a triangle with its reference width corresponding to the amount of variability of NN intervals, its height corresponding to the most frequently observed duration of NN intervals, and its area corresponding to the total number of all NN intervals used to construct it. The triangular HRV index is an estimate of the total HRV.

| Index | Units | Description |
|---|---|---|
| AVNN | ms | Mean of NN intervals |
| SDNN | ms | Standard deviation of NN intervals |
| SDANN | ms | Standard deviation of the averages of NN intervals in all 5 min segments of the entire recording |
| SDNNindex | ms | Mean of the standard deviations of NN intervals for all 5 min segments |
| RMSSD | ms | The Square root of the mean of the sum of the squares of differences between adjacent NN intervals |
| NN50 | | Number of pairs of adjacent NN intervals differing by more than 50 ms in the entire recording |
| pNN50 | | NN50 divided by the total number of NN intervals |

Table 2.1: Statistical indices of HRV.

Geometric methods are less affected by the quality of the recorded data and can provide an alternative to statistical parameters that are easier to obtain. However, the duration of the recording should be at least 20 minutes, which means that in the short term the recordings cannot be evaluated by geometric methods. Table 2.2 sums up the most important geometric indices.

### Spectral Measurements

Spectral methods analysis of HRV [42, 43] are based on the fact that the influences of the two branches of ANS on the heart, as well as on certain other systems, have well-defined and different oscillatory behaviours. In this way, the following division into spectral bands can be established according to the system that has the greatest contribution in that band. Four spectral bands are mainly distinguished in the power spectral density of the NN series, namely, high frequency (HF) band with $f \in (0.15, 0.4)$ Hz, low frequency (LF) band with $f \in (0.04, 0.15)$ Hz, very low frequency (VLF) band with $f \in (0.003, 0.04)$ Hz, and ultra low frequency (ULF) band with $f < 0.003$ Hz.

As shown in table 2.3, a list of Frequency-domain indices have been proposed.

### TI Measurements

Time irreversibility is a characteristic feature [44, 45] of non-equilibrium, complex systems involving cardiovascular control mediated by autonomic nervous system. Its analysis in HRV signal represents a new approach to assess cardiovascular regulatory mechanisms. Henceforth, an estimation of complexity and temporal asymmetry of short-term heart HRV can be given as an index of complex neurocardiac control in response to stress using symbolic dynamics and temporal irreversibility methods which will be further developed in the following chapter.

| Index | Units | Description |
|---|---|---|
| Triangular index | ms | Total number of all NN intervals divided by the maximum of the density function (height of the histogram of all NN intervals) |
| INN | ms | Base width of the minimum square difference triangular interpolation of the highest peak of the histogram of all NN intervals |
| Lorentz plot dispersion | ms | Representation of each NN interval duration versus the duration of the previous interval |
| Differential index | ms | Difference between the widths of the histogram of differences between adjacent NN intervals measured at selected heights |
| Logarithmic index | adim | Coefficient $\phi$ of the negative exponential curve $Kexp - \phi t$ which is the best approximation of the histogram of absolute differences between adjacent intervals |

Table 2.2: Geometric indices of HRV.

| Index | Units | Description |
|---|---|---|
| Total power | $ms^2$ | Total variance of NN intervals over the temporal segment |
| VLF | $ms^2$ | Power in very low frequency range |
| VF | $ms^2$ | SPower in low frequency range |
| LF norm | % | LF power in normalised units LF/(Total power-VLF)*100 |
| CHF | $ms^2$ | Power in High frequency range |
| CHF norm | % | CHF power in normalised units CHF/(Total power-VLF)*100 |
| LF/HR | adim | Ratio LF$[ms^2]$/HR$[ms^2]$ |

Table 2.3: Frequency domain methods of HRV.

### Entropy

The entropy is a central concept of Information Theory [46, 47]. The entropy of a message is a measure of the amount of information contained in it. For example, the message "mmm mmmmmm" does not contain much information. In fact it can be shortened by saying "9*m". Most of the original message is redundant. However, the message "mey jlr yrs" contains a lot of information. There is no redundancy or regularity. Therefore in order to transmit this message at least 9 characters are necessary. The message "mey mey mey" lies in between. It does contain some redundancy, but in order to transmit one would need 5 characters:"3*mey".
A more formal definition of the entropy has been provided by Shannon [48]. For a discrete random variable $X$ having n symbols, each symbol $x_i$ having a probability $p_i$ of appearing. A message source that has n possible messages with probabilities $p_1, ....., p_n$. Then the

entropy of a message is:

$$E_i = -log_2 p(x_i) \ [bit] \tag{2.1}$$

where $E$ denotes mathematical expectation, and $log_2$ the logarithm in base b. A base 2 logarithm is usually used because the entropy then has the units of bit/symbol. The symbols represent the possible realizations of the random variable $X$. In this case, $H(X)$ can be interpreted as the number of yes/no questions to be asked on average by the receiver at the source, or the amount of bit information that the source must provide to the receiver in order for the receiver to unambiguously determine the value of $X$.

### Chaos Measurements

Chaos has been defined as the study of multi variable, non-linear and non-periodic systems, and describes natural systems in a different way because it can reflect the randomness of nature [49, 50]. Perhaps Chaos Theory can help to better understand human resource dynamics, taking into account that healthy heartbeats are slightly irregular and chaotic to some extent, on the assumption that the complex fluctuations of the heart rhythm are partly characterized by a deterministic chaos, and that the pathologies cause a decrease in this non-linear variability. Therefore, HRV dynamics can be analysed by chaotic system methods such as Lyapunov's Exponent, and Correlation Dimension. The Lyapunov spectrum is a central quantity of dynamical systems theory and chaos theory. It is a measure of the sensitivity to the initial conditions of a trajectory, and thus of its stability or chaoticity. Lyapunov exponents also appear as the temporal average of a fluctuating quantity and therefore generally have a typical value for a given system. But it is sometimes interesting to decompose the dynamics into its different ingredients, to elucidate the complex behavior that results from this mixture. From an initial condition called attractor, the correlation dimension is a fractal dimension estimation of the attractor that appears in the reconstructed phase space, since the attractor, if it comes from a chaotic dynamic system, has a fractal structure. The fractal dimension is related to the minimum number of system variables needed to model the attractor, and thus related to the complexity of the system itself. The correlation dimension can be estimated computationally using the Grassberger-Procaccia algorithm.

### Fractal Measurements

Non-linear fractal methods can provide new insights into human resource dynamics in the context of physiological changes and in high-risk situations, particularly in patients after myocardial infarction or in the context of sudden death. Recent data suggest that fractal analysis against standard HRV measurements appears to detect abnormal trends in NN fluctuations more effectively [51, 52]. Since heart rate dynamics are characterized by the singularities, the knowledge of a singularity in time series or in fractal signals is very interesting. Let us consider a continuous function $f(t)$, which mathematically can be developed by a Taylor Series in the vicinity of $t_i$ or power series, as follows:

$$f(t) = a_0 + a_1(t - t_i) + a_2(t - t_i)^2 + a_3(t - t_i)^3 + .... \tag{2.2}$$

When experimental or empirical time series are characterized by their fractal features and for some times $t_i$, function $f(t)$ exhibits singular behavior. In [53], step-like and cup-like singularities features appear as non-integer powers of time in the signal components.

This can be expressed as

$$f(t) = a_0 + a_1(t - t_i) + a_2(t - t_i)^2 + a_3(t - t_i)^3 + ... + a_{h_i}(t - t_i)^{h_i} \tag{2.3}$$

where $h_i$ is a non-integer number quantifying the local singularity of $f(t)$ at $t = t_i$ and $t$ is inside a small vicinity of $t_i$ [54].

Multifractal analysis measures globally the local dynamics of the time series data, based on the Hausdorff dimension, denoted by $f(\alpha)$ (measurement of fractal dimension), where $\alpha$ is the singularity strength of the decomposed interwoven signal sets. The Hausdorff dimension allows us to find the non-integer dimension of fractals. Therefore, to measure the singularity in function $f(t)$, authors in [53] explain a procedure for Hausdorff dimension measurement and for $s = 1, 2, 3$ measures. In case of non-integer $s$, let us consider a set $F$ of fractal signals, thus it exists a unique $d$ such as

$$H^s(F) = \begin{cases} \infty & if \quad s < d, \\ 0 & if \quad s > d, \end{cases} \tag{2.4}$$

Accordingly, $d$ is defined as a measurement of the fractal dimension of the set $H$ defined as $H^d(f)$. According to [53], $F$ is fractal if $d$ is greater than another quantity called the topological dimension, and the singularity spectrum can be written as:

$$f(\alpha) = dim_H\{x \mid \mu(B_x(\epsilon)) \sim \varepsilon^{\alpha},\ for\ \epsilon \to 0\} \tag{2.5}$$

where $B_x(\epsilon)$ is the $\epsilon$ box at point $x$ from tachogram signal, $\mu$ is the measure and $\alpha$ represents the singularity value or singularity strength. The $f(\alpha)$ spectrum is the hump-shaped curve over a finite interval $[\alpha_{min}, \alpha_{max}]$ where $\alpha_{min}$ and $\alpha_{max}$ represent the strongest and weakest singularities, respectively. The different non-integer exponents $h_i$ characterize the statistical properties of different subsets, which are modeled by function $D(h)$, where $D(h_0)$ represents the fractal dimension of the time series subsets and it allows us to alternately measure singularities.

### Choice of MSE, MTI and MFS

The focus of the work is on analyzing the usability of multiscale indices in several-day cardiac monitoring, from different aspects including the algorithmic suitability of currently proposed methods. Multiscale methods can be useful for characterizing long and short-term health states. In particular for MSE, which was first delivered to analyze of nonlinear and non-stationary signals in finite length time series, was of interest to characterize the complex temporal fluctuations that are inherent in permanent AF, and maybe provide additional prognostic information in clinical setting. This path in the work is followed, and focused on obtaining the capability of these indices to characterize different dynamics.

## 2.4 Cluster Headache Overview

The eye, or eyeball, is a hollow structure with a generally spherical shape [55]. It consists of tunics, a lens and liquids. The outer coat is the sclera, a dense, poorly vascular connective tissue. It has a protective role for the eye. It is the white of the eye, it is surrounded by a

http://www.winretina.us/normal-eye-anatomy/(accessed 20 April 2020)

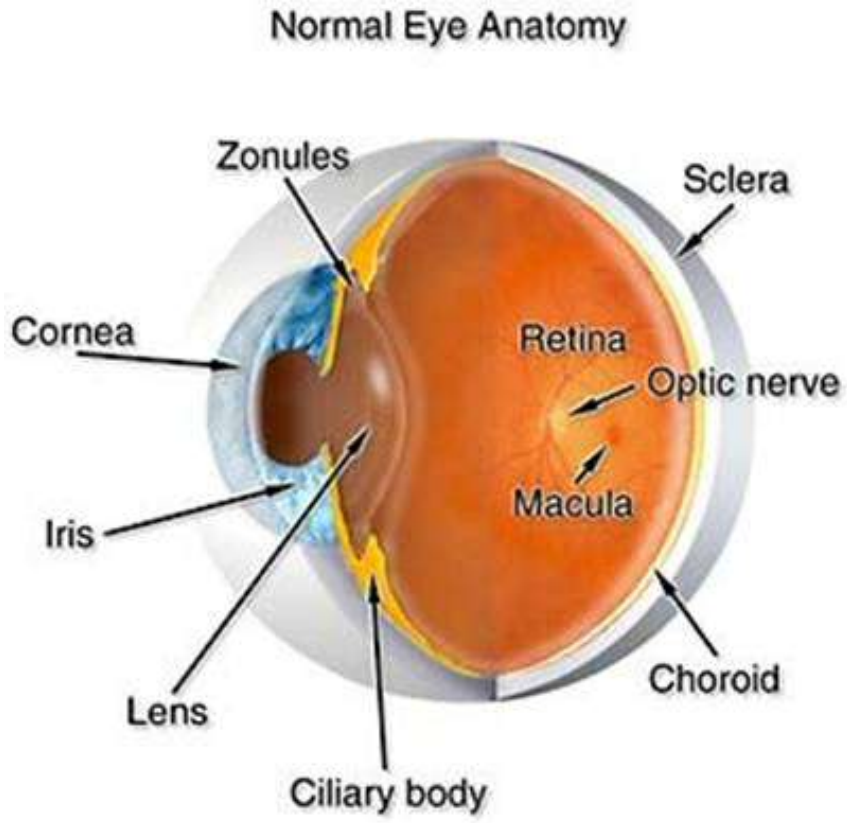


Figure 2.8: Normal eye anatomy.

very thin and transparent membrane, called the conjunctiva. On the anterior side, this sclera is replaced by the cornea, transparent which allows the entry of light rays into the eyeball. It is also rich in nociceptive fibers: contact with an object induces blinking and lacrimal secretion, two protective functions.

The transmission of information obtained from the retina to the brain is effected by the optic nerve. All the optical fibers from the visual cells converge on a specific point in the retina: the pupil. At this point also leads the venous and arterial network of the retina. The optical fibers all join there to form a cable: the optic nerve, there is one optic nerve per eye. The two nerves intersect in an area called the optic chiasm. At this point only part of the fibers intersect as shown in Figure 2.9.

The nervous message is sent to the brain, it is transmitted from one nerve cell to another. The functioning of a synapse which serves as a contact zone between the two neurons is complex. The tip of the pre-synaptic extension is a lump, the synaptic button, rich in neurotransmitters contained in small vesicles. There is a space separating the pre-synaptic zone from the post-synaptic zone: the synaptic cleft. The post-synaptic membrane, supposed to receive the influx, carries receptors specific to a neurotransmitter and when a nerve impulse reaches the synaptic button, it causes the expulsion of the neuromediator in the slit by bursting of the vesicles. This then reaches the receptor sites of the postsynaptic membrane and triggers a nerve impulse there. The pathways of conscious visual sensitivity, partially crossed in the chiasma, terminate in the occipital region. Any damage to the visual area results in partial blindness corresponding to a defined region of

https://www.i.medicine-consultant.com/img/neuroscience/237/congenitally-absent-optic-chiasm.png(accessed 2 April 2019)

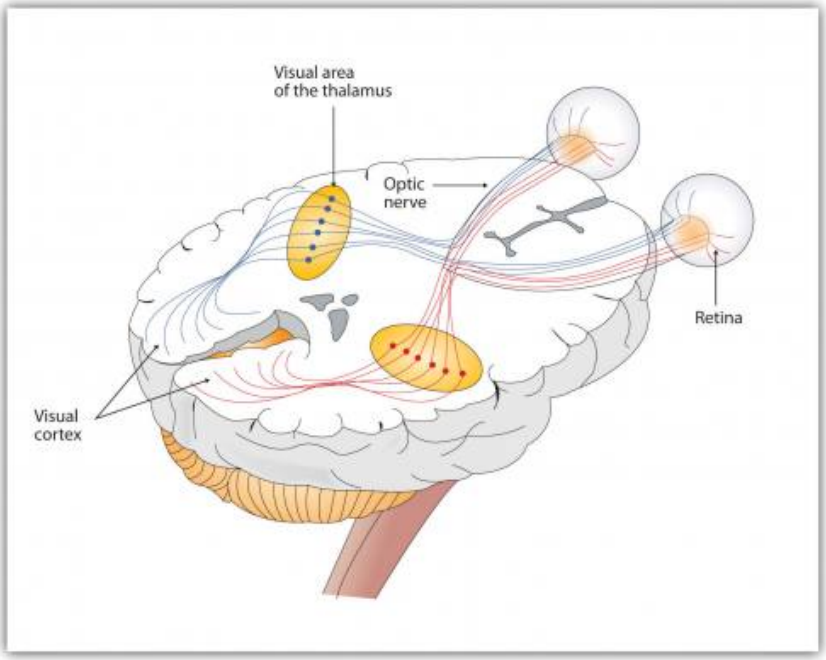


Figure 2.9: From the optic nerve to the visual cortex.

the visual field. The retina projects point by point on the visual area, but the cortical territory corresponding to the fovea is relatively very large. The neurons of the primary visual cortex, on the other hand, have rather elongated receptive fields. They respond well to lines of light with a specific orientation. These receptive fields responding to a given orientation are those of single cells. These rectangular receiving fields often have a central band responding positively to light (ON) flanked by two bands responding to dark (OFF). If the light streak is not on the ON band, the stimulus is simply not transmitted.

The visual area of the brain is divided into several regions of which we do not know everything:

- Areas V1 and V2: these areas play a very important role in the perception of contours. They remain essential in any fine visual perception.
- Area V3: scientists have not clearly identified this area.
- Area V4: this area plays a role in the perception of colors, as demonstrated by Semir Zeki of University College London. But specialists think that other regions are associated with it.
- Area V5: it plays a role in the perception of movements as shown by experiments with magnetic resonance imaging.

Simple eye defects like farsightedness can cause headache [56, 57]. But they are sometimes indicative of much more serious ophthalmological pathologies, therefore, before turning to a neurologist, consulting an ophthalmologist may be wise.

According to the International Headache Society (IHS), headaches in Group IV deserve special attention because they are not associated with visible organic lesions, and they

"4 Common Types of Headaches–Symptoms & Duration",
http://www.drshehadi.com/2020/06/20/4-common-types-of-headaches-symptoms-duration/(accessed 13 March 2020)

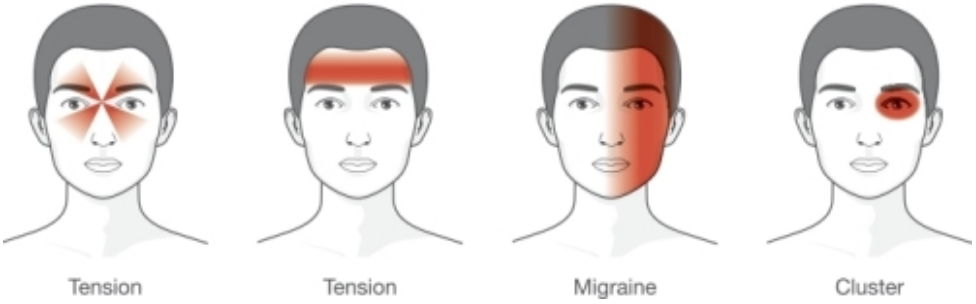


Figure 2.10: Different types of headaches and the location of their symptoms.

are characterized by their short duration, thereby falling into the Primary Headache Short-Term group of the IHS [26]. These are known as Cluster Headaches (CH), they are gender independent, and they can appear from childhood to old ages, with increased prevalence in 30-to-40 year-old patients. The clinical signs in CH mainly include unilateral pain located in the temporal, maxillary, and frontal regions, though they can extend and include the neck and the ear structures. Under some circumstances, these headaches can manifest as multiple pain attacks of short duration, with recurrence during prolonged periods. This allows the clinicians to identify them among other headaches that result from other diseases, such as those ones related to strokes, pancoast and frontal lobe tumors, intracranial hypertension, or severe symptomatic thrombocytopenia [58]. Overall, CH is a relevant pathology, characterized by a complicated diagnosis due to its difficult classification as group IV in the IHS.
One of the CH signs is the different iris color in the patient's eyes, which is not always noticeable by simple visual inspection. Accordingly, the screening and early detection of CH could be addressed by creating a biomarker from subtle color changes in the iris. Newborn has an indeterminate iris color. The coloration of the iris is done in the first months of life. The final color is inherited and determines the progressive pigmentation that is culminated in the first months of life by the activity of pigment cells (melanophores). The sympathetic nervous system exerts a trophic action on the activity of melanophores.

### 2.4.1 Cluster Headache Symptoms

When there is a congenital or acquired sympathetic defect in the neonatal period, there is a deficit of pigmentation in the iris on the side of the sympathetic hypofunction [28]. The result is heterochromia: an eye of each colour, typically a blue eye and a brown eye, with the clear eye being the defective pigmented eye. Heterochromia with a clear difference in colour is easily recognised by the naked eye. If the difference is subtle, a sensitive method would be needed to recognize it.

Some headaches (typically CH) occur with strictly unilateral pain centered in the ocular region [28]. During symptomatic periods, a sympathetic deficit develops on the pain side, causing ptosis (drooping of the upper eyelid) and myosis (small pupil). Both signs of sympathetic hypofunction are known as Horner syndrome. If there is a latent sympathetic defect on the pain side that manifests itself during symptomatic periods there may also be less pigmentation of the iris on that side. If this were so, the sympathetic

https://www.pinterest.com/pin/164803667586203110/ (accessed 03 February 2020)

Figure 2.11: Cluster headache deficit symptoms, Heterochromia and Horner syndrome.

defect would have occurred in the neonatal period or would be congenital.

### 2.4.2 Data Analysis for Irido

Colour, texture, contour are elements that allow a low level analysis in human perception, are also a determining characteristic that leads to the recognition of observed objects and the their interpretation with a large field of applications of segmentation and image classification.

#### Color spaces

A range of colors can be created by the primary colors of pigment and these colors then define a specific color space [59]. Color space, also known as the color model, is an abstract mathematical model which simply describes the range of colors as tuples of numbers, typically as 3 or 4 values or color components (e.g. RGB). Basically speaking, color space is an elaboration of the coordinate system and sub-space. Each color in the system is represented by a single dot.

Color space is a three-dimensional mathematical model representing the set of perceptible, usable or reproducible colors by a human being or a device. Each color it contains is thus associated with coordinates determining a precise point and corresponding, for example, to values such as luminance, saturation and hue. There are three types of color spaces: dependent color spaces, describing only the characteristics of the corresponding device, independent color spaces, describing a set of visible colors without referring to a particular device in the graphic chain; and finally workspaces, which are used by retouching software and file formats to determine the color palette with which it is possible to work. Note that a three-dimensional representation makes it possible to visualize a color space, but makes any comparison between two different spaces difficult. Two-dimensional representations are thus more common, because it is thus possible to superimpose several color spaces, therefore to assess the color palette that they represent in relation to each other. It should be noted, however, that such two-dimensional graphics deprive us of viewing the luminance information contained in the three-dimensional graphics.

https://www.researchgate.net/figure/Color-spaces-a-IHLS-color-space-and-b-L-a-b-color-space_fig1_220135675 (accessed 03 april 2020)

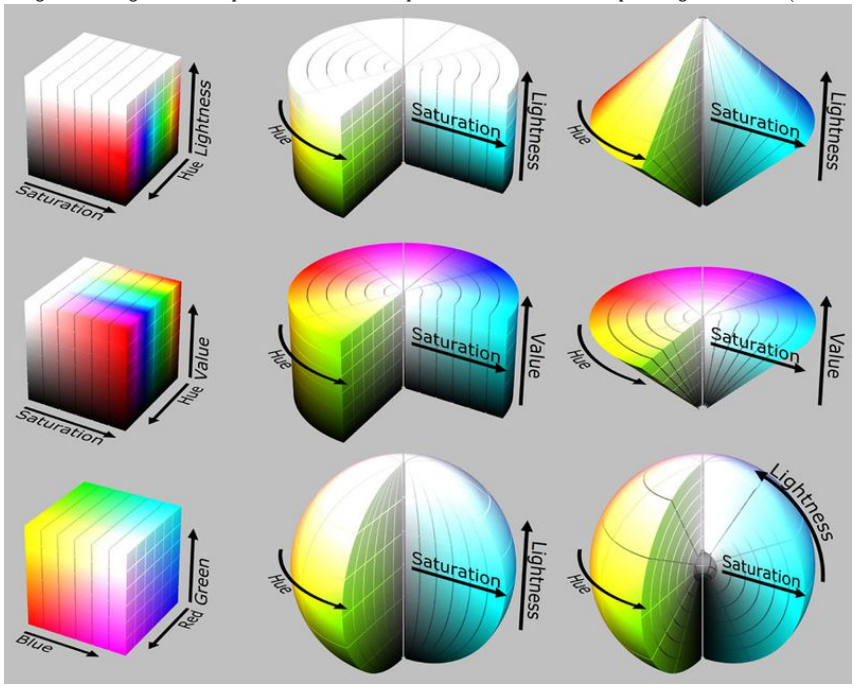


Figure 2.12: Representation of color spaces models.

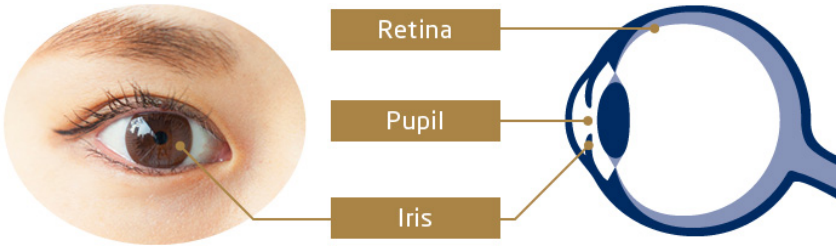


Figure 2.13: The iris location in the eye.

### Textural analysis

Texture analysis remains an open problem in the field of computer vision. There is no exact mathematical definition of texture that results from a coherent perception of an entity observed in an image. For example, in [60], texture is defined as follows:
A texture is a field of the image that appears as a coherent and homogeneous domain, i.e. forming a whole for an observer.
Although the perception of a given texture is obvious to the observer, it remains very difficult to represent it mathematically: on the one hand, it is not trivial to represent the spatial links that exist within the same object, and on the other hand, to define descriptors that ensure invariance by changing scale, orientation, lighting, color, etc. (as is the case for human interpretation) is a delicate task. As a result, a large number of definitions and associated approaches have been developed for specific applications [61].

#### Biometry and iris recognition

The iris is the colored, donut-shaped portion of the eye behind the cornea and surrounds the pupil (Figure 2.13). A person's iris pattern is unique and remains unchanged throughout life. Also, covered by the cornea, the iris is well protected from damage, making it a suitable body part for biometric authentication.

Indeed, biometric identification makes it possible to recognize or verify the identity of people, with a high degree of reliability. For this reason, it was first used in "high security" environments, such as high risk installations, nuclear power plants etc. where iris, fingerprint or face recognition are used. With the advent of user-friendly and affordable systems, biometric identification is increasingly used in our everyday environments such as site access control. Iris recognition [62] is characterized by a very high level of precision. This technique is considered impossible to defraud. The error rate of products available on the market is very low and its stability is extended until the death of individuals. Iris recognition is the only system that can be used on a large number of people with full identification. The biometrics system searches for a positive match among all the models saved in the database. If a matching model is found, the registration number is used as the person's identifier.

### 2.4.3 Analysis methods

Nowadays, machines are capable of reproducing human behavior, but without conscience. Later, their capacities could grow to the point of turning into machines endowed with consciousness, sensitivity and spirit.

#### Machine learning and SVM

Machine Learning (ML) and Deep Learning (DL) are Artificial Intelligence (AI). For example, knowledge graphs or rule engines are AI but do not fall under ML or DL. Deep Learning is a branch of Machine Learning. AI has evolved a lot thanks in particular to the emergence of Cloud Computing and Big Data, which is inexpensive computing power and accessibility to a large amount of data. Thus, the machines are no longer programmed; they learn.

Machine Learning, or automatic learning, is capable of reproducing a behavior thanks to algorithms, themselves fed by a large amount of data. Faced with many situations, the algorithm learns which decision to adopt and creates a model. The machine can automate tasks depending on the situation. For example, for a machine to learn the concept of cat, an engineer compiles a large number of examples on the animal which it transmits to an algorithm. Previously, the engineer had to establish the identity card of a cat (it has a coat, whiskers, it falls on its legs, etc.) and represent these rules in a computer program. Today, he only has to collect the data, which makes the task easier and faster. This new way of automating leads to considerable progress. Support vector machine SVM [63, 64] is a simple algorithm that every machine learning expert should have in his/her arsenal. SVM is highly preferred by many as it produces significant accuracy with less computation power. SVM can be used for both regression and classification tasks. But, it is widely used in classification objectives.

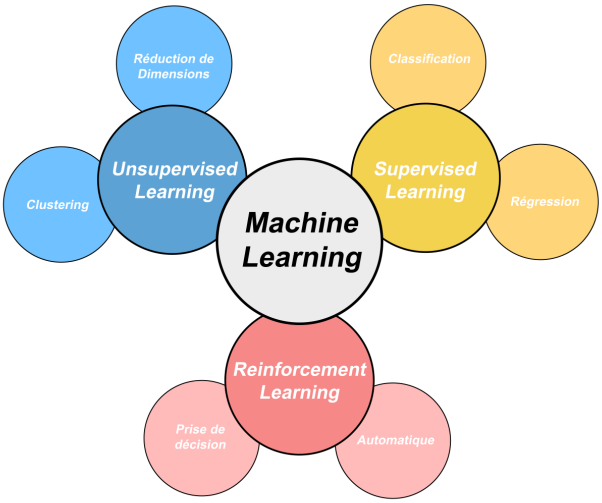


Figure 2.14: Machine learning concept.

**Algorithm 1** K-means clustering

**input:** K, set of pixels $p_1, \cdots, p_n$
**place** centroids $c_1, \cdots, c_K$ at random locations
**repeat** until convergence:
**for** each pixel $p_i$ **do**
  **find** nearest centroid $c_j$ $argmin_j D(p_i, c_j)$
  **assign** the pixel $p_i$ to cluster $j$
**end for**
**for** each cluster $j = 1, \cdots, K$ **do**
  **compute** the new centroid $c_j = mean\ of\ all\ pixels\ p_i$
  **assign** the new pixels to cluster $j$
**end for**
**stop** when none of the cluster assignments change

### K Nearest Neighbours

The basic idea of this algorithm is centred on classifying a new element in the most frequent class where its nearest K neighbours belong, on other words it consists on modifying and adjusting the KNN parameter of the classifier taking into account the new number of samples. The algorithm is therefore based on a very simple and intuitive idea, which coupled with its easy implementation makes it a very widespread classification algorithm.

This algorithm is described as follows:

### Choice of SVM and KNN

The work scrutinizes the scope of an automatic diagnosis-support system for early detection of CH, by using as indicator the error rate provided by an statistical classifier designed to identify the eye (left vs right) from iris pixels in color images. Systematic tests were performed on a database of iris images adopting several aspects to design the classifier,

including: (a) the most convenient color space; (b) whether the used of several color spaces could improve the decision; (c) the robustness of the classification method to iris spatial sub-regions; (d) the contribution of the pixels neighborhood. Although the cost of classifying new instances with is very high due to the fact that practically all the computation takes place at the time of classification instead of when the training examples are first found. KNN is an algorithm that fits properly to the models that can be seen in the improvements obtained in the accuracy rate, when the SVC is faster and robust.

# Chapter 3

# Nonlinear Dynamics and Multiscale Indices in Holter LTM

The identification of patients with increased risk of SCD has been widely studied during last decades, and several quantitative measurements have been proposed from the analysis of the ECG stored in 1-day Holter recordings. Indices based on nonlinear dynamics of HRV have shown to convey predictive information in terms of factors related with the cardiac regulation by the autonomous nervous system, and among them, multiscale methods aim to provide with more complete descriptions than single-scale based measures. However, there is limited knowledge on the suitability of nonlinear measurements to characterize the cardiac dynamics in current LTM scenarios of several days.

In this Tesis, we scrutinized the long-term robustness properties of three nonlinear methods for HRV characterization, namely, the MSE, the MTI, and the MFS. These indices were selected because all of them have been theoretically designed to take into account the multiple time scales inherent in healthy and pathological cardiac dynamics, and they have been analyzed so far when monitoring up to 24 hours of ECG signals, corresponding to about 20 time scales. We analyzed them in 7-day Holter recordings from two data sets, namely, patients with AF and with CHF, by reaching up to 100 time scales.

In addition, a new comparison procedure is proposed to statistically compare the poblational multiscale representations in different patient or processing conditions, in terms of the non-parametric estimation of confidence intervals for the averaged median differences. Results show that variance reduction is actually obtained in the multiscale estimators. The MSE (MTI) exhibited the lowest (largest) bias and variance at large scales, whereas all the methods exhibited a consistent description of the large-scale processes in terms of multiscale index robustness. In all the methods, the used algorithms could turn to give some inconsistency in the multiscale profile, which was checked not to be due to the presence of artifacts, but rather with unclear origin. The reduction in standard error for several-day recordings compared to one-day recordings was more evident in MSE, whereas bias was more patently present in MFS. Our results pave the way of these techniques towards their use, with improved algorithmic implementations and nonparametric statistical tests, in long-term cardiac Holter monitoring scenarios.

## 3.1 Introduction

MSE has been applied to predict stroke-in-evolution in acute ischemic stroke patients using one-hour ECG signals during 24 hours [30], and also recently to predict vagus-nerve stimulation outcome in patients with drug-resistance epilepsy, who were found to have lower preoperative HRV than controls [31]. Different preprocessing stages have been proposed for it, including the use of MSE in the first difference of RR-interval time series instead of the series itself, yielding better statistical support and discrimination capabilities between CHF and control groups [65]. Some authors consider the MSE algorithm biased for two reasons: First, the similarity criteria is fixed for all scales, whereas coarse grained time series variance has been pointed to decrease with the scale; And second, spurious oscillations are introduced due to the suboptimal procedure for eliminating the fast temporal scales of the time series. Accordingly, a modified algorithm was proposed [66], so-called the refined MSE (RMSE), in order to overcome these limitations, and it was tested in simulations and in 24-hour HRV signals from aortic stenosis and control groups. The use of RMSE did not allow to make inferences that could not be made by MSE with real data, however, simulations showed that RMSE can be a more reliable method for the assessment of entropy-based irregularity. A comparative study between MSE and RMSE was performed in [67] confirming that despite the differences they both present similar tendencies with scale factor. MTI has been applied to HRV and blood preasure variability (BPV) signals concluding that TI of beat-to-beat HRV and BPV is significantly altered during orthostasis [68]. Also, recent interest has been raised in the use of some of the multiscale indices in the analysis of AF dynamics, which has been scrutinized in the context of ischemic stroke prediction in patients with permanent AF [69].

We can say that cardiac LTM has been technologically achieved, and previous studies exist which have scrutinized the value of these recordings in simple and well-known clinical indices from practice, such as the number or rate of ectopic beats or the number or rate of different cardiac events [70]. However, algorithm robustness should be paid attention if deeper physiological and pathological information is to be extracted from nonlinear multiscale indices, in order to be sure about their reliability when working with long series in populational data, and to our best knowledge, few previous works can be found noting this point with attention. Therefore, we propose here to study the robustness of nonlinear multiscale HRV measurements to characterize different cardiac health states in LTM recordings.

Specifically, we made a comparative analysis of the three mentioned multiscale methods on a database consisting of patients with 7-dayS Holter in two cardiac conditions, namely, CHF and AF [29]. This study aims to give basic knowledge on the usefulness and current limitations of these methods towards their future and principled use for SCD risk stratification. For this purpose, a nonparametric statistical test is proposed in order to compare and give cut-off comparison levels between two different situations in terms of the confidence intervals (CI) for the median difference across multiscale representations of poblational representations. This method can be used either for establishing comparisons among patients or subjects with different conditions, or to scrutinize the impact of preprocessing or data length on the statistical properties of the multiscale representations. The procedure can be seen as an extension of previously used statistical comparisons [30, 31] in terms of nonparametric bootstrap tests for confidence bands [32, 16].

The structure of the chapter is as follows. In the next section, the fundamentals of the multiscale methods selected here for HRV analysis are described. Then, existing methods and the new procedure based on nonparametric bootstrap tests for median difference are provided, together with the presentation of the available recordings in Physionet [15] used as starting benchmark for this study and the LTM-ECG databases for CHF and AF during 7 days. In Results section, a set of experiments are conducted and results are presented on the suitability, together with some technical limitations and consistency properties, of these benchmarked multiscale algorithms.

## 3.2 Multiscale Methods for HRV Analysis

HRV measurements aim to give a numerical magnitude of the time fluctuations between sets of consecutive beats. The short-term recordings of HRV are usually measured about 3 to 5 min, and they have been traditionally associated with the dynamic control of the ANS on the heart rate and the cardiac properties. The long-term fluctuations of HRV have been described to have a wide physiological meaning in terms of the cardiovascular system self-regulation mechanism description. The ANS is divided into two branches, namely, the sympathetic and the vagal (parasympathetic) ones. Broadly speaking, the activation and excitation of the sympathetic branch has an accelerating effect on the cardiac cycle, whereas the vagal activation has a decelerating effect, but both subsystems are simultaneously and continuously working and compensating themselves, so that oscillations on a dynamic equilibrium are produced on the heart rate [13]. In addition, the ANS receives information through the so-called efferent pathways from a wide variety of systems and organs (heart, digestive system, kidney, respiratory system, and many others), and those influences are part of the genesis of ANS afferent pathways, in which heart rate is affected and is involved through different control mechanisms. Additional influences on the ANS such as humoral factors, night-day cycles, or environmental influences, are slower than the ANS, so that they only can influence the long-term HRV [71]. All these sources are contributors to the HRV modulation, which globally has its origin on a complex dynamic equilibrium arising from diverse mechanisms in the cardiovascular system that are taking place in the short-, the middle-, and the long-term scales.

A number of scientific, technical, and medical studies have focused on the HRV, and it well might be the most studied index in the SCD risk-stratification literature. Nonlinear methods [72] include several subfamilies, according to their calculation being based on Information Theory, on Chaos Theory, or on Fractal Theory. These methods have been paid special attention not only for their attractive theoretical foundations, but also because they seemed to have promising risk capabilities in small-sized studies with patients [11]. A usual situation in the literature of nonlinear HRV indices has been that some basic index has been first proposed, which has shown descriptive capabilities and some independence for SCD risk stratification, and then this index has been subsequently extended to a multiscale formulation, aiming to capture a richer variety of descriptions for the signal behavior. As described next, this is the case of MSE, MTI, and MFS methods for HRV analysis.

We denote the continuous-time ECG signal of a patient by $S(t)$, and we register it during an observed time interval, denoted by $t \in (t_i, t_f)$. As a result of preprocessing

steps devoted to signal filtering and R-wave detection, we can detect the R wave of each beat in $S(t)$, and the time instants associated to each R-wave are denoted as $t_n^R$, with $n = 0, \ldots, N$, so that the detected set of R-waves can be expressed as a point process, given by

$$RR(t) = \sum_{n=0}^{N} \delta(t - t_n^R) \tag{3.1}$$

where $\delta(t)$ denotes the continuous-time Dirac's delta function. It is often useful to work with the so-called *normal beats*, which correspond to R-waves in beats that have been only originated in sinus rhythm conditions and where artifacts and ectopic beats are discarded. Here we assume that the R-waves correspond to cardiac beats but not to artifacts or wrong R-wave detections. The RR-tachogram [13], or just *tachogram*, can be denoted by $x[n]$ and is defined as the discrete-time series given by the indexed time difference between consecutive R-wave times (excluded artifacts and non-physiological beats, as well as conventional quality-control beat filters), this is,

$$x[n] = t_n^R - t_{n-1}^R, \quad n = 1, \ldots, N \tag{3.2}$$

The following algorithms and indices can be expressed and obtained in terms of the tachogram registered in patients.

### 3.2.1 MSE Analysis

The approximate entropy ($ApEn$) can be described as a nonlinear fluctuation measurement that aims to quantify the irregularity of a RR-interval time series [73]. An $ApEn$ increase is usually interpreted as an indicator of irregularity increase in the underlying cardiovascular process. The Sample Entropy ($SampEn$) was subsequently introduced [74] to solve the limitations of the $ApEn$ [75], since the latter compares each pattern in a time series with other patterns but also with itself, which leads to the overestimation of similarity existence in that time series, and hence to strong bias and to some inconsistent results. $SampEn$ is the negative of the natural logarithm of the conditional probability that two similar patterns of $m$ point segments, $x_m(j)$ and $x_m(i)$ of tachogram $x[n]$, remain similar if we increase the number of points to $m + 1$, within a tolerance $r$ that is defined as a noise-rejection filter [74]. SampEn index reduces the statistical bias of ApEn index and it is a measurement rather independent of the data length, but its problem is that it it can be unstable when the counted events are scattered.

The new concept of multiscale analysis was proposed to overcome several limitations pointed out for $ApEn$ and $SampEn$ measurements which could be leading to clinical misinterpretation of HRV in some conditions. The MSE analysis was introduced by Costa et al. in [18], and it was also intended to provide with a richer description of the cardiac dynamics in terms of a set of naturally related indices, rather than to use a single number. For a given discrete-time series, a new series is constructed in a scale $\tau$, the terms of which are the average of the consecutive elements of the original series without overlapping. For a time series with $\tau = 1$, this corresponds to the original series, whereas for $\tau = 2$, the series is constructed with the average of the elements taken from two by two, and so on. We finally calculate the $SampEn$ for each one of these new generated series. When the obtained values are represented versus the scale factor, the dependence of the measured

entropy with the time scale can be scrutinized. The maximum scale to use depends on the number of samples in the time series.

Starting with tachogram signal $x[n]$, we denote $MSE$ as $MSE(x[n], \tau, r, m)$ to explicitly consider the dependence of its design parameters. We obtain the consecutive time series $y^\tau$, determined by scaling factor $\tau$ as follows:

- First, the original time series is divided into non-overlapping intervals with window size of $\tau$ samples. Then the signal mean is obtained for each of the sample windows.

- Each element of the series $y^\tau[j]$ is calculated according to the equation:

$$y^\tau[j] = \frac{1}{\tau} \sum_{n=n_j}^{j\tau} x[n], \qquad 1 \leq j \leq \frac{N}{\tau} \tag{3.3}$$

  where $n_j = (j-1)\tau + 1$ for notation simplicity. For the first scale, the time series $y^1[j]$ is just the original time series. The length of each obtained time subseries is equal to $\frac{N}{\tau}$.

- The sample entropy index is calculated for each time series $y^\tau$, and it is represented as a scale-factor function $SampEn(\tau)$.

The MSE analysis has been applied to a variety of cardiac and cardiopathological situations, including the analysis of CHF [18], hypertensive and sino-aortic denervated conditions in experimental studies [67], as well as the ANS evolution before, during, and after percutaneous transluminal coronary angioplasty [76], as well as for prediction of ischemic stroke in patients with persistent AF [69], among others. In all these cases, the length of the analyzed signals did not exceed 24 hours using 20 as a maximum scale value, which involves $x[n]$ tachograms with about or more than 20 000 samples each.

### 3.2.2 MTI Analysis

Time irreversibility has recently attracted attention in the cardiovascular-signal field. A signal is said to be time irreversible if its statistical properties change after its time reversal. The consistency loss of the statistical properties of a signal when the signal reading undergoes a change through time inversion is measured using the MTI, which represents an asymmetry index. This index is higher in healthy systems (with more complex dynamics) and it decreases in conditions like pathology or aging, as introduced in [19, 20]. On the other hand, physiological time series generate complex fluctuations in multiple depending time scales, due to the existence of different hierarchical and interrelated regulatory systems.

The MTI calculation process is presented next. Considering the time series $x[n]$, for $1 \leq i \leq N$:

- For the first scale, the time series are:

$$Y_1 = y[n], \quad y[n] = x[n+1] - x[n], \quad 1 \leq n \leq N-1 \tag{3.4}$$

- The difference $A_1$ is then calculate as follows:

$$A_1 = \frac{\sum_{n=1}^{N-1} H(-y[n]) - \sum_{n=1}^{N-1} H(y[n])}{N-1} \tag{3.5}$$

where $H$ is the Heaviside function that can be expressed as:

$$H(a) = \begin{cases} 0 \ if \ a \leq 0 \\ 1 \ if \ a \geq 0 \end{cases} \tag{3.6}$$

- For the $j^{th}$ scale, the time series is:

$$Y_j = y[n], \quad y[n] = x[n+j] - x[n], \quad 1 \leq i \leq N-j \tag{3.7}$$

- Then, $A_j$ is calculated for each scale $j$:

$$A_j = \frac{\sum_{n=1}^{N-j} H(-y[n]) - \sum_{n=1}^{N-j} H(y[n])}{N-j}, \ 1 \leq n \leq N-j \tag{3.8}$$

The MTI analysis has been applied to measure nonlinear dynamics in heart-rate time series. For instance, MTI indices were computed in [77] for 20 healthy neonates to detect the presence of nonlinearity in their cardiac-rhythm control system, and temporal asymmetries were detected within their heart rate dynamics even shortly after birth.

### 3.2.3 MFS Analysis

Physiological signals have been shown to present fractal temporal structure under healthy normal conditions [78, 79, 16]. In particular, it was shown in [80] that time series generated by certain cardiovascular control systems in healthy conditions require a large number of exponents to adequately characterize their scaling properties, and that the nonlinear properties of this behavior are encoded in the Fourier phases. The same work used examples of CHF patients to contrast the previous finding with the loss of multifractality in this example of life-threatening condition. In this setting, RR-interval time series have been analyzed in terms of multiple scaling exponents. We next summarize the basic principles for estimating the MFS from RR signals that are usually followed in the literature. The interested reader can consult the original works on its application [80, 23] and the details on the wavelet-transform modulus maxima method [81], which gives a principled calculation method for this purpose.

Whereas monofractal signals have the same scaling properties through time and they can be indexed by a single global exponent (such as Hurst exponent $H$) characterizing their fluctuations, other signals exhibit variations in their local Hurst exponent along time. When several subsets of a signal are characterized by the same local Hurst exponent $h_o$, and when each of these signals can be characterized by a fractal dimension measurement, we denote this estimated dimension as $D(h_o)$. Accordingly, $D(h)$ will have nonzero values on a set of discrete points in $h$ for some class of signals. Local value of $h$ is modernly estimated with Wavelet Theory [81], often using successive derivatives of the Gaussian function as the analyzing wavelet at different scales $a$, in order to remove polinomial trends

with polinomial order up to the wavelet derivative order. In these conditions, the problem reduces to obtain the modulus of the maxima extrema of the time series wavelt transform at eath time instant.

We then estimate the partition function $Z_q(a)$, as the sumation of the $q^{th}$ powers of these local maxima as a function of scale, and for small scales, it is fulfilled that it has the form $Z_q(a) \sim a^{\tau(q)}$, where $\tau(t)$ are exponents that can be estimated. In monofractal signals, a linear scaling exponent spectrum is obtained, given by $\tau(q) = qH - 1$. However, for multifractal signals we obtain a nonlinear expression, and it can be shown that $\tau(q) = qh(q) - D(h)$, where $h(q) = d\tau(q)/dq$ is not constant. Accordingly, the estimated fractal dimensions $D(h)$ are obtained by the Legendre transform of $\tau(q)$, finally yielding

$$D(h) = qh - \tau(t) \tag{3.9}$$

Given that $h = 0.5$ can be related to uncorrelated changing time series, this representation allows to determine to what extent a process conveys anticorrelated ($h < 0.5$) or correlated ($h > 0.5$) behaviour consistently manifested through different time periods.

The multifractal structure of HRV can reflect important properties of the heart-rate autonomic regulation. Multifractal analysis is an expansion of fractal analysis since it characterizes the time series variability with a collection of scaling exponents instead of a single one, which makes possible to investigate and quantify HRV in terms of its multiexponent properties. A right shift has been revealed in the multifractal spectrum peaks for healthy subjects during meditation [82], which points to a better health condition of persons with respect to multifractal nature. Accordingly, a healthy heart-rate regulation promotes a multifractal signal.

## 3.3 Statistical Methods and ECG Databases

### 3.3.1 Previous Indices and Bootstrap Median Difference

A set of metrics were computed in order to quantify population differences in terms of the information conveyed by small, medium, and large scales of MSE and MTI indices. Namely, the area under the MSE and MTI profiles between scales 1 and 5 (so-called $\mathbf{Area1-5}$), between scales 6 and 20 ($\mathbf{Area6-20}$), and between scales 21 and 100 ($\mathbf{Area21-100}$). The area under the complete profiles (so-called **Area**) for MSE, MTI, and MFS was also computed. These metrics have been previously used and validated in studies comparing results of multiscale indices for different populations [31, 30]. The Wilcoxon-Rank Sum Test was subsequently used to evaluate the statistical difference between populations in terms of these metrics, also according to the previous works. As an extension of the previous existing analysis, we contribute in this paper with a statistical procedure allowing to establish simple statistical comparisons, either between two different population groups or within the same group of patients, in terms of a given multiscale representation. The procedure can be summarized and described as follows. We generically denote the scale as $\nu$ (which includes both possibilities for $\tau$ in MSE and MTI, or $h$ in MFS), and the multiscale index as $J(\nu)$ (where $J$ stand for either MSE or MTI or MFS representations). Let us assume that we have available a set of signals from a given patient dataset $A$, and this set is denoted as

$$\mathcal{S}_A \equiv \{x_i[n], i = 1, \cdots, N_A\} \tag{3.10}$$

and that the multiscale parameter can be obtained by using a given operator $\Gamma$ for each signal in the database, i.e.,

$$J_i(\nu) = \Gamma\left(x_i[n], \theta\right) \tag{3.11}$$

where $\theta$ includes the set of preprocessing and processing parameters established for preprocessing and conditioning the signal under analysis.

Note that in this case $J(\nu)$ represents a random process, defined by its statistical distribution $f_{J(\nu)}\left(J(\nu)\right)$, which in general has an unspecified expression. We can define its median value and denote it as $J_M(\nu)$, which in practice can be estimated as the median of the multiscale representations obtained in a given population with a given set of parameters, and denoted as $\bar{J}_M(\nu|\mathcal{S}_A, \theta)$. Therefore, statistical differences can be calculated in two kinds of situations. First, when comparing the multiscale differences in two populations of patients, $\mathcal{S}_A$ and $\mathcal{S}_B$, we can build the statistic accounting for the difference between their corresponding poblational medians, give by

$$\Delta J_M(\nu) = \bar{J}_M(\nu|\mathcal{S}_A, \theta) - \bar{J}_M(\nu|\mathcal{S}_B, \theta) \tag{3.12}$$

In addition, we can have two different sets of preprocessing conditions, given by $\theta_1$ and $\theta_2$, and in this case the differences due to this change in those conditions can be scrutinized in terms of the difference of the median multiscale spectrum in a given population, as given by

$$\Delta J_M(\nu) = \bar{J}_M(\nu|\mathcal{S}_A, \theta_1) - \bar{J}_M(\nu|\mathcal{S}_A, \theta_2) \tag{3.13}$$

Hence, both representations are similar enough to provide a similar-to-handle view of the scales in which differences can be observed. The use of the median gives a robust estimator for cases where non-Gaussian distributions can be present, which was previously observed to be this case.

Since the *PDF* of the multiscale indices is often complex to estimate and to handle, we used nonparametric bootstrap resampling techniques, which provide us with an estimation of the empirical distribution of any statistical magnitude that can be built from computational media [32].In our case, given a set of observed signals, we build a resample of this set by sampling with replacement each of the individuals in $\mathcal{S}_A$ up to $B$ times, so that we get the so-called the $b^{th}$ resample of the patient population, $\mathcal{S}_A^*(b)$, where superscript $^*$ is the usual notation to point out all the bootstrap-estimated magnitudes. For this resample, we obtain an estimate of the statistical magnitude of interest, widely known as its bootstrap replication, and in our case it corresponds to weight vector $\mathbf{w}_{(b)}^*$. By repeating the procedure $B$ times, we get an estimate of the marginal distribution given by the empirical probability density function *(PDF)* of the bootstrap replications of each weight, this is, $\bar{J}_M(\nu|\mathcal{S}_A^*, \theta)$. The estimated distribution of the median difference statistic as a function of the scale can then be estimated from the replications of this statistic, which for the case of two different patient populations is obtained by non-paired resampling as follows:

$$\Delta J_M^*(\nu, b) = \bar{J}_M(\nu|\mathcal{S}_A^*, \theta) - \bar{J}_M(\nu|\mathcal{S}_B^*, \theta) \tag{3.14}$$

whereas for changes in the preprocessing conditions, paired resampling can be addressed, yielding

$$\Delta J_M^*(\nu, b) = \bar{J}_M(\nu|\mathcal{S}_A^*, \theta_1) - \bar{J}_M(\nu|\mathcal{S}_A^*, \theta_2) \tag{3.15}$$

The corresponding CI can be readily obtained just using sorted statistics, with significance level $\alpha$ yielding confidence level $1 - \alpha$ (typically $1 - \alpha = .95$). We expect the relevant

differences to exhibit non-zero overlapping CI. Also, the band confidence width should be consistent with the expected statistical power of the bootstrap test, hence allowing to study the consistency of the estimates when increasing the number of measured days in the Holter signals, and the estimated median average should allow us to scrutinize the presence of bias.

### 3.3.2 ECG Databases

We started by using multiscale methods to asses the variability of the RR-interval signals derived from 24-hour Holter recordings from control subjects and from CHF patients. Both sets of recordings were downloaded from Physionet database [15]. The control group was obtained from 24-hour Holter recordings in 72 healthy subjects (35 men and 37 women, from 20 to 76 years old). The original ECG recordings were sampled at 128 Hz. The CHF group was obtained from 24-hour Holter recordings in 44 subjects (from 22 to 79 years old, including 19 men and 6 women, though gender information was not available for all the recordings). A subset of the original ECG recordings were sampled at 250 Hz (15 recordings), and the rest at 128 Hz. A number of studies have been conducted with these Databases [83, 84, 85, 86] to determine the effect of exercise training on cardiac autonomic modulation in normal older adults using HRV, to establish normal values of RR variability for middle-aged persons, and to determine the effect of beta-blockers on parasympathetic nervous system activity.

We also used a specific LTM database, in which two sets of 7-day Holter recordings were also analyzed, one set from patients with CHF in sinus rhythm (73 recordings), and another set from patients with CHF with chronic AF (14 recordings). For short, we will denote them as CHF dataset and AF dataset, keeping in mind that both of them are CHF patients, but with different basal rhythms. The protocol to collect these recordings was carried out following the principles of Helsinki Declaration. It was approved by the Local Ethics Committee. Patients were recruited during scheduled outpatient visits to the CHF outpatient clinic in Virgen de la Arrixaca University Hospital (Murcia, Spain). From June 2007 to May 2011, patients with an established diagnosis of stable CHF gave written informed consent to participate. All patients had LVEF $\leq 50\%$ and they were clinically stable, without need for hospital admission or intravenous vasoactive agents within the past 3 months. Exclusion criteria included pacemaker-dependent patients, a serious comorbid condition with associated life expectancy $< 1$ year, hospitalization for Myocardial Infarction (MI) and unstable Coronary Artery Disease (CAD) within the past 3 months, or any cardiac revascularization procedure within 30 days before enrolment. The 7-day continuous Holter recordings were obtained using a commercially available device (Lifecard CF$^{TM}$, Del Mar Reynolds, Issaquah, Washington). These databases had been used [70, 87, 79, 16] in previous studies: (a) To demonstrate that the circadian rhythms detected in 7-day recordings could not always be detected in 24-h periods; (b) To compare the diagnostic sensitivity of 1-day Holter monitoring versus 7-days Holter monitoring (7DH); (c) To detect atrial and ventricular arrhythmias in a population of stable patients with CHF and left ventricular dysfunction; (d) To characterize the relationship between heart rate and post-discharge outcomes in patients with hospitalization for CHF with reduced ejection fraction (EF) in sinus rhythm; And (e) and to characterize the infradian, circadian, and ultradian components for each patient, as well as circadian and ultradian

fluctuations.

A standard Holter analysis software (ELA Medical$^{TM}$, Sorin Group, Paris, France) was used to process the data. When needed, a trained cardiologist performed a visual check of the QRS complex classification and every arrhythmic event, therefore, manual corrections were made. Both data sets (Physionet and LTM) were preprocessed to exclude artifacts and ectopic beats, as follows. $RR$ intervals lower than 200 ms and greater than 2 000 ms were eliminated, as well as those which differed more than 20% from the previous $RR$ interval [13]. The nonlinear indices were computed on the resulting time series

## 3.4 Results

In this section, we present a series of experiments in order to analyze the consistency and robustness of the indices for multiscale characterization with 1-day and 7-days Holter registers of healthy subjects, AF patients, and CHF patients. First, a robustness analysis of all these methods is made with datasets from Physionet databases (specifically, healthy subjects and CHF patients) in 1-day Holter recordings, and patients with AF and CHF are then analyzed in 7-day Holter recordings. We also scrutinized how the results can change when using 1-day Holter registers versus 7-day Holter registers and with increased scaling factor. A study on the robustness of the indices on 7-day recordings is checked in terms of 1-day segments, and a quantitative analysis is made for all of them in terms of the confidence bands for the populational medians.

### 3.4.1 Physionet Database and 1-day Holter Recordings

We started our analysis by scrutinizing the effect of calculating multiscale indices in 1-day Holter recordings above 20 scales, which is the usual limit value in the literature. The multiscale indices were obtained in the 72 subjects in the control set of Physionet database. Figure 3.1 (left panels) shows these results, where each plot represents the entropy value (vertical axis) as a function of the multiscale parameter ($\tau$ or $h$), for every patient in the database and with no specific ordering. Typical patterns can be observed for each multiscale index. For instance, in MSE there is often a soft curve for low scales that usually turns to near constant at larger scales. We can observe also a rift effect specially in larger scales, which indicates that the method is being sensitive to noise. We can also observe a bias effect among subjects, as some of them appear to be above increased or decreased average levels compared with others. With respect to MTI, we can see that all the cases start near zero value for low scales, and there is a general trend to increase as a soft-changing curve above zero for all the cases. No rift effect is present in this multiscale index. Finally, MFS often shows an inverted-U shape, as documented in the literature, and there is a bow about $h = 0.5$ in many cases, followed by a flat or slow decaying set of values. Note that some few cases seem to deviate from this populational behavior.

A different behavior is present when we scrutinize the three multiscale indices for the CHF patients in 1-day Holter recordings, as seen in Figure 3.1 (right panels). This figure and its panels allow us to check the individual profiles of a given multiscale index in a population, so that individual profiles can be checked to be consistent with their population, and also non-concordant profiles can be clearly identified. Note that the axis

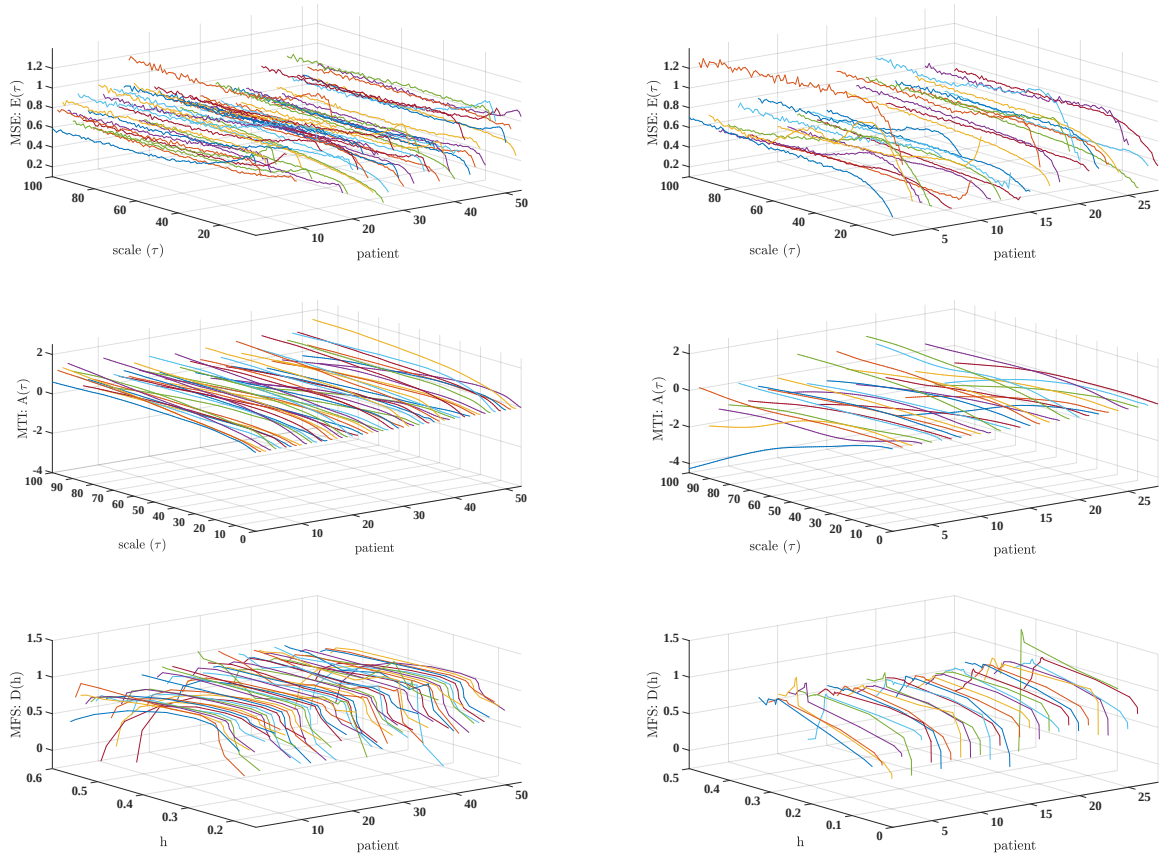


Figure 3.1: Results of multiscale analysis in Physionet Database:
MSE (top), MTI (middle), and MFS (down) for the control database (left) and for the CHF patients (right).

are similar to the control panels, and that the vertical axis have been adjusted with the same range and scale. In MSE there is a diversity of shapes in low scales, though the trend to stabilize at larger scales is again observed, as well as the rift effect. In addition, there are more cases with increased average value, and in general there is a trend to exhibit lower average cases than controls. The MTI again starts from low values for low scales, but then it smoothly and often (not always) tends to go towards negative values. With respect to the MFS, it clearly decreases its width, the bow and the flat set of indices are mostly lost, and it often deviates from 1. Some very atypical cases are present, specially in the CHF set. Several patients are extremely different from the others in MSE and MTI, and several (not few) cases in MFS seem to present a breakdown and even values above 1. We thoroughly checked in all the patients that artifacts were correctly suppressed from the signals with ad-hoc designed software to represent jointly the RR-signals and the ECG signals on a similar time basis.

### Artifact and noise effects

Artifacts and other noisy beat detections are not included in the analysis. We followed a data-quality control process in long-term monitoring, which is, at least, as rigorous and

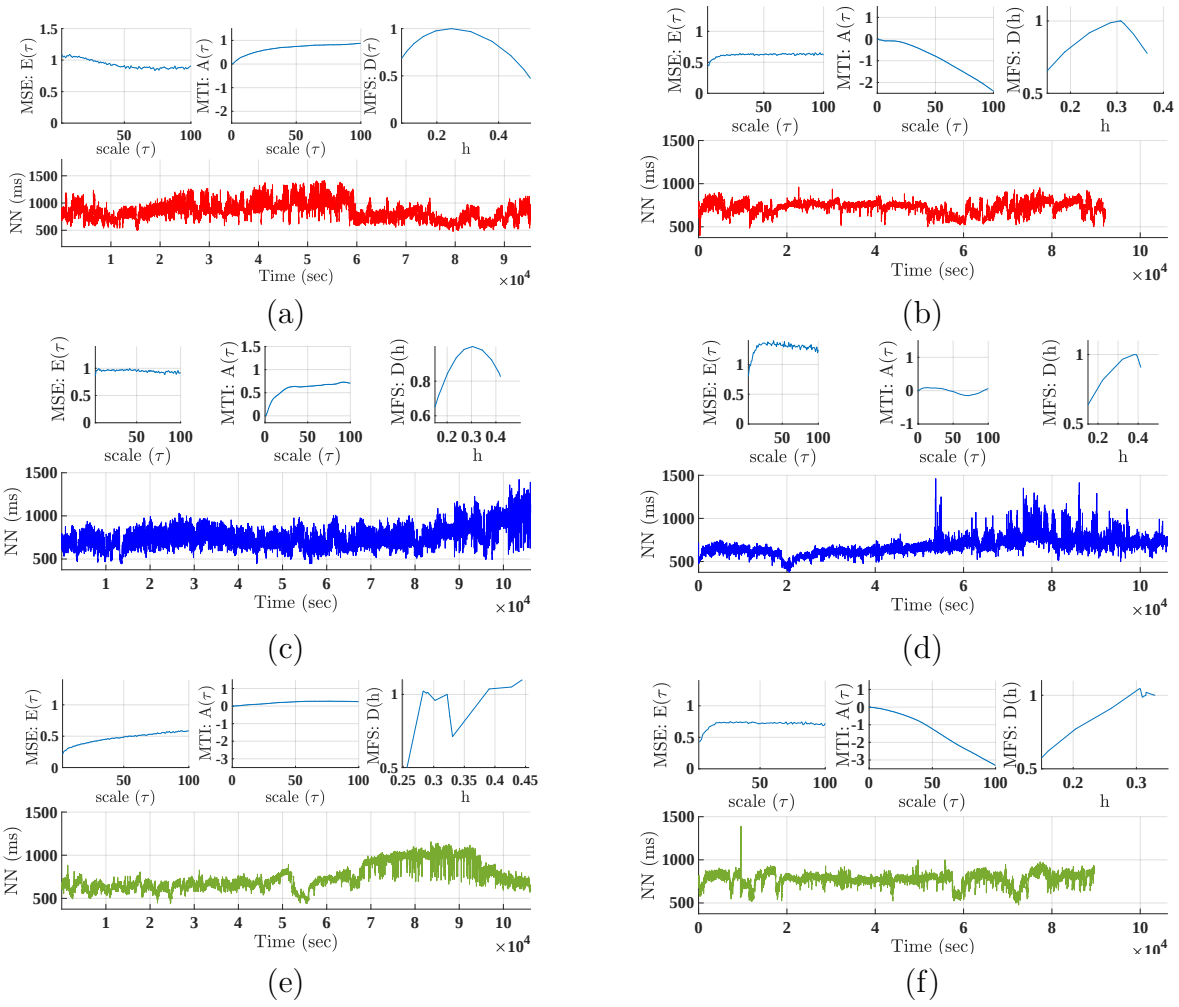


Figure 3.2: Results of multiscale analysis in example patients from Control Database (left) and from CHF Database (right) in Physionet: (a, b) Normal trend; (c, d) Abnormal MSE and MTI profiles; (e, f) Abnormal MFS profile.

detailed as any relevant study in the related literature, the goal is to check that the data are correct, even in long-term recordings.

Ectopic beats are in general included in the cited works on nonlinear analysis (which is not the case in temporal, spectral, or geometrical methods), as they do not affect if they are few, or they are assumed to take part on the dynamics if they are consistently present for time periods. Some beat filter is also often used to discard artifacts (as those due to electrode loose contact or disconnections, synchronization, or artificial pauses of any kind).

In this tesis a usual preprocessing scheme is used [13] for both datasets (1-day and 7-day recordings). The panels in the Figure 3.4.1 show an example in a Physionet case (we thoroughly checked those ones in which the ECGs were available) for which the total RR signal (preprocesed) is used to obtain the multiscale indices (in black), and also the same in each time window (blue, red, green, orange).

The simultaneous ECG recordings (together with the beat detections) were then scrutinized with horizontal zooms in those MS-index windows with worse reproducibility and in those ECG regions with more ectopic beats or with some different trends. It was

checked that the presence of ectopic beats did not affect to the estimated profiles in these cases, and that no artifacts were present in the underlying ECG signals. Furthermore, the underlying signals did not have artifacts or aberrations, and custom software was developed and used for this task.

### Windowing analysis

Since there were these marked deviations in the profiles of some curves compared to others for MSE, MTI and MFS, we subsequently analyzed the effect of calculating these indices in segments of the cardiac signal, with their lengths being smaller but long enough to maintain the multiscale properties. This could allow us to determine whether the profiles deteriorate in a specific segment or just in the complete signal, which is denoted here as the analysis of windowing effects on MSE, MTI, and MFS.

Figure 3.2 presents six example cases (three from healthy subjects and three from CHF patients) in specific cases, namely, a normal-trend patient (typical MSE, MTI, and MFS) (Panels a, b), a patient with atypical MSE and MTI profiles (Panels c, d), and a patient with atypical MFS profile (Panels e, f).

The panels on Figure 3.4 present the windowing analysis applied on the original heart-rate signal by dividing it into 4 sub-signals and applying MSE, MTI, and MFS on each of them. Regarding the first example, Panels a and b, the control patient presents a similar response in terms of the tendency of the signals resulting from applying MSE, MTI, and MFS. The second example, in Panels c and d, represents a result that goes out of the normal in terms of the result of applying MSE and MTI. We observe, in terms of changes in the hear-rate signal, that the resulting signals trend differs in different time windows. A similar view is noted regarding the application of MFS in Panels e and f, where one segments follows an atypical profile compared to the rest of the segments in the same registry by changing the windows. In general we can see that when one single time window looses its consistency with respect to the general shapes, the continuous analysis of the complete segment is compromised too, an effect that seems to be present in all the multiscale indices. Right panels on Figure 3.4 present the windowing analysis done on the heart-rate signals of CHF patients, which are again divided into sub-signals, and then the MSE, MTI, and MFS are applied to this set of series separately. According to Panel b, this CHF patient follows the trend of the complete signal when applying MSE, MTI, and MFS. Panel d shows that the MSE and MTI results disrupt in this example. Despite the appearance of the hear-rate signal at the beginning, it undergoes a degradation in the last window when these methods are applied. A similar remark can be extracted when applying MFS, as seen in Panel f, since the first window notably differs from the last one. Similar considerations can be done as in the healthy subjects windowing analysis. We can conclude from this experiment that the multiscale profile trend depends on the window where the nonlinear methods were applied, sometimes due to the cardiac activity which differs depending on the day or the night periods. It appears that some segments present an anomalous estimation, which affects the whole of the signal. Therefore this can be a limitation of these current methods that should be considered by old and new algorithms in this setting.

### 3.4.2 LTM Database and 7-day Holter Recordings

Figure 3.5 shows the MSE, MTI, and MFS results for AF and CHF 7-day Holter recordings databases. In the right panels, we can observe typical patterns that are similar to the CHF cases in 24-h recordings. In low scales, MSE exhibits a variety of shapes that tend to stabilize at larger scales. MTI indices show decreasing values from low to large scales reaching negative values in some cases. MFS shows a shape with an increased width and a lost of the bow. In the left panels, different trends are observed for AF patients. MSE shows an inverted shape compared to CHF patients, i.e., larger values for low scales and lower values for high scales, or a decreasing soft curve for low scales that usually turns into constant at larger scales. We can also observe a deviation of some of the subjects from the general trend. Regarding MTI, for low scales, values start near zero with a generally slight-decreasing trend curve. MFS shows an inverted-U shape with a bow about $h = 0.2$ for all cases, followed by slowly decreasing values.

We designed a simple experiment accounting for windowing analysis of 7-day recordings in windows of 1-day duration. Our purpose here was to perform a robustness analysis of the 7-days Holter recordings when compared with 1-day recordings, in order to scrutinize the new knowledge provided by the scales up to 100 and to analyze the reproducibility of the multiscale indices throughout the 7 days.

Figure 3.6 presents a comparative analysis between 1-day and 7-day recordings by means of 3 patients with AF and 3 patients with CHF. The heart-rate signal of each patient is presented as well as the MSE, MTI, and MFS profiles. Those profiles present similar trends for every 1-day segment and for the 7-day segment with variable variance depending on the particular case. However this variance is larger in CHF examples than in AF examples for MTI in large scales and mainly for MFS.

We can also check that the consideration of larger scales in the 7-day recordings has relevant effect on the estimation of the multiscale indices. For instance, the ripple in MSE is reduced in the 7-day estimations. Also, the variance in the 1-day estimated indices for larger scales in MSE and MTI seem to stabilize to a profile which is not just the average of the consecutive days, which implies that nonlinear irregularity effects in these larger scales are present and likely they are better accounted by the 7-day calculations. It is interesting the effect that the use of 7-day recordings has on MFS, which is different from a simple day-averaging of the windowed spectra. In some cases, a wider set of 1-day spectra is condensed into a narrower spectrum with 7-day signals. In general, larger variance seems to be present at larger scales with 1-day signals, which is reduced by 7-day based spectrum (often yielding a spectral profile lower than the individual spectra in each day). Even in one case, apparently inconsistent daily spectra turn into a well-shaped spectrum when using the 7-day recording.

### 3.4.3 Statistical Analysis and Confidence Bands

Table 3.1 compares CHF patients and control subjects of Physionet database in terms of $\mathbf{Area1-5}$, $\mathbf{Area6-20}$, $\mathbf{Area21-100}$, and $\mathbf{Area}$ metrics for the multiscale indices. The Wilcoxon Rank-Sum Test reveals significant statistical differences for $\mathbf{Area1-5}$ in MSE and MTI, and for $\mathbf{Area6-20}$ in MTI, hence for small and medium scales. Table 3.2 shows the comparison for the two populations in the LTM database. In this case, statistical

| Scale Test | CHF | Control | p-value |
|---|---|---|---|
| MSE (Area 1 - 5) | 1.30 ± 0.50 | 1.58 ± 0.57 | ¡ 0.05 |
| MSE (Area 6 - 20) | 9.47 ± 3.52 | 9.66 ± 2.75 | 0.53 |
| MSE (Area 21 - 100) | 56.45 ± 18.23 | 52.37 ± 11.88 | 0.38 |
| MSE (Area) | 68.51 ± 22.30 | 65.02 ± 15.27 | 0.69 |
| MTI (Area 1 - 5) | 0.09 ± 0.09 | 0.20 ± 0.14 | ¡ 0.05 |
| MTI (Area 6 - 20) | 1.95 ± 1.79 | 4.41 ± 2.37 | ¡ 0.05 |
| MTI (Area 21 - 100) | 50.46 ± 35.72 | 43.54 ± 27.76 | 0.35 |
| MTI (Area) | 52.77 ± 36.54 | 48.71 ± 29.77 | 0.68 |
| MFS (Area) | 0.32 ± 0.41 | 0.27 ± 0.09 | 0.62 |

Table 3.1: Physionet database, CHF versus Control.
**Area1 − 5**, **Area6 − 20**, **Area21 − 100** and **Area** metrics expressed as mean ± standard deviation for the multiscale indices. Significant statistical differences given by the Wilcoxon Rank-Sum Test are indicated.

| Scale Test | AF-7DH | CHF-7DH | p-value |
|---|---|---|---|
| MSE (Area 1 - 5) | 3.01 ± 1.16 | 1.55 ± 0.47 | ¡ 0.05 |
| MSE (Area 6 - 20) | 12.89 ± 4.89 | 10.22 ± 2.63 | ¡ 0.05 |
| MSE (Area 21 - 100) | 52.34 ± 18.03 | 56.63 ± 12.44 | 0.79 |
| MSE (Area) | 70.16 ± 24.51 | 69.80 ± 15.53 | 0.27 |
| MTI (Area 1 - 5) | 0.04 ± 0.04 | 0.16 ± 0.13 | ¡ 0.05 |
| MTI (Area 6 - 20) | 0.72 ± 1.61 | 3.13 ± 2.17 | ¡ 0.05 |
| MTI (Area 21 - 100) | 19.74 ± 50.62 | 42.78 ± 25.18 | ¡ 0.05 |
| MTI (Area) | 20.60 ± 52.31 | 46.47 ± 26.29 | ¡ 0.05 |
| MFS (Area) | 0.25 ± 0.12 | 0.48 ± 0.91 | ¡ 0.05 |

Table 3.2: LTM database, AF-7DH versus CHF-7DH.
**Area1 − 5**, **Area6 − 20**, **Area21 − 100** and **Area** metrics expressed as mean ± standard deviation for the multiscale indices. Significant statistical differences given by the Wilcoxon Rank-Sum Test are indicated.

| Scale Test | AF-1DH | CHF-1DH | p-value |
|---|---|---|---|
| MSE (Area 1 - 5) | 3.06 ± 1.18 | 1.63 ± 0.58 | ¡ 0.05 |
| MSE (Area 6 - 20) | 12.96 ± 4.74 | 10.58 ± 3.24 | ¡ 0.05 |
| MSE (Area 21 - 100) | 50.58 ± 17.37 | 56.68 ± 14.16 | 0.28 |
| MSE (Area) | 68.54 ± 23.48 | 70.35 ± 18.11 | 0.82 |
| MTI (Area 1 - 5) | 0.04 ± 0.06 | 0.18 ± 0.17 | ¡ 0.05 |
| MTI (Area 6 - 20) | 1.12 ± 2.69 | 3.41 ± 2.47 | ¡ 0.05 |
| MTI (Area 21 - 100) | 31.68 ± 87.92 | 45.79 ± 30.89 | ¡ 0.05 |
| MTI (Area) | 33.00 ± 90.97 | 49.82 ± 32.48 | ¡ 0.05 |
| MFS (Area) | 0.26 ± 0.11 | 0.45 ± 0.51 | ¡ 0.05 |

Table 3.3: LTM database, AF-1DH versus CHF-1DH.
**Area1 − 5**, **Area6 − 20**, **Area21 − 100** and **Area** metrics expressed as mean ± standard deviation for the multiscale indices. Significant statistical differences given by the Wilcoxon Rank-Sum Test are indicated.

differences are present in MSE for small and medium scales, whereas in MTI these are also preset for large scales $\mathbf{Area21-100}$, and in MTI and MFS for the complete **Area**. The same statistical differences are observed when comparing the one day average results of LTM database (Table 3.3). Note that the interpretation of these differences should be taken as descriptive of the different cardiac conditions in terms of the different scales of the signal dynamics, and not as classifying characteristics for them with diagnostic purposes.

Additional details can be scrutinized from the proposed method, aiming to extend the statistical behavior for the previous indices in different scales, populations and conditions, or scale span, in terms of confidence bands width and median differences. Figure 3.7 shows the confidence bands for the median multiscale indices when comparing the control set with the two considered cardiac conditions, namely, CHF and AF. The former is obtained from the Physionet CHF set and the later from the LTM-AF set. Each panel shows the median and confidence bands for the first group (up, left), for the second group (up, right), and for the median difference (down). Panel (a) shows that the MFS is mainly different between both groups for low scales in MSE, whereas significant differences are present in MTI differences in all the scales. For obtaining confidence bands in MFS, an interpolation was done to a regular grid sampling using chirp interpolation, and given the different scale spam for the obtained MFS in each patient, the confidence bands in each point of the scale grid was obtained conditional to the existence of the fractal spectrum in that scale. As it can be seen in the right panel, the control set has a scale span between 0 and 1, with some exceptional case extending out of it, but the confidence band gets wider after 0.6, whereas the scale span is mainly narrower in CHF patients, though sometimes it reaches a similar set of values for different patients, as it can be observed from the wider confidence bands in the left and specially in the right of the graph. The median difference indicates a clear descending trend in the median value (blue line) from left to right, which is only non-overlapping zero at about scale 0.5. Panel (b) in Figure 3.7 shows the result of a similar comparison in this case between the control subjects from Physionet (1D) and the CHF set from the LTM database (7D). The relevant differences with respect to the previous comparison can be summarized as follows. For MSE, the differences in the lowest scales are less present, and there is a trend to the band to be consistently below zero, though it remains non-significantly yet borderline. For MTI, the differences between both populations show a similar trend than in the previous comparison, though the confidence bands in this case are borderline with respect to their zero overlapping. For MFS, the confidence bands in the CHF population from 7D reaches a wider interval of scale values remaining narrow, and the confidence bands for the median difference exhibit a similar trend with smoother band limits than the previous comparison. Panel (c) in Figure 3.7 shows the comparison between the control subjects from Physionet (1D) and the AF set from the LTM database (7D). For MSE, significant differences are present in low scales (below 60), whereas for MTI there are significant differences in all the scales. Also significant differences are present in MFS in almost all the scales, whereas in this case the median trend has the opposite slope than in the preceding comparisons with CHF. Whereas several of these results have been previously documented in the literature, our results are consistent with those precedents and they can be observed at a glance from the representation. It is evident that these indices are measuring different aspects of the complexity and/or nonlinear nature of the cardiac dynamics, and that they probably should be used complementarily.

Figure 3.8 shows the confidence bands of multiscale analyses with the aim of establishing the statistical properties that can be expected due to the use of LTM recordings. In this setting, and as it could be expected, the confidence-band widths are consistently narrower when scrutinizing paired datasets, i.e., those comparisons in which the indices estimated from 7-day recordings are compared to the indices estimated in one day (the third in each set for all of them in the 7D register) of 1D recordings for the same patients. Panel (a) shows the scale-paired confidence bands for the median differences when analyzing the CHF patient set, showing a trend to raise in the very low scales, which could mean that the significance of these scales depends on the number of days considered, when working with CHF patients. The estimated MTI remains very reproducible when obtaining it from 1D or from 7D in each patient. Note the different behavior of MSE and MTI in terms of the confidence band width in terms of increasing scales (mostly constant in MSE and increasing error standard with scale in MTI). With respect to MFS, whereas the median value difference is not significant, the most critical scale regions are again the boundaries of the population spectrum, in terms of confidence band widths. Similar conclusions can be obtained for the AF patients when compared in terms of MSE and MTI. The scale-border effects is even more critical in this case, as AF wide of this spectrum is narrower in the patients compared with control subjects and with CHF condition patients. Panels (c) and (d) show the result of comparing different conditions (CHF and AF) when using 1D or 7D in these two different sets of patients. Note that in this case the confidence bands of the differences are not very different for the cases of MSE and MTI, whereas both the confidence band widths and the scale span are clearly narrower when they are compared in terms of 7D recordings.

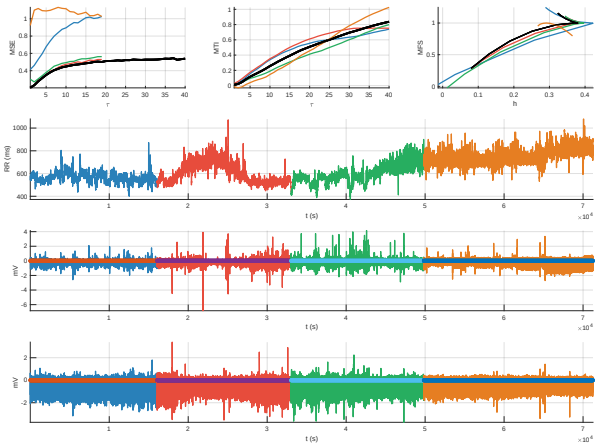

(a)

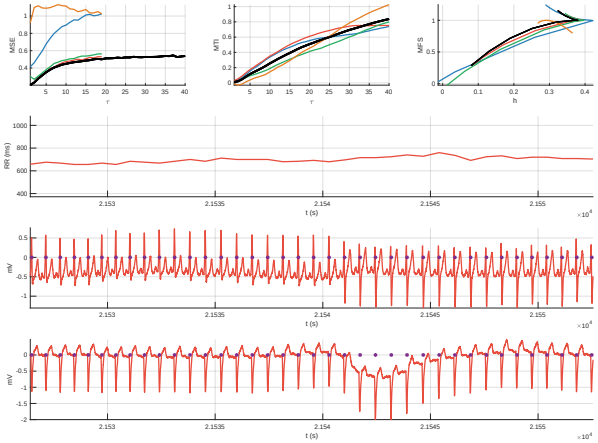

(b)

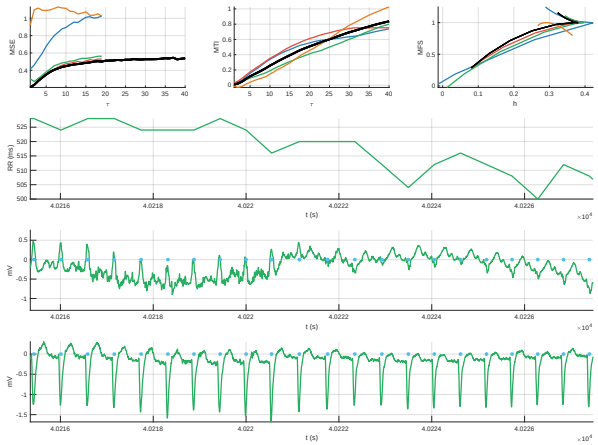

(c)

Figure 3.3: Example of checking the non-presence of artifacts.
(a) MSE, MTI and MFS indices (top row); the RR and ECG signals (two leads, bottom rows) have been synchronized in time, beat detections are marked as * (due to the signal length they look like a continuous thick line). See text for details. (b) Zoom on the red time window. (c) Zoom on the green time window.

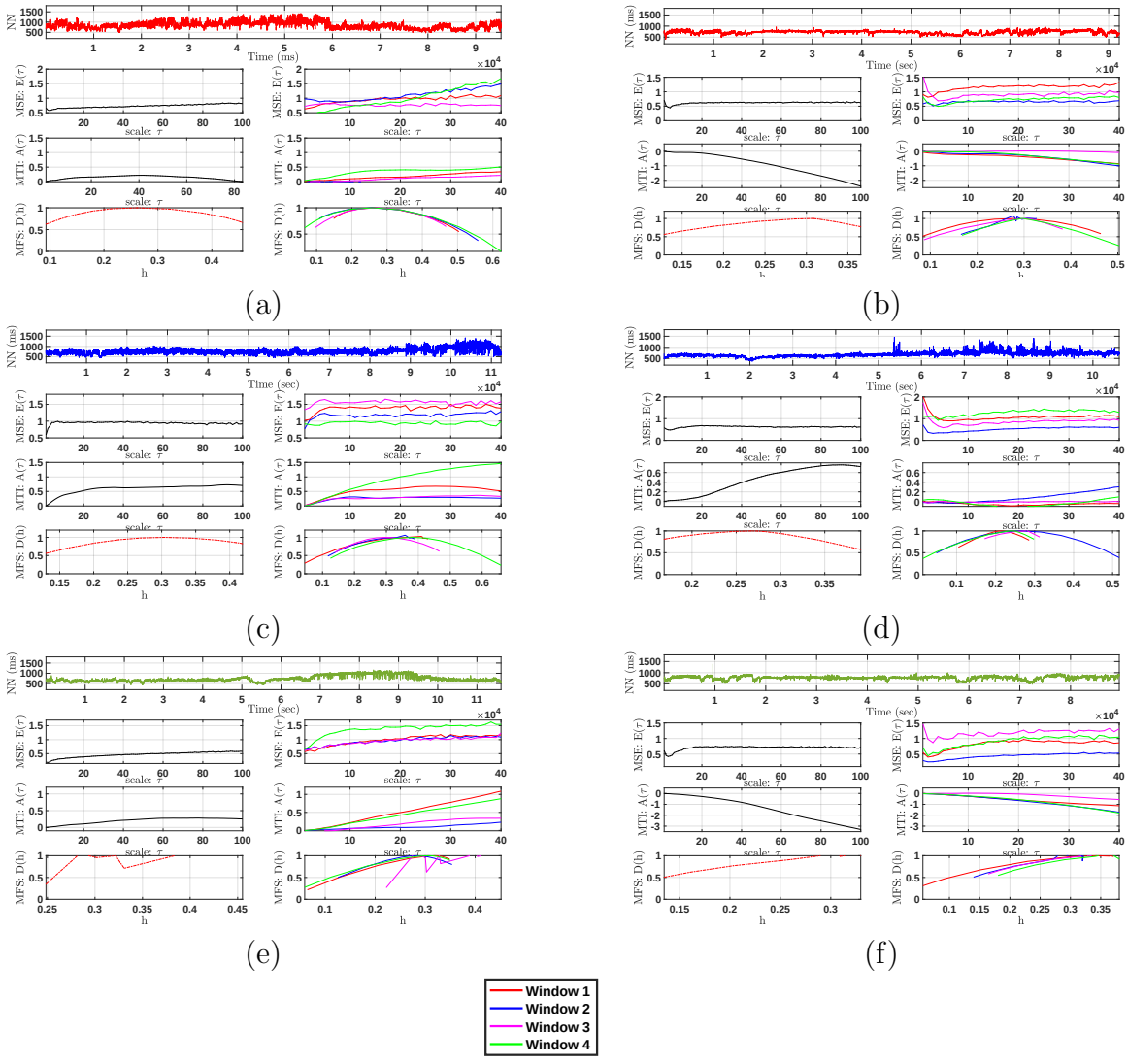


Figure 3.4: Physionet Control Database (left) and CHF Database (right) examples for the windowing analysis: (a, b) Normal curves trend windowing; (c, d) Abnormal MSE and MTI windowing; (e, f) Abnormal MFS windowing.

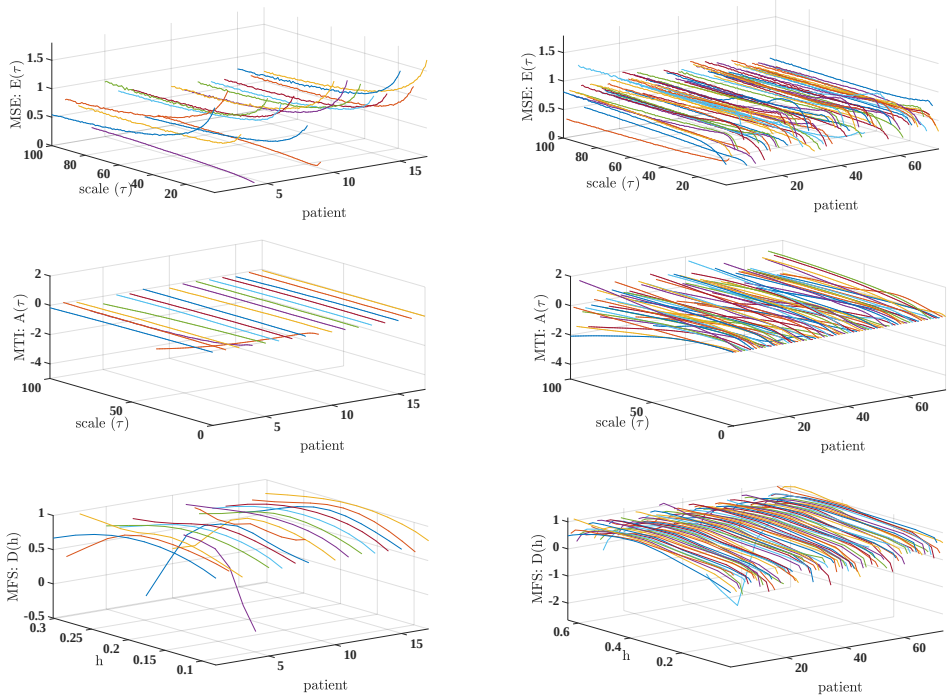


Figure 3.5: Results of multiscale analysis in LTM Database:
MSE (top), MTI (middle), and MFS (down), for the AF database (left) and for the CHF database (right).

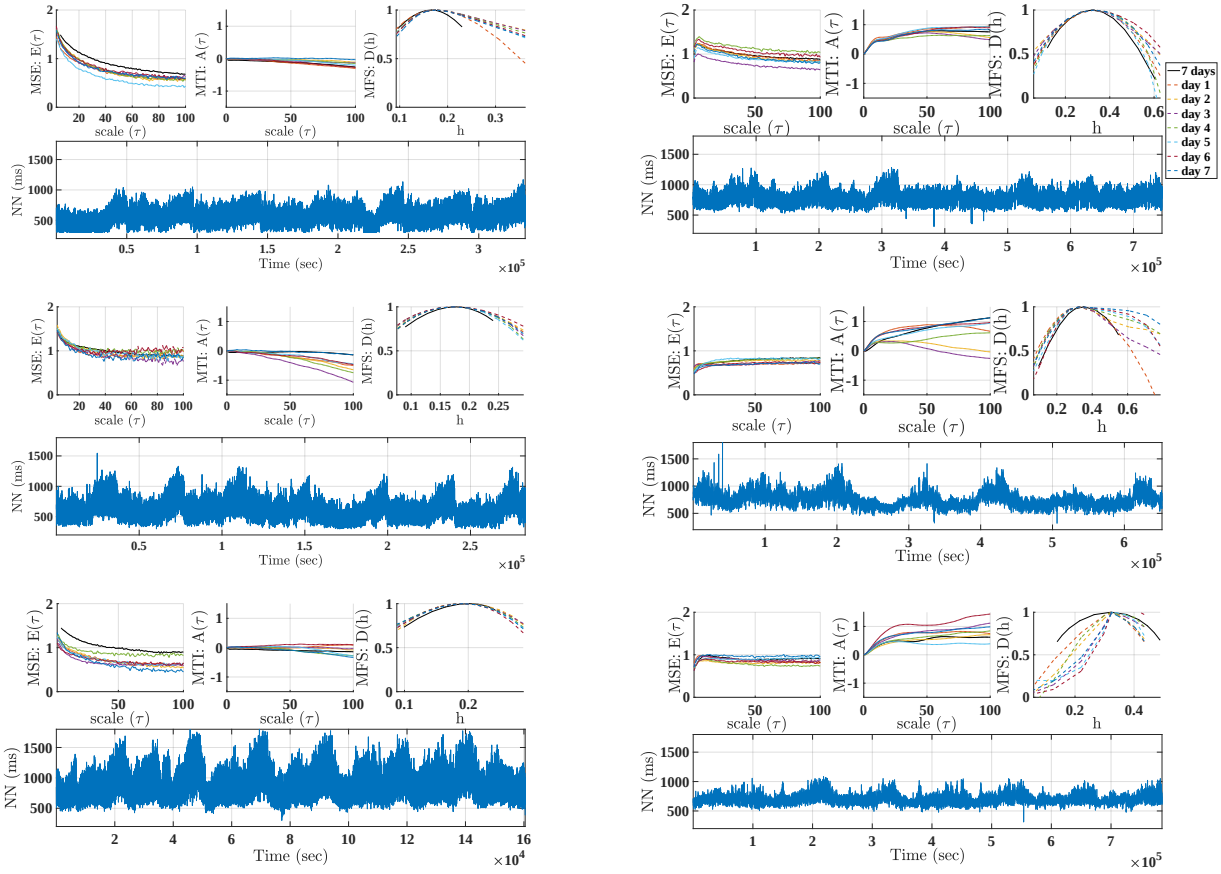


Figure 3.6: Examples of robustness analysis of 1-day versus 7-day Holter recordings in AF (left) and CHF (right) patients.

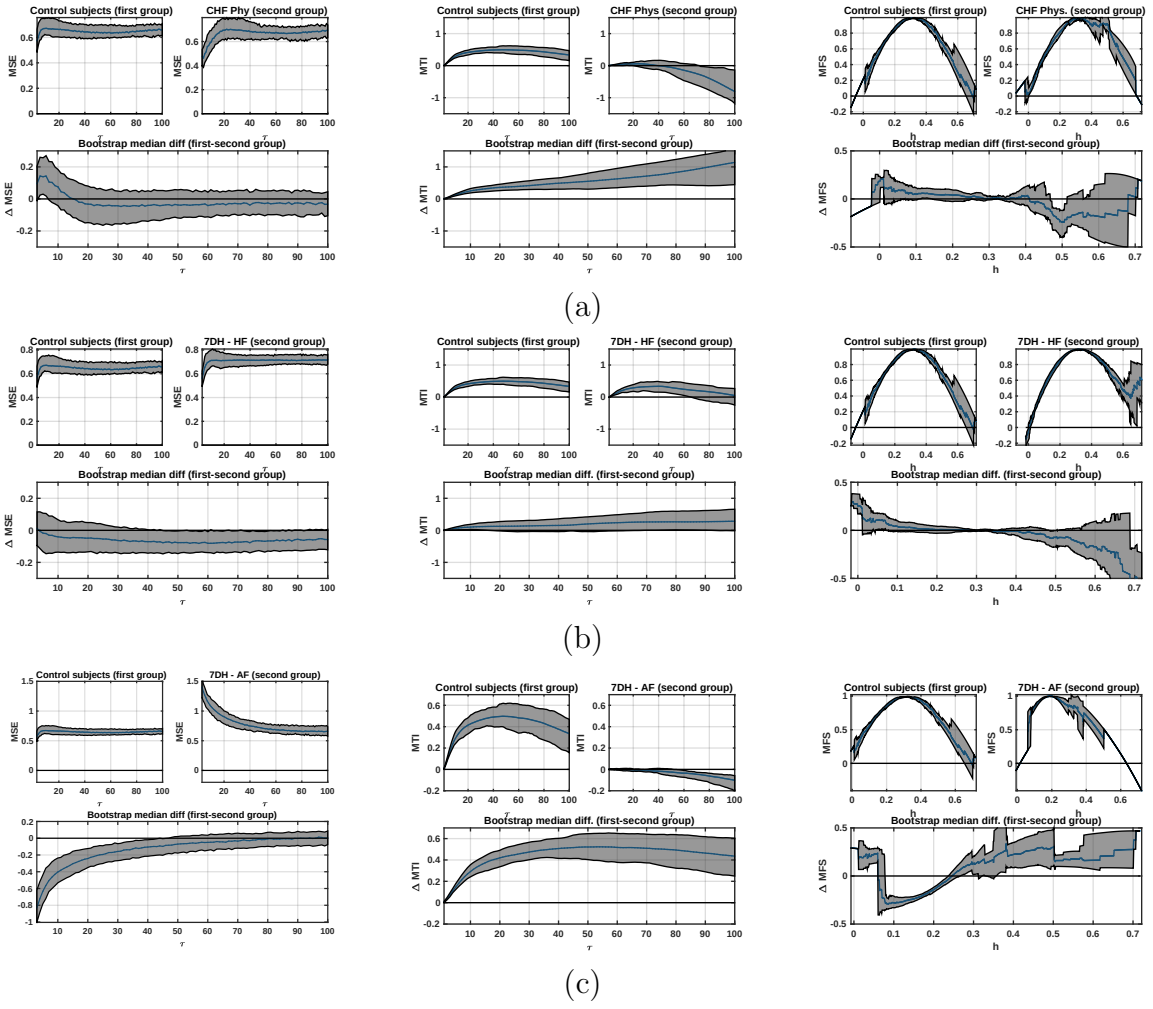


Figure 3.7: Confidence bands of multiscale analysis in control population vs different cardiopathy conditions: (a) Controls from Physionet (1D) vs CHF patients from Physionet (1D); (b) Controls from Physionet (1D) vs CHF patients (7D) from LTM database; (c) Controls from Physionet (1D) vs AF patients (7D) from LTM database. From left to right columns, the MSE, MTI, and MFS confidence bands and their differences are included.

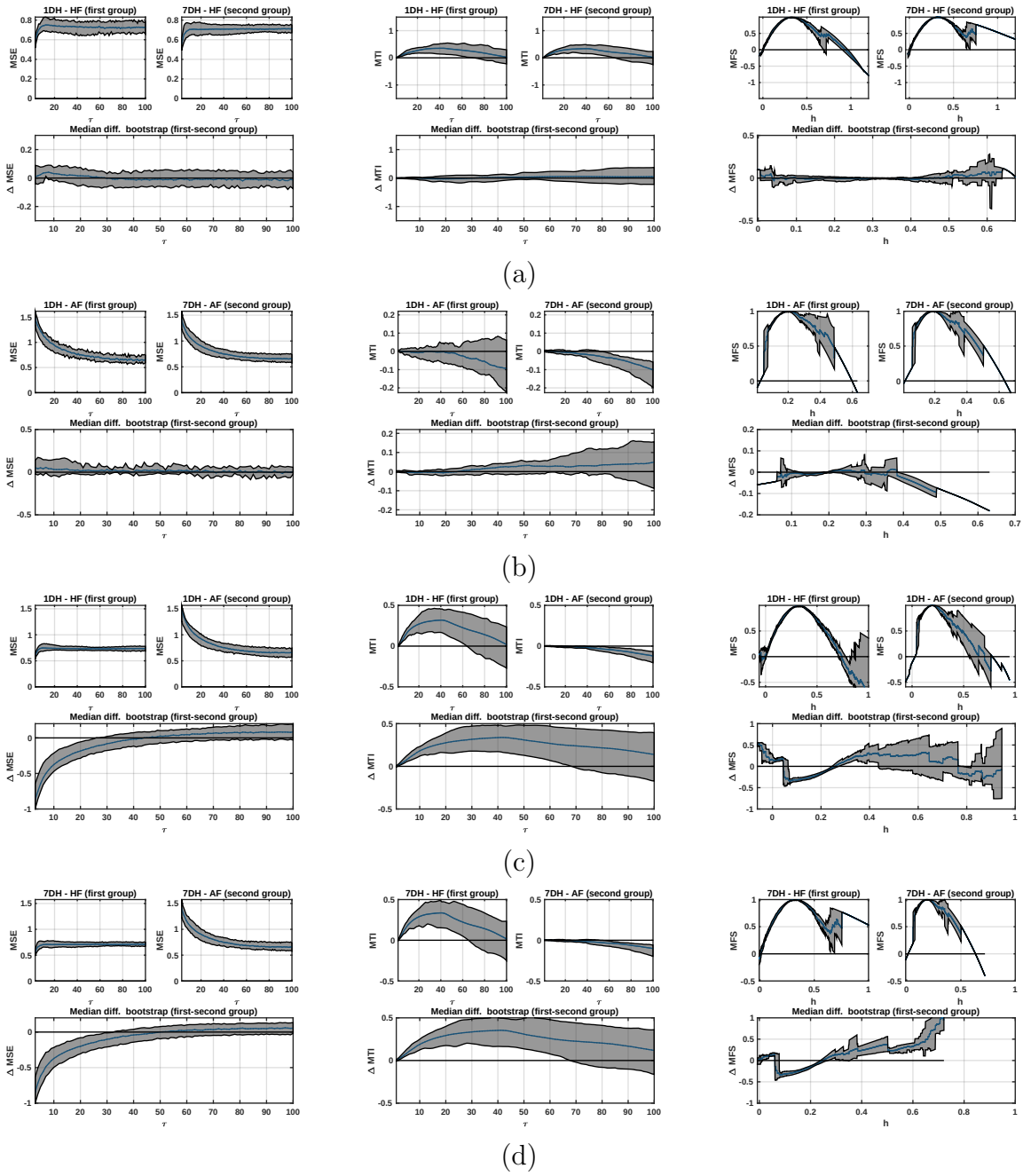


Figure 3.8: Confidence bands of multiscale analysis in LTM database: (a) Paired 1D vs 7D in CHF patients; (b) Paired 1D AF vs 7D in AF patients; (c) Non-paired 1D CHF vs 1D AF patients; (d) Non-paired 7D CHF vs 7D AF patients. From left to right columns, the MSE, MTI, and MFS confidence bands and their differences are included.

# Chapter 4

# ANS Function Evaluation for CH Diagnosis Support Using Iris Color-Pixel Classification

## 4.1 Image Database

Heterochromia of the eye can be sometimes recognized by the naked eye. Thus, in the example shown in Fig. 4.1, the blue eye is abnormal in terms of noticeably different iris color, which is also confirmed by other signs such as a smaller pupil and subtle drooping of the upper eyelid. In other cases, when the difference is subtle, visual identification can be severely limited. In these cases, an automatic method can be extremely useful for supporting medical diagnosis, what is in line with the approach proposed in this work.

Iris images analyzed in this work were obtained from the Ophthalmology Service in Hospital Universitario Fundación de Alcorcón (HUFA) (Madrid, Spain). RGB color images were acquired under the same conditions of light, magnification, and exposition parameters. They were recorded with high resolution (Zeiss FF 450 plus Fundus IR, 768×576 pixel resolution) and stored with a digital image file system (451 Visupac Digital, version 3.2.1). To avoid the potential influence of external elements, pictures were centered in the iris by using a circle shaped frame overlapping the camera. Since the flash effect on the iris cannot be always completely removed, we made sure that the flash was focused on the pupil center when taking the image. The eyelashes presence was also minimized at this acquisition stage.

No primary information regarding the symptomatic side of the patient was known by the ophthalmologist who obtained the images. Clinical diagnosis were made by one of the authors (J.A.P-G), and they were in accordance with the diagnostic criteria of the ICH disorders [88]. A database with 11 patients was created, containing two iris images for each one (left and right eye). Three subject subsets were considered, namely, four subjects with symptomatic CH (Group 1), three control subjects (Group 2), and four with ophthalmic diseases affecting iris pigmentation (Group 3). The iris segmentation could not be done automatically with the usual Daugman algorithm [89], because the presence of flash made it fail sometimes, therefore, the segmentation was done manually by using two size-adjustable ellipses for each iris, one for the sclera outer edge and another one for the pupil contour. Figure 4.1 shows an example of the segmentation for the left and right

Figure 4.1: Screenshots of eyes in a patient with pigmentation deficit when heterochromia is visible to the naked eye.

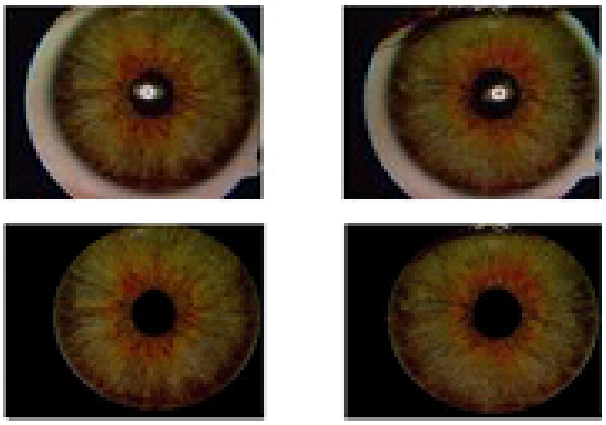

Figure 4.2: Example of right and left iris images (up) and their corresponding segmentation (down).

iris in a subject of our database.

As far as the property which is scrutinized to be used as CH biomarker is conceptually simple (color differences between pixels from both iris), one could thing in using simple statistics on the color image, but we checked that it is not so straightforward. Figure 4.3(a) shows the histogram of the segmented irises for the red component (RGB space) in a control case (no CH). Example of histograms for a patient with CH are in Figure 4.3(b). Note that the histogram shape for both irises is similar for the control case, and also are their means and standard deviations. However, some differences may be observed in the CH example both in the histogram shape and in their corresponding basic statistics. Nevertheless, simple statistics may not be sufficient for providing a good-quality biomarker. Figure 4.4 depicts the scatter plot of the iris pixels when using the three components of the color space (Lab and RGB color space in these examples), showing that complex joint distributions can be further more informative. In addition, the joint distribution can be changing with the subject and with the color space. These observations represent the rationale for proposing a classification strategy from machine learning techniques.

## 4.2 Support Vector Classifier Approach

In this work, we propose a statistical-learning approach to support the diagnosis of CH from iris color differences in the patient's eyes. We propose to use a Support Vector Classifier (SVC) because of its model robustness and good generalization capabilities,

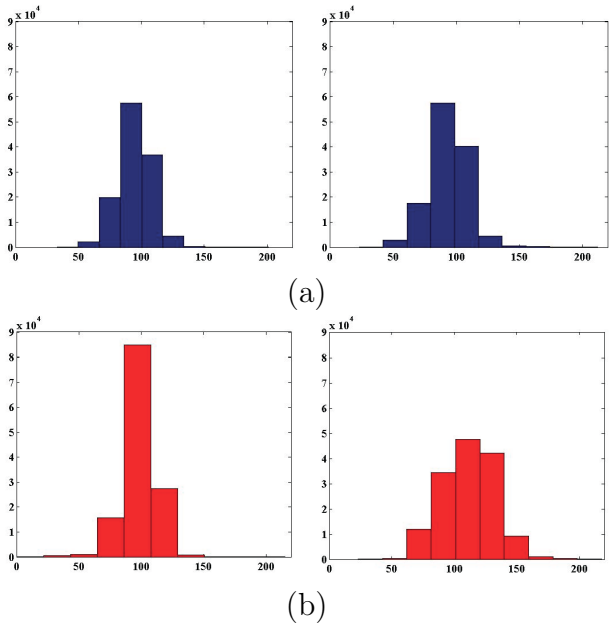

Figure 4.3: Histograms of the red component in the RGB space (after segmentation) for the iris images (mean ± std, CI) of a patient: (a) with no CH, right iris (mean=95.2, std=13.4), left iris (mean=93.5, std=16.0); and (b) with CH, right iris (mean=98.1, std=13.6); left iris (mean=111.7, std=20.8).

arising from the structural risk minimization principle. The SVC principles were developed by Vapnik for the first time [90], and this classifier has been after applied to tackle a dramatically huge number of tasks [91].

The design of statistical classifiers as SVC is conducted by a set of $N$ training samples $\{\underline{x}_i, y_i\}_{i=1}^{N}$ where $\underline{x}_i$ is the input multivariate sample (also named input feature vector) and $y_i$ is a categorical variable indicating the corresponding label (desired output of the model). From a conceptual point of view, the simplest classifier has just to distinguish between two classes, then coding $y_i$ with binary labels +1 and -1. The aim of the SVC is to find the optimal decision boundary based on the maximum margin from the boundary to the training samples of each class. Note that the boundary is just a line in the two-dimensional space, which readily extrapolates to a hyperplane in high dimensional spaces. The decision function can be shown [90] to be expressed as

$$f(\underline{x}) = \sum_{i=1}^{L} \alpha_i y_i \langle \underline{x}_i, \underline{x} \rangle + b \tag{4.1}$$

where $\langle ., . \rangle$ denotes the inner product, $L$ is the number of training samples contributing to build the decision boundary, $\alpha_i$ are the Lagrange multipliers obtained during the optimization process, and $b$ is the interception or bias term. Samples with a non-zero Lagrange multiplier are known as support vectors.

When samples are not linearly separable in the original input space, Equation (4.1) does not provide good performance, and input feature vectors are instead nonlinearly mapped to an intermediate high dimensional feature space. In this case, the SVC constructs an optimal hyperplane in the intermediate space, corresponding to a nonlinear decision

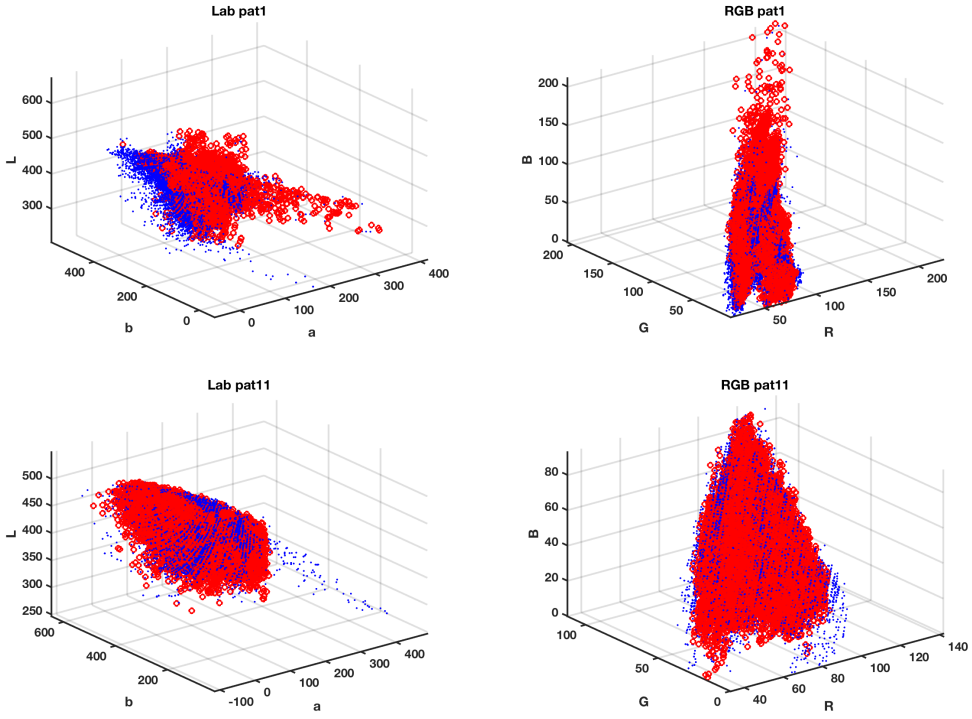


Figure 4.4: Pixel scatter plot in the Lab (left) and in the RGB (right) space for a patient with (up) and without (down) CH. Red circles (blue points) are associated to the right (left) iris pixels.

boundary in the input space. The expression for the decision function can be shown [90] to be as follows,

$$f(\underline{x}) = \sum_{i=1}^{L} \alpha_i y_i K(\underline{x}_i, \underline{x}) + b \tag{4.2}$$

where $K(.,.)$ is a Mercer kernel holding the nonlinear mapping. In our work, the Radial-Basis Function (RBF) kernel has been used, due to its good performance in many other problems. The RBF kernel, which corresponds to a spherical Gaussian function, has the following expression:

$$K(\underline{x}, \underline{x}_i) = \exp\left(-\frac{||\underline{x} - \underline{x}_i||^2}{2\sigma^2}\right) \tag{4.3}$$

where $\sigma$ refers to the Gaussian width, which best value has to be found. When samples of two classes are not fully separable in the transformed space, the SVC includes a penalty term of the structural risk, which is weighted by hyperparameter $C$ in the optimization process. For large $C$ values, the optimization will choose a lower margin hyperplane if it achieves a good classification in training. Conversely, a very small value of $C$ will cause the optimization to look for a separation hyperplane with a higher margin, even if the hyperplane misclassifies more training samples [90].

The proposed method for quantifying the presence of differences in pigmentation between both eyes uses the pixel color features of each patient iris as input vectors. This way, every component of the color space is an input feature to the classifier. For every patient, iris pixels are randomly separated into two subsets, so-called training and test

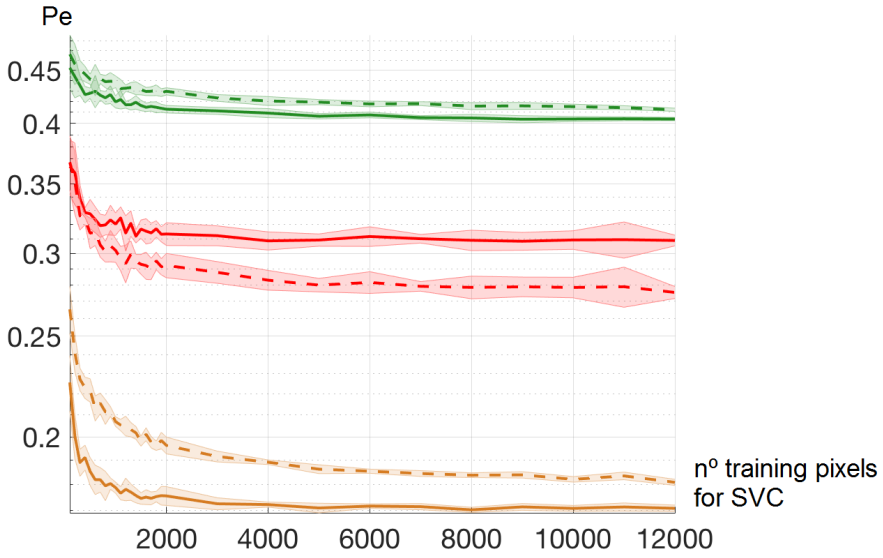


Figure 4.5: Study on the required number of training pixels for the machine learning classification, benchmarked on a control subject (green), on a different pathology (orange) and on a CH patient (red), when using SVC (continuous) and $k$-NN (dashed) classifiers. Shaded bands depict the mean $\pm$ standard deviation of 10 realizations.

subsets. The training subset is used to build the SVC, and the test subset is used to provide with an estimation of the classification error probability, denoted as $P_e$. Note that that this separation between training and test subsets allows to check the generalization capabilities of the SVC by using for this purpose the test pixels, which are different from those used to adjust the SVC parameters. In addition, and since the RBF kernel implicitly uses the Euclidean distance as a similarity measure between vectors, input features are here scaled to a similar range before building the SVC. In our work, each feature was normalized to have zero mean and unit variance.

Hence, the $P_e$ from an SVC on the iris pixels of both eyes can be used as a simple biomarker for a patient, and it can support the clinician on determining whether a patient could have CH in terms of the presence of color differences, as indicated by a reduced $P_e$. In those patients with other pathologies in which the differences in the eye-color are well-known, this method is not necessarily to be run. However, the usefulness for the clinical diagnosis would be focused on those cases of CH which remain asymptomatic but they still can exhibit subtle differences in color.

## 4.3 Experiments and Results

Several experiments were performed in order to determine the most appropriate color space and the classifier parameters ensuring the best system operation. On the one hand, the number of pixels required for training was initially scrutinized, together with a succinct comparison of several classifier architectures. On the other hand, the suitability of different color spaces was analyzed, e.g. RGB, Lab or HSV. In addition, the impact of the possible presence of image structures was tackled by analyzing iris sectors of $45^o$ and comparing

the right and left eyes in different color spaces. Finally, the effect of considering as input features the pixel neighborhood and therefore information about local variability was analyzed.

### 4.3.1 Number of Training Pixels for SVC Learning

Given that we are going to build machine learning classifiers for providing a $P_e$, and given that it is built with pixels on iris images, the number of available pixels is extremely high, and it is unnecessary to use all of them for training the machine. In addition, the use of a too high number of input vectors for training would lead to a excessive computation time and complexity. Therefore, we first addressed the analysis of how many training samples were needed for yielding suitably trained classifiers.

On the other hand, it was also considered convenient to benchmark the SVC with some other classifier, in order to make sure that it represents an adequate classifier structure to be used in this problem. We chose to use the well-known $k$ nearest neighbors ($k$-NN), in which the classification of a sample is established by voting of the labels associated to its $k$ nearest neighbors in terms of the Euclidean distance [92]. In this statistical classifier, only a free parameter ($k$) has to be tuned, and it has been often proven to be strongly competitive with other classifiers, despite its conceptual simplicity [93].

Accordingly, the following experiment was conducted to determine the suitable and lower enough size of the training set in our problem. After extraction of pixels from both irises in each patient, a partition of samples was made, taking $n_p$ pixels for the training set and the same number of pixels for the test set. The free parameter tuning was made using conventional cross-validation [94] in the training set. The ranges searched for $C$ parameter in the SVC classifier was $[1, 10^5]$, and for $\gamma = \frac{1}{2\sigma^2}$ parameter it was $[10^{-12}, 10^3]$. In the $k$-NN classifier, the search range for $k$ was $[1, 20]$. We run 10 realizations for randomly selecting the training and the test set from the complete set of pixels.

Figure 4.5 shows the results in terms of $P_e$ in two subjects, one being a control and the other a CH patient. It can be seen that, for both classifiers, a higher $P_e$ is obtained in the control subject. Note that the $P_e$ is not 0.5, as would correspond to a perfectly matched color distribution in both eyes, but instead its value tends to be around 0.4. The $P_e$ value obtained with the CH patient is in this case noticeably lower. Also, the $P_e$ is in general lower for SVC than for $k$-NN, which is more patent in the CH patient, which gives the rationale for choosing the SVC as classifier for building the CH biomarker. Finally, note that about $n_p = 2000$, the SVC reaches its stability, hence this was considered a sufficient size for the training set in subsequent experiments.

### 4.3.2 Color Spaces

Different color spaces are usually considered in color image processing depending on the scene characteristic and the ultimate goal. Thus, while the RGB color space is characterized because the three components (red, green and blue) are necessary to define the color, other spaces are characterized because they consider two components for describing the chromatic information and one component for the achromatic part [95, 96].

This section scrutinizes the suitability of different color spaces in our system. In addition to the original RGB color space, we benchmarked its normalized version $RG_n$,

where the effect of normalization is reducing the dependence between the red and green components on the brightness, being possible to omit the third component and hence reducing the space dimensionality [97]. Other color spaces based on linear and non-linear transformations of their components have been proposed [96, 98]. We have also considered the Fleck color space [98], based on logarithmic transformations of the RGB components and one of the so-called opponent color spaces. The Fleck transformation is physiologically motivated by the way that the human visual system transforms the RGB values into an opponent color vector with one achromatic and two chromatic components. The Otha color components have been considered too [99]. They are obtained as a linear transformation of the RGB space, proposed when trying to derive three orthogonal color features with large discriminant power on a representative sample of images. The family of perception-based models are quite intuitive to humans because they are related to human color perception (color, saturation, and luminance): e.g., HSI (hue-saturation-intensity) and HSV (hue-saturation-value), which are cylindrical color spaces based on a non-linear transformation of the RGB space [96]. Finally, the CIE Lab (L for lightness, a and b for the color) space has been also considered because, in addition to separate chromatic and achromatic components, distance relations (Euclidean) are in accordance with perceptual color differences. The separability of pixels belonging to the left and right iris was benchmarked for each patient when considering as input features the six color spaces previously presented (RGB, HSI, HSV, Otha, Fleck and Lab).

The estimated mean error probability on the test set for each patient is shown in Table 4.1 for the $k$-NN classifier, and in Table 4.2 for the SVC.

In general terms, the error rate for the SVC is lower than for $k$-NN. Regarding the input features, and though there are no features working best for all patients, we could state that: (1) color spaces Lab, RGB-Lab, and HSI provide reasonable results when considering the three components of the color space; (2) $ab$ components are the best when just considering chromatic components; and (3) HV and Lb could be selected when choosing the achromatic component and one of the chromatic components, though there are some contradictory trends for some patients. Taking into account these conclusions and analyzing the values of $P_e$, we conclude that input features containing the $ab$ components would be the most appropriate for our purpose. This is in accordance with the similarity measure implicitly considered by the statistical classifiers of this work, since both are based on the Euclidean distance. Nevertheless, other options should not be discarded, such as HSI or RGB-Lab.

### 4.3.3 Effect of Neighbor Pixels and Textures

In the previous experiments, the usefulness of different color components as input features to the classifier has been scrutinized on a pixel-basis. Despite the color being a pixel property, it is reasonable to analyse whether the color of a given pixel could be better represented by the color of its neighboring pixels. For this purpose, a new feature space was generated by increasing the size of the $3 \times 1$ vector given by the three components of the pixel in any color space with those provided by the three components associated to its 8 neighbouring pixels. Thus, the new feature space is represented by a vector of 27 elements. On the other hand, to get a better characterization of the iris texture, we increased the neighbouring size to a distance of 2 pixels. This is, each pixel can be characterized by a vector of 75 elements (25 values per neighborhood and color component).

| **Group** | Pat. no. | RGB | Lab | La | Lb | ab | HSI | IH | IS | $HS_{HSI}$ |
|---|---|---|---|---|---|---|---|---|---|---|
| | | HSV | VH | VS | $HS_{HSV}$ | $RG_n$ | Fleck | Ohta | RGBLab | |
| | 1 | 0.34 | 0.32 | 0.34 | 0.35 | 0.32 | 0.35 | 0.34 | 0.33 | 0.35 |
| | | 0.31 | 0.38 | 0.34 | 0.39 | 0.34 | 0.54 | 0.30 | 0.31 | |
| | 2 | 0.37 | 0.39 | 0.40 | 0.41 | 0.42 | 0.40 | 0.41 | 0.41 | 0.42 |
| **1** | | 0.39 | 0.39 | 0.42 | 0.43 | 0.42 | 0.50 | 0.39 | 0.41 | |
| | 3 | 0.43 | 0.45 | 0.49 | 0.48 | 0.48 | 0.47 | 0.48 | 0.45 | 0.45 |
| | | 0.46 | 0.45 | 0.48 | 0.47 | 0.47 | 0.51 | 0.46 | 0.47 | |
| | 9 | 0.39 | 0.38 | 0.41 | 0.40 | 0.44 | 0.41 | 0.41 | 0.40 | 0.44 |
| | | 0.38 | 0.41 | 0.44 | 0.43 | 0.45 | 0.42 | 0.38 | 0.41 | |
| | 4 | 0.44 | 0.40 | 0.45 | 0.44 | 0.41 | 0.43 | 0.45 | 0.42 | 0.43 |
| | | 0.39 | 0.46 | 0.44 | 0.43 | 0.44 | 0.47 | 0.42 | 0.41 | |
| | 8 | 0.37 | 0.38 | 0.40 | 0.43 | 0.46 | 0.37 | 0.39 | 0.42 | 0.41 |
| **2** | | 0.35 | 0.42 | 0.42 | 0.43 | 0.40 | 0.49 | 0.36 | 0.38 | |
| | 11 | 0.43 | 0.43 | 0.46 | 0.46 | 0.46 | 0.44 | 0.46 | 0.47 | 0.44 |
| | | 0.45 | 0.47 | 0.47 | 0.46 | 0.45 | 0.50 | 0.44 | 0.45 | |
| | 5 | 0.19 | 0.18 | 0.21 | 0.24 | 0.22 | 0.21 | 0.20 | 0.27 | 0.24 |
| | | 0.22 | 0.19 | 0.29 | 0.25 | 0.24 | 0.53 | 0.21 | 0.21 | |
| | 6 | 0.22 | 0.20 | 0.41 | 0.27 | 0.24 | 0.20 | 0.35 | 0.24 | 0.26 |
| | | 0.23 | 0.41 | 0.23 | 0.23 | 0.23 | 0.49 | 0.20 | 0.21 | |
| **3** | 7 | 0.28 | 0.31 | 0.30 | 0.38 | 0.31 | 0.29 | 0.34 | 0.39 | 0.44 |
| | | 0.29 | 0.31 | 0.35 | 0.44 | 0.44 | 0.50 | 0.29 | 0.33 | |
| | 10 | 0.17 | 0.20 | 0.22 | 0.22 | 0.22 | 0.18 | 0.23 | 0.22 | 0.24 |
| | | 0.18 | 0.25 | 0.26 | 0.24 | 0.23 | 0.52 | 0.17 | 0.17 | |

Table 4.1: Mean $P_e$ on the test partitions when applying the $k$-NN classifier on the iris pixels of each patient (rows, organized according to the group they belong to). Double column header represents two designs, each one with a different feature space (values in cells keep the order in the column header).

Figure 4.6 shows the comparison of input spaces as given by individual pixels and when extending to 8 neighbors, and more neighbors (texture). Classifiers were trained and tested with 5,000 and 10,000 samples, respectively. Results are shown for the Lab input space. The $k$-NN classifier shows a defined trend to bring closer all the cases in terms of $P_e$ with increasing size of the pixel neighborhood, whereas the SVC is less sensitive to the increase of the pixel neighborhood. Nevertheless, there is a trend in some specific cases (specially for patient P4 in the figure) for which $P_e$ decreases despite being a control case. Then, it can be concluded for this problem that feature spaces just associated with individual pixels are better suited than extended spaces considering neighborhood pixels.

### 4.3.4 Iris Image-Region Analysis

In previous experiments, we considered the whole iris area and different number of neighbors and components of the color space as features to design the statistical classifier. In addition, some structures can be expected to be present in iris images, like spots or patches, which could modify the color structure and affect the performance of the SVC in this setting. We conducted an experiment for the analysis of the iris by taking the pixels in sectors of $45^o$, as depicted in Figure 4.7. The features used for this purpose were components of the

| **Group** | Pat. no. | RGB | Lab | La | Lb | ab | HSI | IH | IS | $HS_{HSI}$ |
|---|---|---|---|---|---|---|---|---|---|---|
| | | HSV | VH | VS | $HS_{HSV}$ | $RG_n$ | Fleck | Ohta | RGBLab | |
| | 1 | 0.32 | 0.29 | 0.34 | 0.32 | 0.37 | 0.33 | 0.33 | 0.36 | 0.38 |
| | | 0.30 | 0.36 | 0.32 | 0.34 | 0.35 | 0.47 | 0.29 | 0.28 | |
| | 2 | 0.38 | 0.40 | 0.41 | 0.42 | 0.40 | 0.40 | 0.41 | 0.42 | 0.41 |
| **1** | | 0.38 | 0.39 | 0.41 | 0.41 | 0.41 | 0.49 | 0.38 | 0.38 | |
| | 3 | 0.44 | 0.46 | 0.47 | 0.48 | 0.46 | 0.46 | 0.47 | 0.46 | 0.46 |
| | | 0.45 | 0.47 | 0.47 | 0.47 | 0.47 | 0.49 | 0.44 | 0.45 | |
| | 9 | 0.37 | 0.36 | 0.38 | 0.38 | 0.42 | 0.36 | 0.40 | 0.39 | 0.42 |
| | | 0.34 | 0.40 | 0.39 | 0.43 | 0.43 | 0.51 | 0.34 | 0.37 | |
| | 4 | 0.42 | 0.39 | 0.43 | 0.42 | 0.44 | 0.40 | 0.45 | 0.42 | 0.42 |
| | | 0.39 | 0.44 | 0.43 | 0.40 | 0.40 | 0.45 | 0.41 | 0.37 | |
| | 8 | 0.36 | 0.37 | 0.35 | 0.42 | 0.43 | 0.38 | 0.37 | 0.41 | 0.42 |
| **2** | | 0.38 | 0.42 | 0.42 | 0.41 | 0.43 | 0.50 | 0.35 | 0.32 | |
| | 11 | 0.43 | 0.43 | 0.44 | 0.43 | 0.40 | 0.45 | 0.45 | 0.43 | 0.42 |
| | | 0.48 | 0.43 | 0.45 | 0.44 | 0.43 | 0.50 | 0.43 | 0.41 | |
| | 5 | 0.19 | 0.18 | 0.20 | 0.24 | 0.22 | 0.20 | 0.19 | 0.26 | 0.25 |
| | | 0.19 | 0.18 | 0.25 | 0.27 | 0.21 | 0.52 | 0.20 | 0.17 | |
| | 6 | 0.22 | 0.21 | 0.39 | 0.25 | 0.21 | 0.19 | 0.34 | 0.24 | 0.24 |
| | | 0.22 | 0.38 | 0.20 | 0.23 | 0.23 | 0.48 | 0.19 | 0.18 | |
| **3** | 7 | 0.28 | 0.27 | 0.27 | 0.45 | 0.39 | 0.29 | 0.30 | 0.39 | 0.46 |
| | | 0.27 | 0.29 | 0.34 | 0.45 | 0.43 | 0.49 | 0.28 | 0.27 | |
| | 10 | 0.17 | 0.16 | 0.19 | 0.19 | 0.22 | 0.17 | 0.20 | 0.19 | 0.23 |
| | | 0.17 | 0.19 | 0.23 | 0.23 | 0.23 | 0.48 | 0.16 | 0.15 | |

Table 4.2: Mean $P_e$ on the test partitions when applying the SVC classifier on the iris pixels of each patient (rows, organized according to the group they belong to). Double column header represents two designs, each one with a different feature space (values in cells keep the order in the column header).

previously analyzed RGB-Lab space.

We analyzed two strategies. Firstly, a classifier was designed using only those pixels of the same iris angular sector on each eye. This approach aimed to account for the presence of structures and for regional differences, being more noticeable in some sectors than in others. Secondly, the impact of including pixels from increasingly accumulated sectors was also studied. Each classifier was trained with 5,000 samples and tested with 10,000 samples for getting the $P_e$.

Figure 4.8 shows that the four patients in Group 3 (P5, P6, P7 and P10) generally exhibited a noticeable reduced $P_e$, which was consistent throughout all the angles, although for some sectors their $P_e$ was increased. In general terms, the concatenation of all sectors softened its $P_e$ and made it constantly low. Also, the three healthy subjects in Group 2 showed a consistently increased $P_e$, both in every sector (with some occasional drop in $P_e$) and in the accumulated.

However, results on CH patients in Group 1 exhibited a more complex behavior. In the accumulated classifiers, patients P1 and P9 were readily and consistently identified by the classifiers, P2 showed a trend to be identified but still it remained in the $P_e$ values of control subjects, and P3 could not be identified and exhibited in general a high $P_e$. On

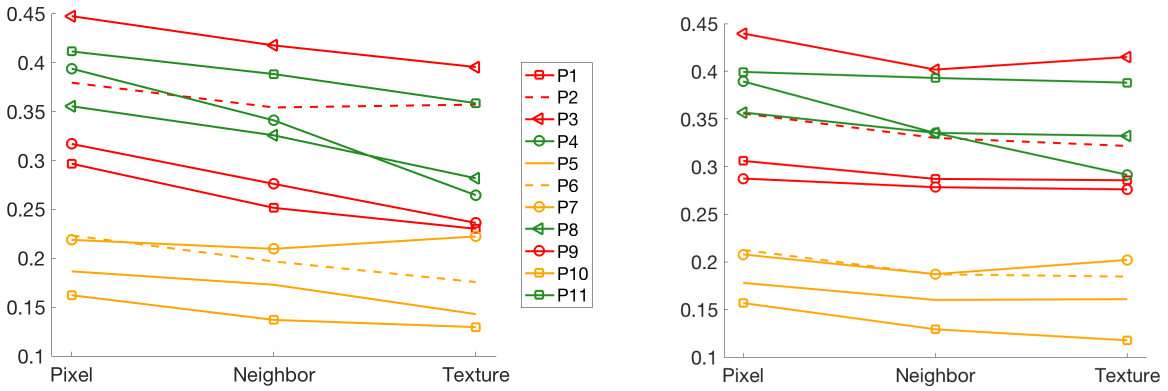


Figure 4.6: Comparison of the mean $P_e$ obtained when considering three approaches (one pixel-based and two extensions to the neighbor pixels, see the abscisas axis), both for $k$-NN (left panel) and SVC (right panel) classifiers.

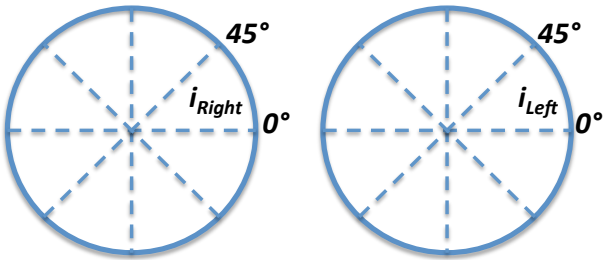


Figure 4.7: Scheme of the iris segmentation in sectors of $45^o$ for evaluating the impact of image structures on the classifier performance.

the other hand, the identification by accounting for each sector separately exhibited a larger variance, nevertheless, some sectors were more adequate to better separate Groups 1 and 3 from 2, namely, sectors of 180-225 degrees, and 270-315 degrees. Overall, a perfect discrimination could not be achieved. Iris images of patients P2 and P3 often showed a behavior strongly overlapping with an increased $P_e$, which not seems to support the hypothesis that the iris color features can provide with a universal criterion for CH detection, at least as considered in this work. By visual iris inspection on our database, we consider this can be mainly due to two facts: First, the iris tissue in those cases actually contains a variety of spots and marks; and second, the subtle differences in color are in these cases more patent on some sectors. Therefore, even when the sector analysis increases its sensitivity, the reduction in the number of pixels makes it more sensitive to spots and marks.

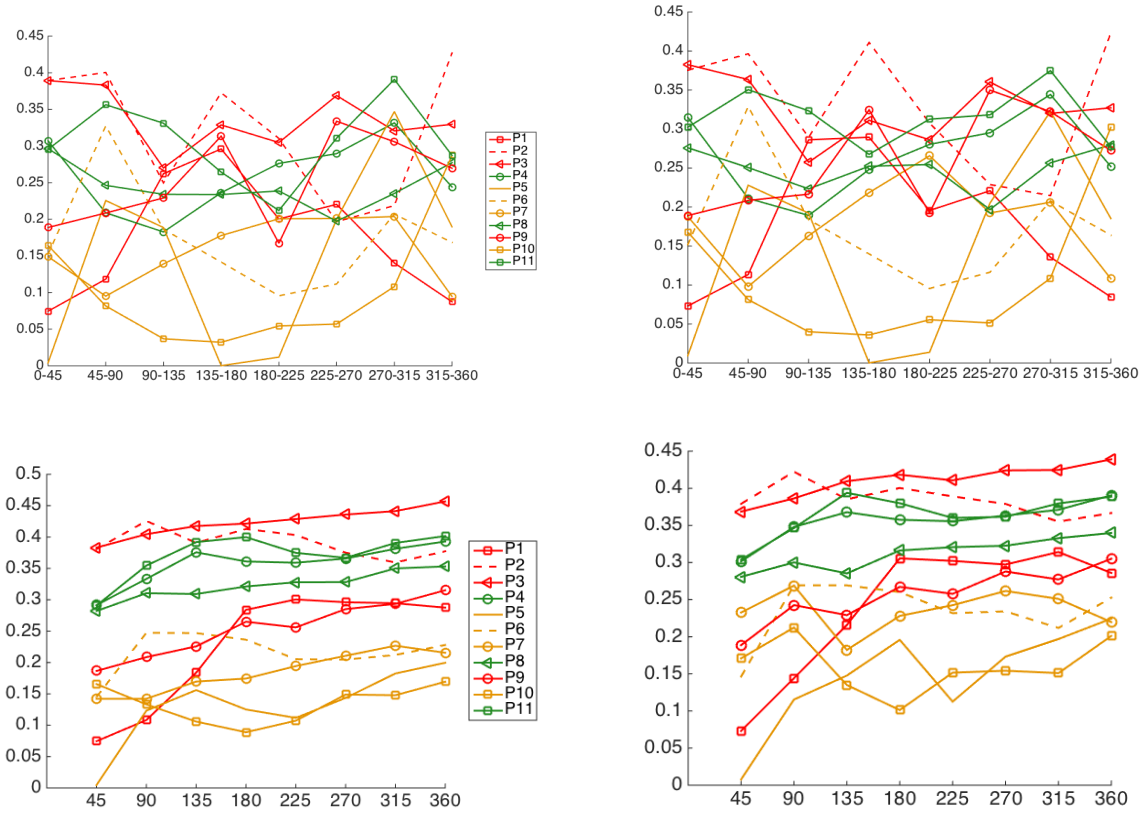


Figure 4.8: Study of the $P_e$ per iris sector (abscissa axis), for each separate sector (top) and for accumulated sectors (bottom), using $k$-NN (left panels) and SVC (right panels).

# Chapter 5

# Conclusions and Future Works

## 5.1 Conclusions

### 5.1.1 Nonlinear Dynamics and Multiscale Indices in Holter LTM

In this work, we have addressed the calculation of three representative multiscale indices, namely, MSE, MTI, and MFS, on 1-day and 7-day Holter recordings. From our results, we can conclude that, when present, the trends are consistent between the additional scales provided by 1-day recordings and by the 7-day recordings, but the second ones can give a statistically better view of this kind of representations, specially in the MFS representations.

#### Contributions

Several preceding results can be found in which descriptions of 1-day estimated indices are shown, however few works address from this perspective the 7-days case with scales up to 100. Accordingly, and given the advances in the monitoring and well-being technology in our days, this represents a good moment to determine the possible advantages and issues of using these methods in larger observation scales. Non-linear methods used in this work (MSE, MTI, and MFS) have previously been proposed and widely used in the literature. The contributions of our work are twofold. On the one hand, we analyzed the dynamics, the consistency, and especially the robustness of these indices when applied to the new long term scenarios (7 days) and to point out that algorithms may need to be improved when using them in this area. On the other hand, to find out if further information is conveyed in the temporal scales that have not been analyzed before in shorter recordings.

#### Summary and Discussion of Results

Results showed significant differences between CHF and AF populations not only for short-term scales but also for long-term and very long-term scales in some indices, MSE (MTI) being higher (lower) for AF. These results are consistent with previous studies [18, 19, 20]. Here we confirmed the same trends, but we also obtained several differences in very long-term scales that had not been analyzed before. MSE was not further significantly different for very long-term scales. This may be attributed to the fact that statistical characteristics of AF signals resemble those from noise, and being MSE a entropy-based

measure, it is higher for AF than for CHF for short-term and long-term scales, but not for very long-term scales, where the surrogate signals present attenuated these erratic characteristics. On the other hand, MTI shows that time irreversiblity is for all time scales lower in AF patients, i.e., for those presenting a more severe pathology.

We detected that 1-day estimations of the multiscale indices can show a distorted profile. The different estimations observed in the different time windows could be due to several reasons. In addition, this effect could have statistical roots, in terms of consistency and variance of the estimation with shorter time series. On the other hand, it also could be due to the fact that some frames had some properties in their dynamics which made the multiscale algorithm fail or disrupt. The differences in daily activities should not be a limitation, as far as the multiscale algorithm measurements are the correlations present in the signal at different time scales. In the conventionally used surrogate-signal test, which is built with lower-pass versions of the original signal, the more we increased the scales, the more the short-term relationships were eliminated to manifest the long-term. Thus, the short-term differences would be hidden for high scales. We thoroughly checked that the underlying signals did not have artifacts or aberrations with a specifically customized software to support an observer to watch at the heart-rate signals and at the original ECG signals simultaneously. Accordingly, one of our conclusions is that these multiscale algorithms, while likely informative, should trust not only on the increase of the length of the signals for their consistency, but also on improving their algorithmic robustness. Although stationarity can not often be assumed for HRV signals, MSE was originally proposed and applied in 24-hour Holter recordings, and later many other works have used MSE to study different dynamics in 24-hours. The analysis of the underlying dynamics during the day or night can be complex with these methods. Nevertheless, we observed that the disruption effect in one day does not have any significant impact in the 7-day analysis, which promotes their use in favor of improved statistical consistency.

**Usefulness of Median-difference Tests**

An extension of previously proposed statistical comparisons for scales has been proposed here in terms of nonparametric bootstrap resampling, which allows us to establish poblational comparisons in terms of the median difference of the multiscale representations, either for different health conditions, or for different acquisition conditions. Our results with this method were consistent with the results identified in the literature and showed some non-observed differences, specially the ones related with AF patients, and with different statistical consistency behavior and retrieved information about the patient given by these three multiscale indices, which suggests their use jointly in these and other populations.

**Related Relevant LTM Applications**

With the technological availability of cardiac monitoring systems for extended time periods, LTM is expected to bring interest to new applications in health, wellness, and research. For instance, it has been recently pointed out [71] that energetic environmental phenomena can affect psychophysical processes on people in different ways depending on their sensitivity, health status, and ability of the ANS to self-regulate. In that study, the HRV was recorded for 72 consecutive hours per week over a five-month period in 16 participants, in order to

examine ANS responses during normal background environmental periods. Interestingly, HRV measurements were negatively correlated with the solar wind speed, and the low-frequency and high-frequency power were negatively correlated with the magnetic field. This study confirmed that the daily activity of the ANS responds to changes in geomagnetic and solar activity during periods of undisturbed normal activity, it starts at different times after changes in various environmental factors, and it persist for variable time periods. As far as the activity of the ANS reflected by HRV measurements is affected by solar and geomagnetic influences, the analysis of HRV should take into account these effects when possible. This study is focused on the ANS modulation, and hence spectral measurements were mostly used, nevertheless, this kind of data could be analyzed with multiscale indices to provide with a wider view on the long-term behaviour of HRV.

#### On the Clinical Usefulness of Multiscale Indices

As described with detail in [11], many indices have been proposed in the last years to develop risk stratification from different kinds of analysis of electric cardiac signals. However, these techniques from the academic research world rarely are used in the clinical practice. In that reference, our team analyzes the possible reasons by decoupling the sometimes limited accuracy and the lack of consensus on the robustness with the appropriate signal processing implementations. In this line of search, the present work aims to first establish the need for robustness in the methods that are widely used nowadays, as a requirement before enrolling in risk stratification studies, which require high-cost and high effort to yield clinically useful use to these techniques. Our future research would consider first to perform the same multiscale analysis (MSE, MTI, and MFS) in LTM healthy subjects, in order to study the dynamic behavior in normal conditions when increasing the number of scales. As indicated, the development of more robust multiscale indices is a desirable target in order to continue to progress in this informative characterization of the cardiac dynamics. On the other hand, AF and CHF are different heart diseases with different dynamics, though in this study we only could analyze AF patients as a subset of CHF patients. CHF is a syndrome of the deterioration in short-term and long-term regulatory mechanisms, while AF, and especially the persistent one, is an intrinsic short-term mechanism. Whereas long-term mechanisms can be present in AF, it seems that LTM recordings should be better used to analyze their presence or deterioration.

### 5.1.2 ANS Function Evaluation for CH Diagnosis Support Using Iris Color-Pixel Classification

A SVC-based approach was developed with the aim to support the diagnosis detection system of CH by an automatic system. Statistical analysis of its performance was based on sample-based algorithms for learning to classify the pixels of each iris image of the same individual. The corresponding error probability when classifying iris image pixels of an individual is inversely associated to the risk the individual suffers from CH.

We obtained better CH identification results with features containing both luminance and chrominance information. Also, the SVC was a good option as machine learning classifier to be used in this task. Moreover, some color spaces were found to be more suitable (Lab, RGB, and HSI). And finally, single-pixel input spaces were found to be

better than pixel-neighborhood input spaces. However, CH patients with extremely subtle changes in their eye color could not always be identified by the method. Though this could be alleviated by considering more reduced regions of the iris for increasing its sensitivity to color differences, it also increases the sensitivity of the method to marks and spots.

From a clinical viewpoint, the implications of this study can be relevant. According to recent works, newborns have an inherited and indeterminate iris coloration, which is performed during the first months of life by the cell-coating activity (melanophors). The sympathetic nervous system exerts a trophic action on the activity of the melanophors. When there is a congenital or acquired sympathetic defect in the neonatal period, pigmentation deficiency occurs in the side of the sympathetic hypofunction [27, 28]. This results in hetherochromia, which can be noted in the different colored eyes, typically blue and brown, the clearer iris being the defectively pigmented one. Some headaches (typically CH) occur with strictly unilateral pain centered in the ocular region. During symptomatic periods, a sympathetic deficit on the side of the pain causes ptosis, and miosis is developed. Both signs of sympathetic hypofunction are known as Horner's syndrome. If there is a latent defect in the sympathetic side of pain that occurs during the symptomatic periods, then decreased pigmentation of the iris in that side could also exist. In that case, sometimes the sympathetic defect has occurred in the neonatal period, or sometimes it can be congenital [28][100].

## 5.2 Future Works

### 5.2.1 Nonlinear Dynamics and Multiscale Indices in Holter LTM

Despite the need for more robust algorithms in long-term nonlinear indices, we still consider that the effort is worth to use these indices, as vast literature supports their informativeness in other scenarios in addition to the very long-term monitoring. In general terms, the underlying hypothesis in precedent studies is that heart rate oscillations respond to phenomena with very different characteristic times, ranging from seconds to months. The former are well evaluated in a 24-hour recording, but the low frequency (such as circadian cycles, many hormonal cycles, or secondary to changes in activity during the week) would only be represented in long-term monitoring. The response to these stimuli has been moderately studied, but it could provide us with interesting information on some clinical aspects, such as the prediction of decompensation in heart failure, the evolution of cardiovascular remodelling after acute injury (e.g., in the weeks following acute myocardial infarction), the evolution of sports training, or the susceptibility to the development of malignant arrhythmias (related with sudden cardiac death). All these aspects involve hormonal processes, inflammatory processes, adaptations of different organs or systems, and they are characterized by the interaction of mechanisms with slow response times, so that they develop in days or weeks, rather than in minutes or hours. Therefore, methods of analyzing the very long-term behavior of heart rate responses could be of interest, especially in noisy rhythms such as AF, in which almost all the usual HRV parameters are difficult to interpret. We still do not know if these methods will be widely used in the future clinical practice because we are still in the phase of describing how these indices behave, their variability, their comparison with the results in 24 h, among others. In any case, all these efforts should be supported by robust algorithms for multiscale nonlinear

indices, an idea that had not been previously paid much attention in the nonlinear HRV literature.

### 5.2.2 ANS Function Evaluation for CH Diagnosis Support Using Iris Color-Pixel Classification

The second work has been aimed to open the wave towards an automatic system. As such, it has highlighted the scope and limitations of the color as sole criterion. The main limitation of this study is the reduced number of available examples. A larger database will allow to create technically improved systems, likely improving the performance by efficiently and robustly accounting for the regional information of the iris.

The method has provided encouraging results, and it arises as a possibility to provide the clinicians with diagnostic support for early detection and screening of CH patients with a low-cost system.

Also it will be very interesting to use the entropy as a measure to compare between left and right eye of patients. On another hand the mutual Information (MI) is an alternative to adopt for the same comparison. Both methods can provide a good information so as to confirm our previous results.

Since deep learning is one of the ways of executing machine learning, and is, nowadays, a suitable method for extracting meaningful features from the raw data, we will consider this deep learning as a method in a future work.

The development of cluster headache analysis opened up another research topic, which would address the assessment of the pain degree that would then be used as an index of response to medication. As an example, it would be the case of patients in palliative cancer therapy avoiding the supply of overdose of pain relief medication.

# Bibliography


[1] S. R. Devasahayam. *Signals and Systems in Biomedical Engineering*. 2013.

[2] R. B. Northrop. *Signals and Systems Analysis in Biomedical Engineering*. 2010.

[3] G. Wong J. R. Chapman, A. C. Webster. Cancer in the transplant recipient. *Cold Spring Harb Perspect Med*, 3(7):1–16, 2013.

[4] W.H.O. *Recent Advances in Biological and Physical Sciences and Their Implications for Health Care*. 2000.

[5] WHO. *Cardiovascular disease*, 2016. `http://www.who.int/topics/cardiovascular\_diseases/en/` (accessed 08 July 2018).

[6] WHO. International classification of diseases. Technical report, US Department of Health and Human Services, Centers for Disease Control and Prevention, Health Care Financing Administration, 2005.

[7] S. G. Priori, E. Aliot, C. Blomstrom-Lundqvist, L. Bossaert, G. Breithardt, P. Brugada, A. J. Camm, R. Cappato, S. M. Cobbe, C. D. Mario, B. J. Maron, W. J. McKenna, A. K. Pedersen, U. Ravens, P. J. Schwartz, M. Trusz-Gluza, P. Vardas, H. J. J. Wellens, and D. P. Zipes. Task force on sudden cardiac death of the european society of cardiology. *European Heart Journal*, 22(16):1374–1450, 2001.

[8] D. P. Zipes, A. J. Camm, M. Borggrefe, A. E. Buxton, B. Chaitman, M. Fromer, G. Gregoratos, G. Klein, A. J. Moss, R. J. Myerburg, S. G. Priori, M. A. Quinones, D. M. Roden, M. J. Silka, C. Tracy, S. C. J. Smith, A. K. Jacobs, C. D. Adams, E. M. Antman, J. L. Anderson, S. A. Hunt, J. L. Halperin, R. Nishimura, J. P. Ornato, R. L. Page, B. Riegel, S. G. Priori, J. J. Blanc, A. Budaj, A. J. Camm, V. Dean, J. W. Deckers, C. Despres, K. Dickstein, J. Lekakis, K. McGregor, M. Metra, J. Morais, A. Osterspey, J. L. Tamargo, and J. L. Zamorano. Guidelines for management of patients with ventricular arrhythmias and the prevention of sudden cardiac death: A report of the american college of cardiology/american heart association task force and the european society of cardiology committee for practice guidelines (writing committee to develop guidelines for management of patients with ventricular arrhythmias and the prevention of sudden cardiac death). *Journal of the American College of Cardiology*, 48(5):247–346, 2006.

[9] C. Soguero-Ruiz, I. Mora-Jiménez, J. Ramos-López, T. Q. Fernández, A. García-García, D. Díez-Mazuela, A. García-Alberola, and J. L. Rojo-Álvarez. An interoper-

able system toward cardiac risk stratification from ecg monitoring. *International Journal of Environmental Research and Public Health*, 15(3):428, 2018.

[10] J. Villacastín, R. Bover, N. Castellano, J. Moreno, R. Morales, and A. García-Espinosa. Risk stratification and prevention of sudden death in patients with heart failure. *Revista Española Cardiología*, 57(8):768–782, 2004.

[11] F. J. Gimeno-Blanes, M. Blanco-Velasco, O. Barquero-Pérez, A. García-Alberola, and J. L. Rojo-Álvarez. Sudden cardiac risk stratification with electrocardiographic indices - a review on computational processing, technology transfer, and scientific evidence. *Frontiers in Physiology*, 7(82):1–17, 2016.

[12] A. Corana, G. Bortolan, and A. Casaleggio. Most probable dimension value and most at interval methods for automatic estimation of dimension form time series. *Chaos, Solitons & Fractals*, 20(4):779–790, 2004.

[13] M. Malik, T. Cripps, T. Farrell, and A. Camm. Prognostic value of heart rate variability after myocardial infarction. a comparison of different data processing methods. *Medical and Biological Engineering and Computing*, 27(6):603–611, 1989.

[14] R. E. Klabunde. *Cardiovascular physiology concepts*. Lippincot Williams and Wilkings, Philadelphie, Pennsylvanie, USA, 2011.

[15] A. L. Goldberger, L. A. N. Amaral, L. Glass, J. M. Hausdor, P. Ch. Ivanov, R. G. Mark, J. E. Mietus, G. B. Moody, C.-K. Peng, and H. E. Stanley. Physiobank, physiotoolkit, and physionet: Components of a new research resource for complex physiologic signals. *Circulation*, 101(23):215–220, 2000.

[16] R. Goya-Esteban, I. Mora-Jiménez, J. L. Rojo-Álvarez, O. Barquero-Pérez, F. J. Pastor-Pérez, S. Manzano-Fernandez, D. A. Pascual-Figal, and A. García-Alberola. Heart rate variability on 7-day holter monitoring using a bootstrap rhythmometric procedure. *IEEE Transactions on Biomedical Engineering*, 52:1366–1376, 2014.

[17] M. El-Yaagoubi, R. Goya-Esteban, Y. Jabrane, S. Muñoz-Romero, J. L. Rojo-Álvarez, and A. García-Alberola. Multiscale entropy and multiscale time irreversibility for atrial fibrillation and heart failure from 7-day holter. In *Congreso Anual de la Sociedad Española de Ingeniería Biomédica*, Bilbao, Spain, 2017.

[18] M. Costa, A. L. Goldbergez, and C. K. Peng. Multiscale entropy analysis of complex physiologic time series. *Physical Review Letters*, 89(6):68–102, 2002.

[19] M. Costa, A. L. Goldberger, and C. K. Peng. Broken asymmetry of the human heartbeat: Lost of time irreversibility in aging and disease. *Physical Review Letters*, 95(19):102–198, 2005.

[20] M. Costa, C. K. Peng, and A. L. Goldberger. Multiscale analysis of heart rate dynamics: Entropy and time irreversibility measures. *Cardiovascular Engineering*, 8(2):88–93, 2008.

[21] Md Aktaruzzaman and R. Sassi. Parametric estimation of sample entropy in heart rate variability analysis. *Biomedical Signal Processing and Control*, 14:141—-147, 2014.

[22] H. E. Stanley, L. A. Amaral, A. L. Goldberger, S. Havlin, P. Ivanov, and C. K. Peng. Statistical physics and physiology: monofractal and multifractal approaches. *Physica A*, 270(1-2):309–324, 1999.

[23] P. Ivanov, A. Luis, A. L. Goldberger, H. Shalomo, H. E. Stanley, and Z. Struzik. From 1/f noise to multifractal cascades in heartbeat dynamics. *Chaos*, 11(3):641–652, 2001.

[24] T. Sarna A. Wielgus. Melanin in human irides of different color and age of donors pigment cell res. 18(6):454–64, 2005.

[25] E. Moore V. Silvestri C. C. Patterson A. P. Maxwell G. J. McKay A. McGowan, G. Silvestri. ©. *Invest Ophthalmol Vis Sci*, 56(1):382–387, 2014.

[26] Headache classification committee of the international headache society classification and diagnostic criteria for headache disorders, cranial neuralgia and facial pain. *Cephalalgia*, 8(7):1–96, 1988.

[27] Gladstone. Development and significance of heterochromia iridis. *Arch Neurol*, 21(2):184–192, 1969.

[28] M. Trigo O. Sjaastad J. A. Pareja, M. Espejo. Congenital horners syndrome and ipsilateral headache. *Funct Neurol*, 12(3-4):123–131, 1997.

[29] L. Mainardi, S. Cerutti, and L. Sörnmo. *Understanding Atrial Fibrillation, the Signal Processing Contribution*. Morgan and Claypool, San Rafael, CA (USA), 2008.

[30] C. H. Chen, P. W. Huang, S. C. Tang, J. S. Shieh, D. M. Lai, A. Y. Wu, and J. S. Jeng. Complexity of heart rate variability can predict stroke-in-evolution in acute ischemic stroke patients. *Nature*, 5:17552, 2015.

[31] H. Y. Liu, Z. Yang, F. G. Meng, Y. G. Guan, Y. S. Ma, S. L. Yang, J. L. Lin, L. S. Pan, M. M. Zhao, W. QU, H. W. Hao, G. M. Luan, J. G. Zhang, and L. M. Li. Preoperative heart rate variability as predictors of vagus nerve stimulation outcome in patients with drug-resistant epilepsy. *Nature*, 8(1):3856, 2018.

[32] E. Bradley and R. J. Tibshirani. *An introduction to the bootstrap*. CRC press, 1994.

[33] L. K. McCorry. Physiology of the autonomic nervous system. *American Journal of Pharmaceutical Education*, 71(4):1–11, 2007.

[34] W. Struhal R. D. Thijs M. Hilz H. Lahrmann, I. Rocha. Diagnosing autonomic nervous system disorders – existing guidelines and future perspectives. *European Neurological Review*, 6(1):52–56, 2011.

[35] M. Varacallo J. A. Waxenbaum. *Anatomy, Autonomic Nervous System*. 2019.

[36] S. S. Po Y. Wang, L. Yu. Ablation of neuroaxial in patients with ventricular tachycardia. *Card Electrophysiol Clin*, 11:625–634, 2019.

[37] Emile L. Boulpaep Walter F. Boron. *Medical Physiology second edition.* Elsevier SAUNDERS, 2009.

[38] L. W. Stevenson W. H. Maisel. Atrial fibrillation in heart failure: epidemiology, pathophysiology, and rationale for therapy. *The American Journal of Cardiology*, 91(6):2–8, 2003.

[39] M. Poglitsch R. M. Touyz J. C. Burnett Jr. C. Llorens-Cortes M. R. Ehlers E. D. Sturrock L. B. Arendse, A. H. J. Danser. Novel therapeutic approaches targeting the renin-angiotensin system and associated peptides in hypertension and heart. *American Society for Pharmacology and Experimental Therapeutics*, 71(4):539–570, 2019.

[40] M. Malik and al. Heart rate variability standards of measurement, physiological interpretation, and clinical use. *European Heart Journal*, 17:354–381, 1996.

[41] J. W. Christle D. Hadley D. Plews N. Singh, K. J. Moneghetti and V. Froelicher. Heart rate variability: An old metric with new meaning in the era of using mhealth technologies for health and exercise training guidance. part one: Physiology and methods. *Arryhthmia and Electrophysiology Review*, 7(3):193–8, 2018.

[42] K. S. Heffernan G. V. Mendonca, B. Fernhall and F. D. Pereira. Spectral methods of heart rate variability analysis during dynamic exercise. *Clin Auton Res*, 19(4):237–45, 2009.

[43] P. M. Blanche F. Badilini and P. Coumel. Heart rate variability in passive tilt test: Comparative evaluation of autoregressive and fft spectral analyses. *Pacing Clin Electrophysiol*, 21(5):1122–32, 1998.

[44] A. Luceño. On time-irreversibility and other non-linear features in time series. *Communications in Statistics-Simulation and Computation*, 29(1):295–313, 2000.

[45] M. Javorka D. Mokra M. Gala A. Jurko A. Calkovska Z. Visnovcova, M. Mestanik and I. Tonhajzerova. Complexity and time asymmetry of heart rate variability are altered in acute mental stress. *Communications in Statistics-Simulation and Computation*, 35(7):1319–34, 2014.

[46] A. Schirdewan A. Voss N. Wessel, A. Schumann and J. Kurths. Entropy measures in heart rate variability data. *Computer Science*, 1933:78–87, 2000.

[47] E. H. Jang S. Kim K. W. Choi H. Y. Yu S. Byun, A. Y. Kim and H. J. Jeon. Entropy analysis of heart rate variability and its application to recognize major depressive disorder: A pilot study. *Computer Science*, 27(1):407–424, 2019.

[48] C. E. Shannon. A mathematical theory of communication. *Bell System Technical Journal*, 27(4):379–423 and 623–656, 1948.

[49] L. L. Shen D. K. Tang D. A. Zheng N. Q. Zhao-D. L. Eckberg G. Q. Wu, N. M. Arzeno and C. S. Poon. Chaotic signatures of heart rate variability and its power spectrum in health, aging and heart failure. *PLoS ONE*, 4(2):e4323, 2009.

[50] T. Santiago P. Sarreira J. Melo E. D. Soares M. Costa, I. R. Pimentel. No evidence of chaos in the heart rate variability of normal and cardiac transplant human subjects. *Cardiovasc Electrophysiol*, 10(10):1350–7, 1999.

[51] H. V. Huikuri J. S. Perkiömäki, T. H. Mäkikallio. Fractal and complexity measures of heart rate variability. *Clin Exp Hypertens*, 27(2-3):149–58, 2005.

[52] S. Murakami G. Yamanakaa Y. Kuboa O. Matsuokaa T. Yamanaka M. Shinagawaa S. Nunodaa-Y. Nishimuraa K. Shibata H. Saitoh M. Nishinaga M. Ishine T. Wada K. Okumiya K. Matsubayashi S. Yano K. Ichihara G. Cornrlissen N. Hotta, K. Otsukaa and F. Halberg. Fractal analysis of heart rate variability and mortality in elderly community-dwelling people – longitudinal investigation for the longevity and aging in hokkaido county (lilac) study. *Biomed Pharmacother*, 59(45), 2005.

[53] C. N. Jani. *Multifractal Analysis Of Heart Rate Variability Using Wavelet-Transform Modulus-Maxima Method. Master thesis.* New Jersey Institute of Technology, New Jersey, USA, 2005.

[54] Y. G. Sinai. Gibbs measures in ergodic theory. *Russian Mathematical Surveys*, 27(4):21–64, 1972.

[55] C. König. *Anatomie, fonctionnement et physiologie de l'œil.* Futura Santé, 2020. `https://www.futura-sciences.com/sante/dossiers/medecine-oeil-vision-dela-vision-667/page/4/` (accessed 27 January 2020).

[56] L. Rossant J. R. Lumbroso. *Céphalée de tension : des symptômes au traitement.* Doctissimo, 2019. `https://www.doctissimo.fr/html/sante/encyclopedie/cephalee-tension.htm#` (accessed 27 January 2020).

[57] F.-X. Borruat. *Céphalées et œil.* Rev Med Suisse, 2007. `https://www.revmed.ch/RMS/2007/RMS-98/31576` (accessed 27 January 2020).

[58] A. J. Agualimpia Y. T. Takeuchi. Cefaleas primarias de corta duracion. *http://www.acnweb.org*, 2010.

[59] P. Nicoué. *Les espaces colorimétriques.* lesnumeriques, 2020. `https://www.lesnumeriques.com/photo/les-espaces-colorimetriques-pu102215.html` (accessed 28 January 2020).

[60] A. Lefebvre. *Contribution de la texture pour l'analyse d'images à très haute résolution spatiale : application à la détection de changement en milieu périurbain.* thesis, 2011.

[61] M. Tuceryan and A. K. Jain. *The Handbook of Pattern Recognition and Computer Vision: Texture Analysis.* World Scientific Publishing C., 1998.

[62] J. Daugman. *How Iris Recognition Works.* Elsevier Academic press, 2009.

[63] G. Guo Y. Ma. *Support Vector Machines Applications*. Springer, 2014.

[64] C. Zhang N. Deng, Y. Tian. *Support Vector Machines: Optimization Based Theory, Algorithms and Extensions*. CRC Press Taylor & Francis Group, 2012.

[65] C. Liu and R. Gao. Multiscale entropy analysis of the differential rr interval time series signal and its application in detecting congestive heart failure. *Entropy*, 19:430, 2017.

[66] J . F. Valencia, A. Porta, M. Vallverdú, F. Clarià, R. Baranowski, E. Orlowska-Baranowska, and P. Caminal. Refined multiscale entropy: application to 24-h holter recordings of heart period variability in healthy and aortic stenosis subjects. *IEEE Transactions on Biomedical Engineering*, 56(9):2202–2213, 2009.

[67] L. Silva, R. Lataro, J. Castania, C. D. Silva, J. Valencia, L. Murta, H. Salgado, R. Fazan, and A. Porta. Multiscale entropy analysis of heart rate variability in heart failure, hypertensive, and sinoaortic-denervated rats: classical and refined approaches. *American Journal of Physiology-Regulatory, Integrative and Comparative Physiology*, 311(1):150–156, 2016.

[68] L Chladekova, B Czippelova, Z Turianikova, I Tonhajzerova, A Calkovska, M Baumert, and M Javorka. Multiscale time irreversibility of heart rate and blood pressure variability during orthostasis. *Physiological Measurement*, 33(10):1747–1756, sep 2012.

[69] E. Watanabe, K. Kiyono, J. Hayano, Y. Yamamoto, J. Inamasu, M. Yamamoto, T. Ichikawa, Y. Sobue, M. Harada, and Y. Ozaki. Multiscale entropy of the heart rate variability for the prediction of an ischemic stroke in patients with permanent atrial fibrillation. *PLOS ONE*, 10(9):137–144, 2015.

[70] F. J. Pastor-Pérez, S. Manzano-Fernández, R. Goya-Esteban, D. A. Pascual-Figal, O. Barquero-Pérez, J. L. Rojo-Álvarez, M. D. M. Martinez-Espejo, M. V. Chavarri, and A. García-Alberola. Comparison of detection of arrhythmias in patients with chronic heart failure secondary to non-ischemic versus ischemic cardiomyopathy by 1 versus 7-day holter monitoring. *The American Journal of Cardiology*, 106(5):677–681, 2010.

[71] M. Atkinson et al A. Alabdulgader, R. McCraty. Long-term study of heart rate variability responses to changes in the solar and geomagnetic environment. *Scientific Reports*, 8, article no. 2663, 2018.

[72] M. Malik, T. Cripps, T. Farrell, and A. Camm. Prognostic value of heart rate variability after myocardial infarction. a comparison of different data processing methods. *Medical and Biological Engineering and Computing*, 27(6):603–611, 1989.

[73] B. Singh, M. Singh, and V. K. Banga. Sample entropy based hrv: Effect of ecg sampling frequency. *Biomedical Science and Engineering*, 2(3):68–72, 2014.

[74] J. S. Richman and J. R. Moorman. Physiological time-series analysis using approximate entropy and sample entropy. *Heart Circulatory Physiology*, 278(6):2039–2049, 2000.

[75] S. M. Pincus and Ary L. Goldberger. Physiological time-series analysis: what does regularity quantify? *American Journal of Physiology*, 266(4):1643–1656, 1994.

[76] J. F. Valencia, M. Vallverdu, P. Gomis, G. Wagner, and P. Caminal. Multiscale information analysis of the autonomous nervous system during myocardial ischemia. In *Computers in Cardiology*, Durham, NC, USA, 2007. IEEE.

[77] B. Czippelova, L. Chladekova, Z. Uhrikova, K. Javorka, M. Zibolen, and M. Javorka. Time irreversibility of heart rate oscillations in newborns – does it reflect system nonlinearity? *Biomedical Signal Processing and Control*, 19:85–88, 2015.

[78] M. G. Signoriniand, R. Sassi, F. Lombardi, and S. Cerruti. Regularity patterns in heart rate variability signal: the approximate entropy approach. In *Annual International Conference of the IEEE Engineering in Medicine and Biology Society. Vol.20 Biomedical Engineering Towards the Year 2000 and Beyond*, Hong Kong, China, 1998. IEEE.

[79] R. Goya-Esteban, F. Sandberg, O. Barquero-Pérez, A. García-Alberola, L. Sornmo, and J. L. Rojo-Álvarez. Long-term characterization of persistent atrial fibrillation: wave morphology, frequency, and irregularity analysis. *Medical and Biological Engineering and Computing*, 57(6):1053–1060, 2010.

[80] P. C. Ivanov, L. A. N. Amaral, A. L. Goldberger, S. Havlin, M.G. Rosenblum, Z.R. Struzik, and H.E. Stanley. Multifractality in human heartbeat dynamics. *Nature*, 399:461–465, 1999.

[81] J. F. Muzy, E. Bacry, and A. Arnéodo. Multifractal formalism for fractal signals: The structure-function approach versus the wavelet-transform modulus-maxima method. *Physical Review*, 47(2):875–884, 1993.

[82] R. G. R. Lekkala and S. Kuntamalla. The effect of chi meditation on the multifractal nature of heart rate variability. *International Journal of Signal Processing Systems*, 4(2):128–132, 2016.

[83] J. E. Mietus, C. K. Peng, I. Henry, R. L. Goldsmith, and A. L. Goldberger. The pnnx files: re-examining a widely used heart rate variability measure. *Heart*, 88(4):378–380, 2002.

[84] P. K. Stein, A. A. Ehsani, P. P. Domitrovich, R . E. Kleiger, and J. N. Rottman. Effect of exercise training on heart rate variability in healthy older adults. *American Heart Journal*, 138(3):567–576, 1999.

[85] J. T. Bigger, J. L. Fleiss, R. C. Steinman, L. M. Rolnitzky, W. J. Schneider, and P. K. Stein. Rr variability in healthy, middle-aged persons compared with patients with chronic coronary heart disease or recent acute myocardial infarction. *Circulation*, 91(7):1936–1943, 1995.

[86] G. L. Rochelle, J. T. Bigger, M. Daniel Bloomfield, H. Krum, R. C. Steinman, J. Sackner-Bernstein, and M. Packer. Long-term carvedilol therapy increases parasympathetic nervous system activity in chronic congestive heart failure. *American Journal of Cardiology*, 80(8):1101–1104, 1997.

[87] F. J. Pastor-Pérez, S. Manzano-Fernández, R. Goya-Esteban D. A. Pascual-Figal, O. Barquero-Pérez, J. L. Rojo-Álvarez, E. Everss, M. D. M. Martinez-Espejo, M. V. Chavarri, and A. García-Alberola. Prognostic significance of long-period heart rate rhythms in chronic heart failure. *Circulation*, 76(9):2124–2129, 2012.

[88] International headache society the international classification of headache disorders. *2nd ed Cephalalgia*, 24:1–160, 2004.

[89] J. Daugman. The importance of being random: Statistical principles of iris recognition. *Patt. Recog.*, 36:279–291, 2003.

[90] V. Vapnik. The nature of statistical learning theory. *Springer-Verlag*, 2000.

[91] V. Vapnik E. Boser, I. Guyon. A training algorithm for optimal margin classifiers. *In Fifth Annual Workshop on Computational Learning Theory ACM Press*, page 144–152, 1992.

[92] P. E. Hart T. M. Cover. Nearest neighbor pattern classification. *IEEE Trans. Inform. Theory.*, 13:21–27, 1968.

[93] A. K. Ghosh. On optimum choice of k in nearest neighbor classification. *Computational Statistics*, 50:3113–3123, 2006.

[94] C. Huttenhower-G. Parmigiani L. Trippa, L. Waldron. Bayesian nonparametric cross-study validation of prediction methods. *The Annals of Applied Statistics*, 9(1):402–428, 2015.

[95] A. N. Venetsanopoulos K. N. Plataniotis. Color image processing and applications. *Springer-Verlag*, 2000.

[96] R. Gonzalez. *Digital Image Processing. 3rd.* 2008.

[97] A. Andreeva V. Vezhnevets, V. Sazonov. A survey on pixel-based skin color detection techniques. *Proc. GraphiCon*, pages 85–92, 2003.

[98] H. Palus. *Color Spaces.* 1998.

[99] T. Sakai Y. I. Ohta, T. Kanade. Color information for region segmentation. *Computer Graphics and Image Processing*, 13(5):222–241, 1980.

[100] H. Grehl A. Lindner M. Krasnianski, D. Georgiadis. Correlation of clinical and magnetic resonance imaging findings in patients with brainstem infarction. *Fortschr Neurol Psychiatr*, 69(5)(5):236–41, 2001.